

Sheffield Hallam University

FTIR and X-ray investigation of triphenylene based discotic liquid crystals.

FORDE, Declan J.

Available from the Sheffield Hallam University Research Archive (SHURA) at:

<http://shura.shu.ac.uk/19655/>

A Sheffield Hallam University thesis

This thesis is protected by copyright which belongs to the author.

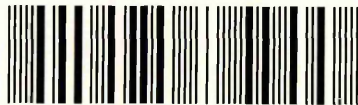
The content must not be changed in any way or sold commercially in any format or medium without the formal permission of the author.

When referring to this work, full bibliographic details including the author, title, awarding institution and date of the thesis must be given.

Please visit <http://shura.shu.ac.uk/19655/> and <http://shura.shu.ac.uk/information.html> for further details about copyright and re-use permissions.

CITY CAMPUS, POND STREET,
SHEFFIELD, S1 1WB.

101 657 641 2



KEY TEXT LOAN

Return to Learning Centre of issue
Fines are charged at 50p per hour

15 AUG 2007

24 AUG 2007 *5pm* *5pm*

516 *5pm*

ProQuest Number: 10694536

All rights reserved

INFORMATION TO ALL USERS

The quality of this reproduction is dependent upon the quality of the copy submitted.

In the unlikely event that the author did not send a complete manuscript and there are missing pages, these will be noted. Also, if material had to be removed, a note will indicate the deletion.



ProQuest 10694536

Published by ProQuest LLC (2017). Copyright of the Dissertation is held by the Author.

All rights reserved.

This work is protected against unauthorized copying under Title 17, United States Code
Microform Edition © ProQuest LLC.

ProQuest LLC.
789 East Eisenhower Parkway
P.O. Box 1346
Ann Arbor, MI 48106 – 1346

**FTIR and X-ray Investigation of
Triphenylene Based Discotic Liquid Crystals.**

Declan J. Forde (BSc Hons)

A thesis submitted in partial fulfilment of the
requirements of
Sheffield Hallam University
for the degree of Doctor of Philosophy

November 2000

Sponsored by the Materials Research Institute :
Sheffield Hallam University
Collaborating Organisation: DRA Malvern



I wish to dedicate this thesis to Eliška who encouraged me throughout the years, and to say 'Thank you for everything.'

Děkuji - Mám tě ráda - Myslim si to!

I would also like to thank the Staff and members of Sheffield Hallam University, especially the many helpful members of the Physics Department and the MRI, in particular my supervisors Dr. J.D.Bunning and Dr. S.J.Spells.

Thanks to the DRA Malvern and John Goodby's chemistry group from Hull - without whom the compounds investigated here would never have been synthesised.

Finally a special thanks to my examiners Prof. J.Yarwood and Prof. J.Lydon for finding the time to examine my thesis despite extenuating circumstances - I appreciate what you did.

FTIR and X-ray Investigation of Triphenylene Based Discotic Liquid Crystals.

Author: Declan J. Forde

Supervisors: J.D. Bunning S. J. Spells

Novel disc like molecules based on hexa-n-alkoxy benzoates of triphenylene were synthesised at Hull university. The compounds exhibited thermotropic liquid crystalline behaviour. The compounds differed chemically based upon the number and position of methyl additions to the ester benzoate linkage. Unsymmetrical compounds based on hexa-n-alkoxy triphenylenes were also examined.

A number of techniques were employed to observe and measure the physical properties of these compounds. Polarising optical microscopy was used to observe and record the phase behaviour. Typical schlieren nematic textures were often observed in the liquid crystalline phase. The transition temperatures of the phase transitions were recorded to within $\pm 0.1^\circ\text{C}$. Methyl additions to the ester benzoate linkage plays a major role in determining transition temperatures and also the ranges of liquid crystal phase.

X-ray diffraction investigations allowed the molecular planar spacings to be measured, use of a heating stage enabled measurements to be taken in the liquid crystalline phase. All the samples produced a diffuse broad diffraction ring in the liquid crystalline phase, indicating that the samples are not highly ordered and that they are likely to have adopted a hexagonal packing arrangement. Planar spacings measured were in the range 22 - 30Å, only one sample, DB26, showed a diffraction ring corresponding to a planar spacing of 4.1Å, indicating that molecular columns or partial columns were able to form from molecules stacking one on top of another. Thus methyl groups on the ester benzoate linkage disrupt the formation of columns, in turn reducing transition temperatures.

A number of methods of successfully aligning the discotic materials using surface treatments are presented. Rubbed PVA and HTAB layers aligned the samples homotropically, while SiO deposited layers aligned the samples homogeneously. (The SiO deposition used an evaporation angle of 45° , a deposition angle of 5° is commonly used to obtain homotropic alignment of calamitic materials.) Methods that produced homogenous alignment of calamitic materials produced homotropically aligned discotic materials and vice-versa.

FTIR allows conformational information about a molecule to be determined. The CH_2 wagging region was investigated to determine conformational information relating to the alkyl arms. Combination of FTIR and aligned samples allowed the alignment process to be investigated, it was determined that the alignment of the molecules occurs in a series of stages, the triphenylene cores align first on cooling, followed by the ester benzoate linkages and finally the alkyl arms.

Computer modelling simulations allowed various molecular conformations to be observed, combination with X-ray diffraction data allowed molecular structures to be generated. The software allowed various molecular dimensions to be easily measured and the effect and extent of interdigitation of molecular arms to be observed. The molecular dynamics calculations were only able to calculate energy minimisations for crystalline structures, but the crystalline results offered valuable insights into the liquid crystalline structures and behaviour.

Contents

| | |
|--|-----------|
| Nomenclature. | V |
| Chapter 1. Liquid crystals. | 1 |
| 1.1. History of liquid crystals. | 1 |
| 1.1.1. Lyotropic liquid crystals. | 2 |
| 1.1.2. Thermotropic liquid crystals. | 6 |
| 1.2. Rod-like molecules. | 10 |
| 1.3. Development of discotic liquid crystals. | 11 |
| 1.3.1. 1977 - 1980 | 11 |
| 1.3.2. 1981 - 1985 | 16 |
| 1.3.3. 1986 - 1990 | 19 |
| 1.3.4. 1991 - 1995 | 29 |
| 1.3.5. 1996 - 1998 | 42 |
| 1.4. Discotic compounds - Hull University. | 46 |
| Chapter 2. Optical Microscopy. | 50 |
| 2.1. Optical Microscopy. | 50 |
| 2.1.1. Optical Microscopy and Liquid Crystals. | 50 |
| 2.1.2. Experimental Set-Up and Sample Preparation. | 51 |
| 2.1.3. Hot Stage Calibration and Temperature Gradient. | 51 |
| 2.1.4. Sample Preparation. | 52 |
| 2.2. Transition Temperatures Obtained by Optical Microscopy. | 53 |
| 2.2.1. Symmetrical Substituted Compounds. | 53 |
| 2.2.2. Unsymmetrical Substituted Compounds. | 54 |
| 2.3. Accidental Alignment | 56 |
| 2.4. Intentional Alignment. | 57 |
| 2.4.1. Alignment by Magnetic and Electric Fields. | 57 |
| 2.4.2. Alignment by Surface Treatments. | 58 |
| 2.4.3. Alignment of Discotic Mesophases. | 59 |
| Chapter 3. X-Ray Diffraction. | 65 |

| | |
|--|-----------|
| 3.1. Discovery of X-rays. | 65 |
| 3.2. X-ray Analysis. | 68 |
| 3.2.1. Powder Diffraction Camera. | 68 |
| 3.2.2. Combining Bragg's Law and Camera Geometry. | 70 |
| 3.2.3. Sample Preparation and Determination of Exposure Time. | 71 |
| 3.2.3.1. Sample Preparation. | 71 |
| 3.2.3.2. Determination of Exposure Time. | 71 |
| 3.3. Ring Diameter Measurements. | 72 |
| 3.3.1. Use of Vernier Callipers and a Light Box. | 72 |
| 3.3.2. Use of Wooster Mark III Mod III Microdensitometer. | 73 |
| 3.3.3. Mode of Operation of the Microdensitometer. | 74 |
| 3.3.4. Planar Spacings. | 75 |
| 3.4. Planar Spacings. | 76 |
| Chapter 4. Infra Red Analysis. | 81 |
| 4.1. Background | 81 |
| 4.1.1. Normal modes of vibration. | 83 |
| 4.1.2. Coupled interactions. | 86 |
| 4.2. FTIR spectrometer development. | 87 |
| 4.2.1. Michelson interferometer. | 88 |
| 4.2.2. Interferograms. | 90 |
| 4.2.3. Fourier transformation and the fast Fourier transformation. | 92 |
| 4.2.4. Apodization. | 93 |
| 4.2.5. FTIR advantages. | 94 |
| 4.2.6. FTIR disadvantages. | 95 |
| 4.3. Software. | 96 |
| 4.3.1. Advanced FIRST feature - second derivative. | 96 |
| 4.3.2. Advanced FIRST feature - curve fitting. | 97 |
| 4.4. Experimental set up and sample preparation. | 98 |
| 4.4.1. Experimental Set-up. | 98 |

| | |
|---|------------|
| 4.4.2. Sample preparation. | 98 |
| 4.5. IR. analysis. | 101 |
| 4.5.1. Peak identification. | 101 |
| 4.5.2. Peak shifts from subtraction spectra. | 103 |
| 4.5.3.1. Effect of the addition of methyl groups pointing away from the core. | 105 |
| 4.5.3.2. Effect of the addition of a methyl group pointing towards the core. | 105 |
| 4.5.3.3. Addition of two methyl groups pointing away from the core. | 106 |
| 4.6. CH ₂ wagging vibration analysis. | 107 |
| 4.6.1. CH ₂ wagging vibrations. | 107 |
| 4.6.2. Rotational isometric state model (RIS). | 110 |
| 4.6.3. Curve fitting. | 112 |
| 4.7. FTIR studies on aligned samples. | 119 |
| 4.7.1. Use of PVA alignment. | 119 |
| 4.7.2. Use of SiO alignment. | 120 |
| 4.7.3. Effect of SiO layer on sample alignment. | 121 |
| 4.8. Order parameter determination. | 124 |
| 4.8.1. Background theory. | 124 |
| 4.8.2. Neff's method of analysis. | 124 |
| 4.8.3. Order parameter results | 127 |
| 4.8.4. Order parameter conclusion | 139 |
| Chapter 5. Computer Modelling. | 141 |
| 5.1. Introduction. | 141 |
| 5.2. Alchemy. | 145 |
| 5.3. Cerius 3.2 running on a Silicon Graphics workstation. | 150 |
| 5.3.1. Energy minimisation. | 150 |
| 5.3.2. Cerius force fields. | 151 |
| 5.3.3. DREIDING I and II force fields. | 152 |
| 5.3.4. Crystal builder. | 154 |

| | | |
|-------------------|--|------------|
| Chapter 6. | Results and Discussion. | 157 |
| 6.1. | Reduction of Transition Temperature. | 157 |
| 6.1.1 | Methyl Additions to the Benzene of the Ester Benzoate Linkage. | 158 |
| 6.1.2. | Additional Methyl Addition to the Alkyl Arm. | 161 |
| 6.1.3. | Conclusion on Methyl Substitutions. | 163 |
| 6.2 | X-ray Diffraction. | 164 |
| 6.2.1 | Symmetrical Compounds. | 165 |
| 6.2.2. | Unsymmetrical Compounds. | 169 |
| 6.3. | Alignment | 171 |
| 6.3.1 | Accidental Alignment | 171 |
| 6.3.2 | Alignment by Magnetic Fields. | 172 |
| 6.3.3 | Alignment by Surface Treatments. | 173 |
| 6.3.4 | Alignment conclusion | 175 |
| 6.4 | Infra Red Analysis | 177 |
| 6.4.1 | Alkyl arm conformations | 177 |
| 6.4.2 | Curve fitting to the I.R. data | 177 |
| 6.4.3 | CH ₂ wagging results | 178 |
| 6.4.4 | FTIR studies of aligned samples | 181 |
| 6.4.5. | Order Parameter determination | 182 |
| 6.5 | Computer Modelling Simulations. | 183 |
| 6.6 | Further Work | 185 |
| 6.6.1 | Reduction of Transition Temperatures through Mixtures and Dopants. | 185 |
| 6.6.2 | Alignment | 185 |
| 6.6.3 | Computer Modelling. | 186 |
| 6.6.4 | Viscosity Measurements. | 186 |
| Appendix A | Optical Textures. | |
| | Optical Microscopy Scale | |
| Appendix B | X-ray Diffraction Photographs. | |
| | References. | |

Nomenclature.

| Symbol | Description | Unit |
|---------------------------|--|------------------------------------|
| $B(\bar{\nu})d\bar{\nu}$ | Spectral component of power | |
| $B(\bar{\nu})$ | Spectrum | |
| $\bar{\nu}$ | Wavenumber | cm^{-1} |
| $\bar{\nu}_{\text{asym}}$ | Antisymmetrical mode of vibration | cm^{-1} |
| $\bar{\nu}_{\text{sym}}$ | Symmetrical mode of vibration | cm^{-1} |
| λ | Wavelength of the radiation used | m |
| $\Delta\epsilon$ | Dielectric anisotropy | |
| $\epsilon_{ }$ | Parallel component of dielectric anisotropy | |
| ϵ_{\perp} | Perpendicular component of dielectric anisotropy | |
| α, β, γ | Unit cell angles | $^{\circ}$ |
| δd | Uncertainty in the planar spacing | \AA |
| Δn | Optical anisotropy | |
| ϵ_r | Relative permittivity | |
| a, b, c | Unit cell lengths | \AA |
| AgCl | Silver chloride | |
| B | Magnetic flux density | T |
| C | Crystal phase | |
| c | Velocity of light in a vacuum | $2.997 \cdot 10^8 \text{ ms}^{-1}$ |
| c_m | Velocity of light through a medium | m s^{-1} |
| CAD | Computer aided design | |
| CaFl | Calcium Fluoride | |
| CCD | Charge coupled device | |
| cm^{-1} | Wavenumber | |
| $\text{Cu K}_{\alpha 1}$ | $\alpha 1$ component of Cu radiation | 1.5405\AA |
| $\text{Cu K}_{\alpha 2}$ | $\alpha 2$ component of Cu radiation | 1.5443\AA |

| | | |
|-----------------|---|-----------------------|
| Cu K_{α} | Weighted mean of $K_{\alpha 1}$ and $K_{\alpha 2}$ | 1.5418Å |
| d | Planar spacing | Å |
| D | Sample to film separation | 94mm |
| $D(x)$ | Box car function | |
| DCM | Dichloromethane | |
| DSC | Differential scanning calorimetry | |
| E ray | Extraordinary ray, apparently contradicts Snell's law | |
| E_{angle} | Energy associated with the bond angle | J |
| E_{bond} | Bond stretching energy term | J |
| EG | End gauche conformer | |
| E_{hb} | Energy term related to hydrogen bonded components | J |
| $F(x)$ | Interferogram | |
| FFT | Fast fourier transform | |
| FTIR | Fourier-transform infra red | |
| g | Gauche state | |
| g' | Gauche prime state | |
| GG | Double gauche conformer | |
| GTG | Gauche-trans-gauche conformer | |
| GTG' | Gauche-trans-gauche prime conformer (kink), | |
| hd | Hexagonal disordered | |
| HET | Hexaalkoxytriphenylene | |
| ho | Hexagonal ordered | |
| HTAB | Hexadecyl trimethyl ammonium bromide | |
| IR | Infra red | |
| ITO | Indium tin oxide | |
| k | Force constant of the bond | $5 \cdot 10^{-2}$ N/m |
| K | Resolution enhancement | |
| k_{11} | Splay elastic constant | |
| k_{33} | Bend elastic constant | |

| | |
|------------------------|---|
| K_b | Force constant |
| KBr | Potassium bromide |
| n | Refractive index |
| n_e | Extrardinary refractive index |
| n_o | Ordinary refractive index |
| $\Delta n = n_e - n_o$ | Optical anisotropy |
| \underline{n} | Director average of the molecular long axis |
| N_{C-C} | Number of C-C bonds in the alkane chain |
| N_D | Nematic disc-like phase |
| N_D^* | Twisted N_D phase |
| N_{eg} | No. of end gauche |
| N_{gg} | No. of double gauche |
| N_k | No. of kink |
| P_{eg} | % end gauche |
| P_{gg} | % double gauche |
| PI | Polyamide |
| P_k | % kink |
| PVA | Poly vinyl alcohol |
| rd | Rectangular disordered |
| S | Order parameter |
| S_A | Smectic A |
| SiO | Silicon monoxide |
| t | Trans state (i.e. gtg) |

Chapter 1. Liquid crystals.

1.1. History of liquid crystals.

Liquid crystalline materials were first observed during the middle of the last century by Rudolf Virchow [1], a German physicist, who in 1853 observed through a microscope an interesting form of matter. Myelin, which forms an outer coat around certain nerve fibres, produces a number of different forms when withdrawn from the nerve core into water. Similar effects were also observed with other biological samples e.g. lecithin and protagon, a group of phospholipids found in animals, egg yolk and some higher plants. By 1888 Otto Lehmann had investigated these materials as well as cholesterol esters that underwent iridescent colour changes during cooling [2]. Lehmann initially used the term "flowing crystals" in 1889 to describe these compounds. By 1890 he was describing the systems as "crystalline liquids" and by 1900 the term "liquid crystal" first appeared [3]. The term liquid crystal describes a state of matter that exhibits a greater degree of molecular order than an ordinary liquid, but less order than a crystalline solid. A liquid crystal may pass through one or more regions of decreasing order, mesomorphic states, or mesophases, before becoming an isotropic liquid.

There are currently two main classifications for liquid crystals.

LYOTROPIC - these liquid crystals are not pure substances but are a solution of a compound in a solute e.g. water. Such solutions show liquid crystalline properties only above a certain concentration, with properties that are very much dependent upon the concentration.

THERMOTROPIC - liquid crystal phases formed by either heating a solid or cooling a liquid. The transfer between phases is purely dependent on the thermal processes.

1.1.1. Lyotropic liquid crystals.

Lyotropic liquid crystals are generally made up of two or more components, an *amphiphilic* molecule and a solute, commonly water. Water belongs to a group of molecules which are polar; the bonding of atoms in these molecules results in an uneven distribution of electrical charge, one part of the molecule being slightly positively charged and another part slightly negatively charged. Molecules where the charge is distributed fairly uniformly are non-polar.

An amphiphilic molecule consists of two parts (Fig. 1.1.), a polar head group that is hydrophilic (water loving) and is therefore easily soluble in water, and a non-polar tail usually consisting of one or more alkyl chains which are hydrophobic (water hating) and as a consequence are insoluble in water [4].

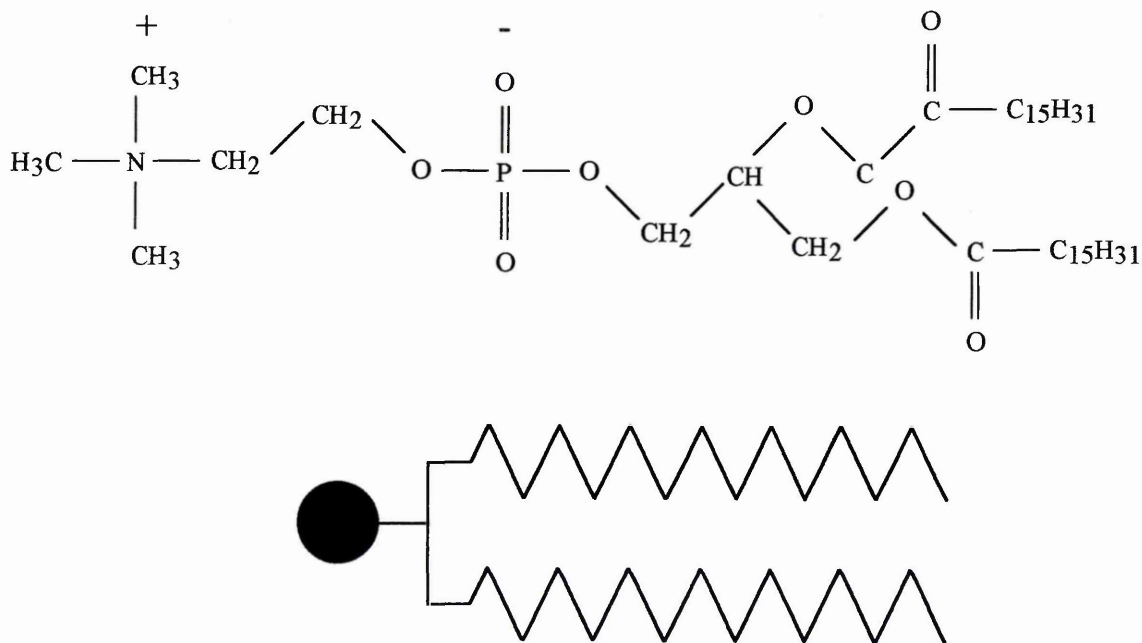


Figure 1.1. An example of an amphiphilic molecule.

These molecules are able to display characteristics from both their components, which leads to interesting behaviour. Two important amphiphilic types of molecule are phospholipids, which make up the cell membranes of all biological systems, and soaps.

When an amphiphilic molecule is mixed with water, the hydrophilic head group tends to maximise its interfacial surface contact with the water while the hydrophobic tails tend to minimise their interfacial surface contact. When the concentration of amphiphilic molecules is low, two possible structures may form depending on the strength of the polar head group relative to the non-polar tail.

For a strong polar head group the amphiphilic molecules arrange into spheres, maximising head group contact with the water and minimising water tail contact. This spherical structure with the heads on the outside and the tails pointing towards the middle is called a *micelle* (Fig. 1.2. a). If the head groups are not as strongly polar, spherical vesicles are formed in which double layers of amphiphilic molecules form a shell with water both inside and outside. These double layers of amphiphiles are known as *bilayers* and this is the basis of biological cell membranes (Fig. 1.2. b).

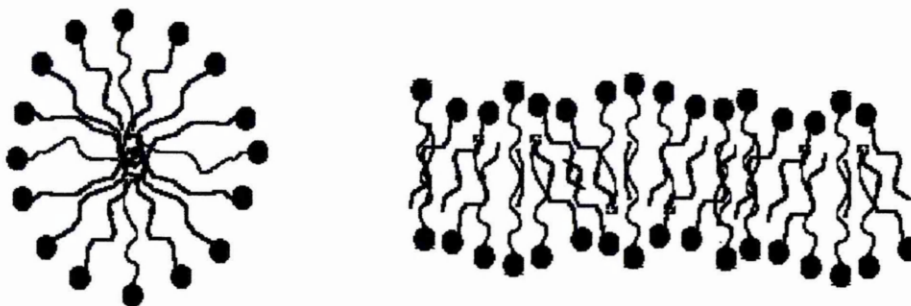


Figure 1.2. a. Micelle.

b. Bilayer.

In some cases several bilayers may form inside each other, the structure resembling an onion with each bilayer separated by a water layer. These structures are stable provided the amphiphilic concentration is above the critical micelle concentration.

The structures described above occur when an amphiphilic molecule is placed in a polar solute. If the solute is non-polar e.g. oil, similar structures will form. In these cases it is the non-polar tail that shows an affinity for the solute and the molecules arrange themselves with the tails at the oil-micelle interface and with the heads pointing towards the centre, resulting in *inverted* structures.

When the amphiphile concentration is increased to approximately 50% the spherical micelles combine to form larger more complex structures i.e. *hexagonal phase, lamellar phase, cylinders and bilayer sheets*.

The hexagonal phase sometimes referred to as the middle soap phase, no longer consists of spherical micelles, but instead consists of long cylindrical rod-like collections of amphiphiles, where the long axes of these rod-like groups are arranged into a hexagonal array (Fig. 1.3. a). At even higher concentrations the lamellar phase or neat soap phase forms, in which the amphiphilic molecules form relatively flat bilayers separated by a region of water (Fig. 1.3. b).

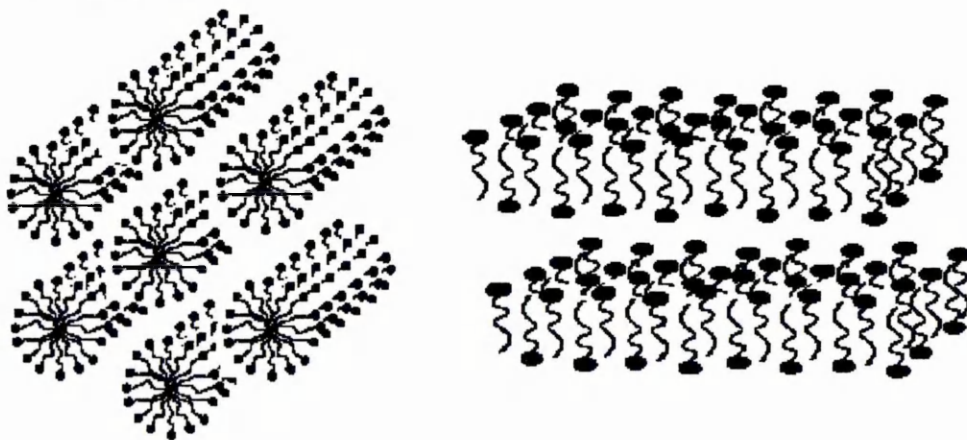


Figure 1.3. a. Hexagonal Array. b. Lamellar phase.

For some phospholipid systems a *gel phase* may form; this is very similar in appearance to the lamellar phase, but the hydrocarbon chains are more rigid than in the lamellar phase where the chains are free to adopt a number of differing and constantly changing configurations. The increased tail rigidity allows the phospholipid head groups to adopt a closely spaced hexagonal array when packing together. Cubic phases and intermediate phases are also possible

All the structures mentioned are liquid crystalline, the amphiphilic molecules being free to diffuse throughout each structure and also into the water region.

Only the effect of amphiphilic concentration has been described above. Temperature also has a significant effect on phase formation and stability. If the temperature is too low, none of these phases can form, and the amphiphilic molecules become fixed into rigid crystalline structures and are no longer able to move relative to each other. When the temperature is too high only the isotropic phase is visible.

1.1.2. Thermotropic liquid crystals.

Traditionally, the structures of thermotropic liquid crystals have been based on molecules having a rod-like shape, (calamitic), (see 1.1). Within the thermotropic division there are three classes of mesophases, *nematic*, *smectic* and *cholesteric*. A brief description and simplified views of each of these three phases are given below. The order within a crystal and an isotropic liquid are described in order as to be used as a reference.

CRYSTAL - a crystal is a structure that has both long range translational and orientational order. A crystal may be thought of as consisting of a regular repeating lattice of points with each lattice point corresponding to the position of an atom, molecule or compound. If a molecule or compound is situated at the lattice point, then they are all oriented in the same direction in a perfect crystal (Fig. 1.4.).

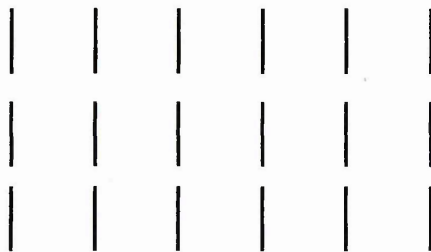


Figure 1.4. Crystal.

ISOTROPIC - this is the name for a completely disordered phase, with no preferred orientation direction. It also has the lowest viscosity and is more commonly known as the liquid phase (Fig. 1.5.).

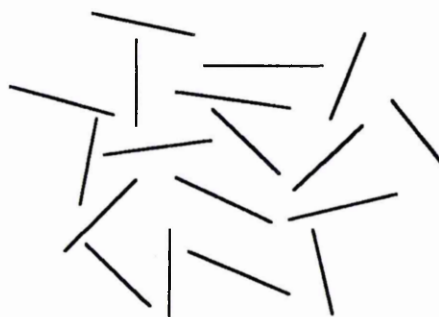


Figure 1.5. Isotropic.

NEMATIC - comes from the Greek for thread - *nematos*, and is used to describe a mesophase that consists of a collection of curved threadlike lines when viewed in the optical microscope between two crossed polarisers. The arrangement of crossed polarisers would normally ensure that no light can pass through, but due to orientational ordering within the liquid, the plane of polarisation of the light is altered and the sample appears visible and coloured. The dark / light regions without polars arise from defects within the liquid crystal. Exactly how this occurs will be discussed in Chapter 2.

If a unique molecular axis is identified and used to represent the orientation of the molecules, an overall molecular orientation can be calculated by averaging over all orientations. This gives a preferred orientation direction referred to as the *director* \underline{n} .

In the nematic phase the unique molecular axes are spontaneously oriented approximately parallel to one another. The ordering is strictly one dimensional (Fig. 1.6.). The phase displays long range orientational ordering but no long range translational order. The orientation direction may vary from one region of the sample to another, this variation of orientation direction giving rise to grain boundaries.

The phase is not as viscous as other liquid crystalline phases but still has a peculiar turbid appearance, the fluidity of the phase being due to the ease with which molecules slide past each other whilst retaining their parallelism. Nematic calamitic materials are to be found in many display applications. The term *calamitic* is used to describe rod-like molecules.

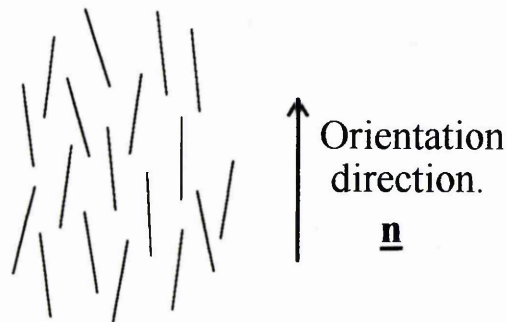


Figure 1.6. Nematic.

CHIRAL - Chiral nematics also referred to as cholesterics derive their name from cholesterol, many of them are chemical derivatives of cholesterol, although cholesterol itself does not form a liquid crystal phase. The phase is similar to a nematic in that the mesophase consists of a series of layers within each of which the molecules are packed with their long axes approximately in the plane of the layer (Fig. 1.7.).

The molecules are optically active, the molecular axes in adjacent layers are not parallel, but they are in fact oriented at slightly different angles due to intermolecular forces that favour alignment at a slight angle to one another. This progressive twist leads to the production of a screw axis perpendicular to the preferred molecular orientation direction. This results in a progressively twisting or helical structure, which may be either right-handed or left-handed, depending on the molecular conformation. The twist described in the cholesteric liquid crystal is very small: it takes approximately 1500 molecular layers in order for the top and bottom layers to be aligned. Thus the pitch of the twist is of similar magnitude to optical wavelengths and the visible iridescent colouring of the material arises from varying twist pitches.

Cholesteric liquid crystals are very sensitive to changes in temperature where the screw pitch is altered by the temperature variation and are commonly used in temperature sensing devices and paints, displaying different colours corresponding to different temperatures, going from red to yellow to green and then to blue as the temperature is increased. In the last few years T-shirts incorporating a cholesteric dye have become almost obligatory for the fashion conscious teenager.

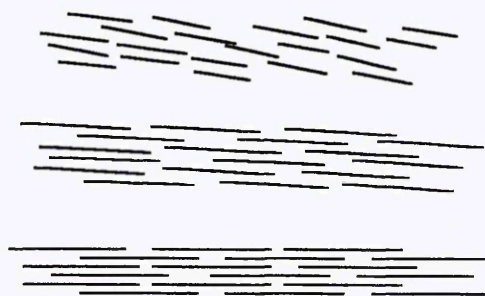


Figure 1.7. Helicoidal.

SMECTIC - derived from the Greek word *smectos* for soap. In this example the rod-like molecules pack together in strata or layers that stack on top of each other. Interlayeral attractions are weak when compared with lateral forces between molecules, allowing the layers to slide over one another relatively easily. The molecules within each layer all point in approximately the same direction although they may pack in a regular or an irregular manner (Fig. 1.8.). Molecules within each layer may be perpendicular to the plane of the layers or be tilted relative to it.

Ordering of, tilting within and correlation between layers of molecules permit over 12 distinct smectic mesophases to be successfully identified [5, 6, 7]. For example, in the Smectic A (S_A) phase, molecules are arranged in layers and within the layers the molecules are on average perpendicular to the layer plane but are positionally disordered within it. The smectic C, S_C , phase is similar to the S_A except that the molecules are tilted with respect to the plane of the layer. This type is thus ordered in at least two dimensions, depending on which form is considered. S_E , S_G , S_H , S_J and S_K have three dimensional long range positional order, similar to a crystal but have weak interlayer forces and are usually referred to as smectic crystal phases.

The nature of this molecular arrangement means that the smectic phase is the most solid-like, being turbid and quite viscous. When drops with freed surfaces are formed they have an unusual terraced surface, the edges of which often displaying focal conic textures.

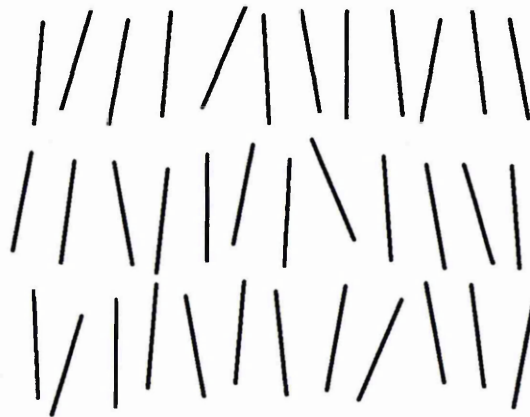


Figure 1.8. Smectic A.

1.2. Rod-like molecules.

Until quite recently it was accepted that in order to exhibit liquid crystalline properties (e.g. thermotropic or lyotropic mesomorphism) the molecule had to be rod-like in shape. The rod-like molecules are usually composed of a semi flexible core with highly flexible tails on either side of the core (Fig. 1.9.). One of the molecular axes is many times longer than the other two molecular axes. By adjusting the core and altering the tail lengths, it is possible to alter the liquid crystalline properties e.g. melting point, dielectric constant and magnetic susceptibility.

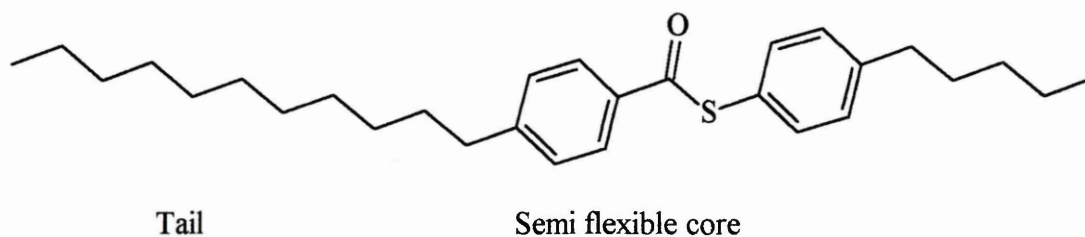


Figure 1.9. Rod-like molecule.

1.3. Development of discotic liquid crystals.

1.3.1. 1977 - 1980

1977

Up until 1977, all materials that showed liquid crystalline properties involved rod-like molecules that were usually composed of a semi flexible core with highly flexible tails on either side of the core. It was therefore believed that only these rod-like molecules would be capable of displaying liquid crystalline mesophases. Chandrasekhar *et al* postulated and showed in 1977 [8] that the only geometrical constraint for liquid crystalline behaviour is that the molecule is anisometric (non spherical) in shape. Thus compounds composed of disc-like molecules should also be able to exhibit stable liquid crystal mesophases. These new liquid crystal types are referred to as discotic liquid crystals. The first compounds to be prepared and identified as liquid crystalline were hexa substituted esters of benzene, specifically the hexa-*n*-alkanoates of benzene (Fig. 1.10.). Through optical investigation and X-ray studies a new kind of mesophase was identified in which the discs stack on top of one another to form columns that exhibit liquid crystal like behaviour.

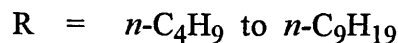
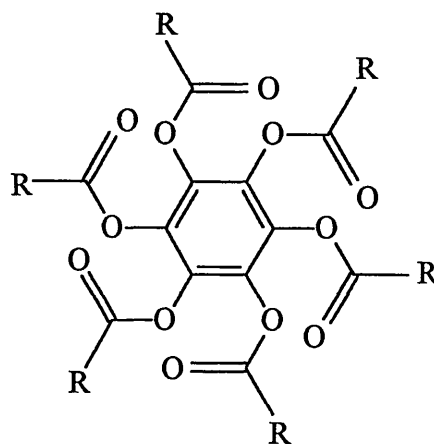


Figure 1.10. Hexa-*n*-alkanoate of benzene.

Billard *et al* [9] introduced the word *discotic* to distinguish disc-shaped mesogens from the rod-shaped or calamitic mesogens. They identified liquid crystalline behaviour in hexa-*n*-alkanoates of triphenylene (Fig. 1.11.) and hexa-*n*-alkoxytriphenylene.

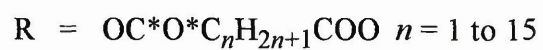
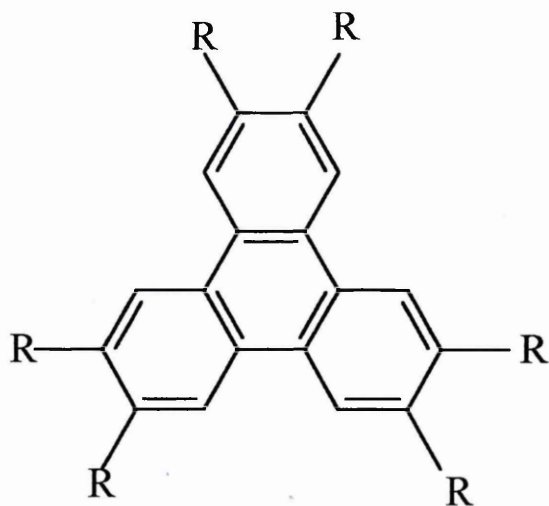


Figure 1.11. Hexa alkoxy derivatives of triphenylene.

Destrade *et al* [10] in 1979 identified liquid crystalline behaviour in hexa alkanoyloxy derivatives of triphenylene (Fig. 1.11.).

The first hexa-*n*-alkyl and -alkoxy benzoates of triphenylene (Fig. 1.12.) were synthesised and identified in 1979 by Tinh *et al* [11]. A new phase, the discotic nematic was shown to exist.

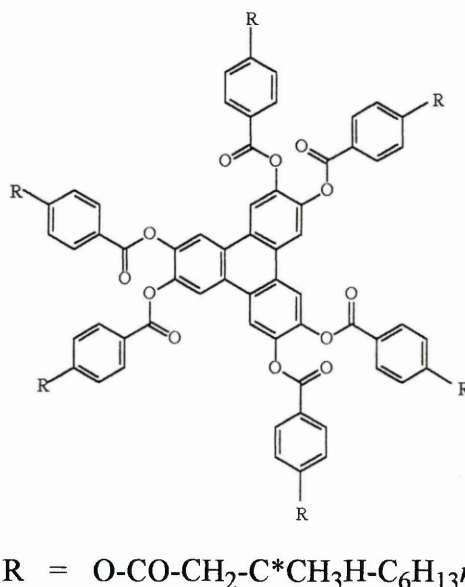


Figure 1.12. Hexa-*n*-alkyl and -alkoxy benzoates of triphenylene.

These discotics exhibit the new columnar phase and/or a nematic like phase, but a smectic like phase has yet to be observed. In the case of discotic liquid crystals the director, the preferred axis of orientation of the molecules, which for the calamitic compounds was parallel to the long axes of the molecule, is now defined as the:

"Preferred axis of orientation of the disc normal (or molecular short axis)." [5].

Hence the medium is optically negative unlike the classical rod-like nematics which are optically positive.

During the late 70s and early 80s, a lot of work was concentrated on synthesising these new discotic compounds and new liquid crystalline phases were identified by use of optical microscopy and X-ray diffraction. The first compounds synthesised, the hexa-*n*-alkanoates [8], exhibited a columnar phase, where the discs tend to stack one on top of another to form long parallel columns that are free to slide past each other.

Two years after the first columnar discotics were synthesised and identified, Tinh *et al* [11] in 1979 synthesised and identified the :

"first example of disc-like mesogens which present at high temperatures a highly fluid mesophase with a nematic optical texture."

This was the first example of a nematic disc-like phase which Tinh and co-workers labelled N_D . The compound, a hexadecyloxy benzoate of triphenylene, exhibited a classical Schlieren texture when viewed in a polarising optical microscope at 165°C. The texture was very similar to the textures produced by various calamitic nematics and was a complete contrast to the focal conical textures of the discotics that had been observed and which previously only formed columnar phases.

In the new nematic disc-like phase, the discs no longer stack one above another, but stack in a more disordered manner. The directors tend to align in approximately the same direction, but the discs are now able to slide past one another and over one another more easily. Tinh *et al* [11] proposed molecular structures for the columnar phase (Fig 1.13. a) and the nematic phase (Fig. 1.13. b).

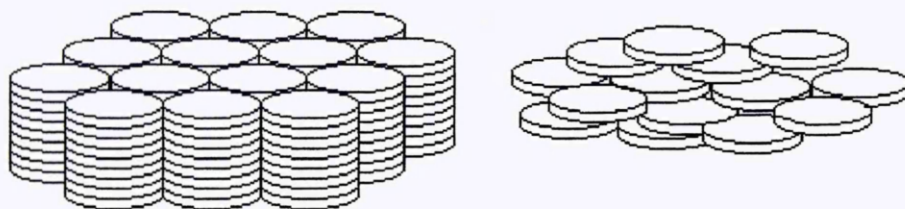


Figure 1.13 a. Columnar phase b. Nematic phase

By the end of 1979 several columnar phases: D_{ho} , D_{hd} , D_{rd} , D_t had been proven to exist by Destrade *et al* [12] in a range of discotic compounds.

ho - hexagonal ordered

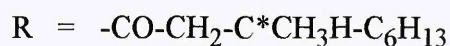
hd - hexagonal disordered

rd - rectangular disordered

t - tilted.

1980

In the summer of 1980, Destrade and Tinh [13] reported the first evidence of a "cholesteric" phase in a disc-like mesogen, where a chiral triphenylene based compound dissolved in the N_D nematic phase in a 50/50 mixture was able to twist the N_D nematic phase. The chirality was achieved by taking a compound that previously displayed a N_D phase and altering the arms by a methyl addition at the third carbon unit on the alkyl chain, giving the general formula for the chiral 3-methyl nonanoyl group



The compounds displayed non chiral columnar phases at lower temperatures and at higher temperatures domains with very typical cholesteric optical textures were observed, characterised by oily streaks and fingerprints of polygonal textures.

1.3.2. 1981 - 1985

1981

Malthete *et al* [14] reported the first evidence of a cholesteric phase in a pure disc-like molecule, 2,3,6,7,10,11-hexa-[s-(4-methyl)-4-*n*-hexyloxybenzoyloxy] triphenylene, which displayed a twisted N_D or N_D* phase from 192.5°C - 246.5°C.

A classification of disc-like mesogens was published by Destrade *et al* [15] describing the five identified mesomorphic phases of several disc-like liquid crystals. Optical textures, nomenclature and proposed structures were described. Experiments were also underway at attempting to orientate discotic mesophases by Levelut *et al* [16] using a rotating magnetic field and Vauchier *et al* [17] using various surface treatments. Homeotropic alignment, with the directors perpendicular to the walls, was obtained by use of glass surfaces coated with flat molecules possessing six polar side functions e.g. polysiloxanes. Parallel alignment was obtained using glass surfaces coated with obliquely deposited silicon oxides at relatively large angles of 20°.

Tinh *et al* [18] synthesised hexa-4-*n*-alkylbenzoates of triphenylene, similar to the compounds first synthesised by Tinh *et al* [11].

1982

Destrade *et al* [19] found in a mixture of two truxene based discotic liquid crystals the occurrence of a re-entrant isotropic phase. The term *re-entrant* was used when a more disordered phase appeared out of sequence after a more ordered phase on cooling.

The hexa-*n*-alkanoates of benzene synthesised by Chandrasekhar *et al* [8] in 1977 were originally synthesised as long ago as 1937 by Backer and Van der Bann at Groningen Universitat Germany [20], but they did not report the compounds showing any liquid crystalline behaviour. However 46 years later in 1983, de Jeu [21] also working at Groningen, found that the materials were still in stock in the organic chemistry department and upon investigation they were indeed seen to exhibit the mesomorphic behaviour already reported by Chandrasekhar *et al* [8].

In 1983 Giannessi [22] treating the nematic-hexagonal discotic phase transition in the framework of the Landau theory of phase transitions, theorised the pre transitional enhancement of the elastic constants. Chandrasekhar [23] produced a brief review of disc-like liquid crystal structures and considered an extension of Mc Millan's mean field model for smectic A modified for disc-like molecules. Theoretical studies of the fluctuations of the discs within the columns in a columnar liquid crystal were carried out. Dowell [24, 25] produced a general lattice model partition function using hard repulsions for ordered phases of rigid cores having semi flexible tails. The molecules although not discotic possessed a rigid core with one or two semi flexible tails. They approximated rod-like molecules and re-entrant nematic phases were simulated. Dowell [25] suggested the important role of the intrachain flexibility constraints in the molecular lattice model for the rod-like compounds could be extended to incorporate the discotic class of compounds. Re-entrant phases had not been identified in the discotic class of compounds, although they were known to exist in a number of calamitic compounds.

Levelut [26] and Destrade *et al* [27] produced reviews of the columnar mesophases discovered so far.

In 1984 Destrade *et al* [27] and Tinh *et al* [28] reported the existence of re-entrant liquid crystalline sequences in pure compounds; both re-entrant columnar and re-entrant nematic phases for truxene derivatives were seen to exist. The existence of re-entrant columnar and re-entrant nematic phases had been shown to exist in pure compounds [27, 28], but the re-entrant isotropic was only observed in a mixture [21] and did not appear in either of the two compounds separately.

Safinya *et al* [29] obtained highly oriented discotic liquid crystal fibres of the columnar mesophase of hexaalkoxytriphenylene HET-*n* and triphenylene-hexa-*n*-alkanoate HAT-*n* by a new strand alignment technique. Freely suspended fibres were drawn from a two stage oven consisting of a mechanically operated pin and a reservoir cup. The temperature of the system was monitored to a stability of 0.01°C and a slow drawing motion was employed to produce fibres of 1-3 mm length with a diameter of 50-400 µm. The single crystal quality of these drawn fibres was determined by synchrotron X-ray scattering studies, which indicated that the drawn fibre contained a few single columnar lattice domains.

Chiang *et al* [30] in 1985 improved the technique and the single crystal quality was further improved by annealing. The strand technique proved to be a reliable method to align discotic liquid crystals and has subsequently been employed by a number of other groups to align samples. This strand technique is able to produce aligned samples from the relatively viscous columnar mesophases, but is of no use for studies of the physical properties of the more fluid nematic mesophase.

1.3.3. 1986 - 1990

1986

In 1986 X-ray diffraction of powder samples of alkylthio substituted triphenylenes were obtained for both the D_{ho} and D_{hd} phases by Gramsbergen *et al* [31]. The Bragg spacing for the inter columnar separation was obtained and when this spacing was converted to a hexagonal lattice it yielded a molecular separation of 21.2 Å to 24.8 Å depending on alkyl chain length. This implied either a large degree of penetration of the alkyl chains into the aliphatic regions of neighbouring columns and/or a high degree of orientational disorder within the chain. X-ray powder diffraction was unable to answer the problem and determine if the alkyl chains were interdigitated or highly disordered or if both cases existed. Results from conformationally sensitive techniques needed to be considered. Kardan *et al* [32] employed vibrational spectroscopy to analyse the micro structure of some disc-like crystalline macromolecules. From this work it appeared that the structure of the polymethylene sequence was correlated to the phase behaviour of the compounds studied. It was also suggested that there were two distinct conformations associated with the ester linkage attached to the core. The C=O stretching vibration was found to be particularly sensitive to the phase transitions. From analysis of the CH₂ rocking vibrations in the 720 cm⁻¹ region it was determined that the polymethylene sequence of the compound that did not show any liquid crystalline mesophases was quite disordered, while for the other two compounds the polymethylene chain vibrations were observed and in particular for one compound it appeared that the chains were in a fully trans conformation i.e. fully extended, in the crystalline region. As the temperature was raised however, the polymethylene sequences were observed to disorder rapidly and in the intermediate discotic liquid crystal region the degree of disorder was similar to that observed in the isotropic region. Giannessi [33] building on previous theoretical work [22] calculated the critical behaviour of the Frank energy near the transition for a theoretically predicted nematic phase with six fold orientational order to the hexagonal discotic phase.

In 1987 the bend and splay elastic constants of a discotic nematic liquid crystal, hexa-*n*-dodecanoyloxy truxene were determined by Raghunathan *et al* [34] using the Freederickz transition technique. This method initially involves capacitance measurements of a parallel plate capacitor, where the dielectric between the plates is air. The liquid crystal to be investigated is then replaced as the dielectric for the capacitor. The relative permittivity ϵ_r of the liquid crystal is calculated by dividing the capacitance of the full cell by the capacitance of the empty cell. The perpendicular and parallel components of the dielectric permittivity are determined graphically from plots of ϵ_r against $1/\text{applied voltage}$. The splay elastic constant k_{11} and the bend k_{33} can then be calculated. Values of $\approx 10^{-7}$ N were produced, which are of the same order as for nematic rod-like molecules. The k_{33} (bend) was found to be greater than k_{11} (splay) probably arising as a consequence of the columnar short range order in the medium. In order for this method to work it is a requirement that the liquid crystal sample is aligned in the capacitor.

Homeotropic alignment, where the director is perpendicular to the glass substrate, was obtained by placing the sample between two clean glass plates; spontaneous alignment occurred. Homogeneous alignment was more difficult to achieve. Using the parallel alignment techniques of Vauchier *et al* [17], obliquely coating with silicon monoxide only produced homeotropic alignment due to the strong affinity of the aromatic cores of the molecules to the SiO surface. By further treatment of the obliquely SiO coated plates with octadecyl triethoxy silane, to produce an aliphatic surface that preserved the underlying undulations of the SiO coating, parallel alignment of the sample was achieved. Raughunathan did not indicate the oblique angle used for the SiO deposition: assuming the work of Vauchier *et al* [17] was followed, an angle of 20° would have been used.

Kardan *et al* [35] investigating the conformations of discotic compounds deposited on metallic surfaces found that the cores lay flat on the surface, while the arms tended to lie

with the plane of their skeletal backbone perpendicular to the surface and the chain axis parallel to the surface, although the relative orientations changed significantly during phase transitions. The ester group was oriented perpendicular to the metallic surface. The spectra were obtained using reflectance infrared spectroscopy from ultra thin films 20-80Å thick or approximately 3-14 molecular layers of the disc-like molecules deposited on a gold substrate. It should be noted that the results were for thin films and that the results do not easily translate into the bulk. The transition temperatures of the thin films were slightly lower than those measured for the bulk material.

1988

In 1988 Yang *et al* [36] using site-specific deuterated hexahydroxybenzene hexaoctanoate discotic liquid crystals revealed conformational information about the C₂-C₃, C₅-C₆ and C₆-C₇ bonds on the side chains. Previous work from this group [32, 35] revealed dramatic spectral changes that accompanied the phase transitions in discotics, but they were unable to quantitatively determine the structural disorder distribution along the flexible arms, due to uncertain infra-red band assignments. Selective deuteration of the methylene chains enabled this information to be obtained, due to the spectral properties of a CD₂ group. The rocking vibration of an isolated CD₂ group in a polymethylene chain is uniquely sensitive to the conformation of the chains in the immediate vicinity. By placing CD₂ units at selected positions along the chains the defect distribution at these positions can be identified. Work using this technique had previously been carried out on *n*-alkanes and fatty acids by Snyder and coworkers [37, 38, 39] in 1985, but it was employed here to investigate chain conformations of discotic liquid crystal compounds.

Yang *et al* [36] determined that in the crystal phase the chains were in the fully trans conformation. Disordering of all of the bonds occurred at 32°C at a crystal-crystal transition. Conformational disorder increased slowly and continuously to the crystal-

discotic transition at 80°C. At both the crystal-discotic and discotic-isotropic transitions at 80°C and 90°C respectively, there was an associated major increase in side chain disorder. It was determined that the side chains in the discotic phase were more highly ordered than in the isotropic state where the spectral characteristics resembled those of molten alkanes.

Boden *et al* [40] determined the X-ray crystal structure of the discotic amphiphile 2,3,6,7,10,11-hexa-(1,4,7-trioxaoctyl) triphenylene (TP6E02M) using the thin hair-like needles that formed the crystal habit. Due to the low melting temperature of the compound the X-ray diffraction was carried out at 0°C in order to obtain X-ray data of sufficient quality to define the interesting features. The lattice parameters and space group were defined, with the most interesting feature of the X-ray data being the fact that the molecules were arranged in tilted stacks. They also investigated the one-dimensional electronic conductivity of some discotic liquid crystals [40] in particular the discotic mesogen 2,3,6,7,10,11-hexa-hexyloxytriphenylene (HAT 6) which forms a columnar hexagonal phase and is an electrical insulator. When this material is doped with 1mol% of the Lewis acid AlCl₃ it is converted into a p-type semiconductor, where the direction of conductivity is along the columnar axis.

Fontes *et al* [41, 42] using the strand alignment technique developed by Safinya and coworkers [29, 30] generated oriented strands of 2,3,7,8,12,13-hexa(*n*-tetradecanoyloxy) truxene and hexa-hexylthiotriphenylene. Using X-ray diffraction two types of behaviour were revealed from the samples in the columnar phase: the alkyl arms were highly disordered producing a nearly isotropic scattering pattern, whereas the rigid cores were orientationally ordered but translationally disordered along the columns.

Warmerdam *et al* [43] were the first to observe a re-entrant isotropic for a pure compound 2,3,7,8,12,13-hexa(octadecanoyloxy) truxene. They carried out a number of physical parameter measurements on the compounds that they synthesised, including the

compound that produced the re-entrant isotropic behaviour [44]. Transition temperatures from both optical microscopy and differential scanning calorimetry (DSC) along with the various optical textures produced were reported. A temperature controlled Abbe refractometer was used to measure the refractive indices, with the birefringence of the nematic phase being clearly detectable. The optical anisotropy $\Delta n = n_e - n_o$ for the discotic compounds was negative as expected (which is contrary to that commonly observed for rod-like liquid crystals.) The elastic constants were measured using the Freederickz transition technique [44, 45, 46]. The nematic material was homeotropically aligned using a thin polymer film, Dupont P12566. A magnetic field was used to switch the compounds. It was found that the splay elastic constant k_{11} was greater than the bend elastic constant k_{33} . This is in contrast to calamitic nematics, but the values were of the same order of magnitude as those of rod-like compounds.

1989

In 1989 Lee *et al* [47] also observed a re-entrant isotropic phase in a discotic mixture similar to that previously reported by Destrade *et al* [27] as having only re-entrant columnar and re-entrant nematic phases. It was suggested that nematic and even isotropic re-entrancy for truxene based discotics arises from a delicate balance between the positional entropy of the entire molecule and the conformational entropy of the tails.

Yang *et al* [48] using Fourier transform infra red spectroscopy (FTIR) obtained the molecular orientation of two hexasubstituted benzene derivative discotic liquid crystals. Previous vibrational spectroscopy measurements by this group [36] provided a measure of the temperature-induced changes in the conformation of the side chains attached to the central core. The work of Kardan *et al* [32, 35] using site-specific deuterium labelled samples prepared in Yang's laboratories, measured the amount of conformational or orientational disorder for each carbon unit in the alkyl chains as a function of

temperature. This previous work [32, 35, 36] did not address the conformation of the C*O*-C bond orientation relative to the central core, how the cores pack relative to the columnar axis and what changes occur as a function of temperature. By use of a film cast on a KBr plate and a sample mull in KBr, significant spectral differences were observed. These spectral differences are associated in part with the molecular orientation on external surfaces. Kardan *et al* [35] determined that, under certain experimental conditions, the liquid crystal compounds orientate significantly on external surfaces. By heating a thin film on the KBr plate into the isotropic region and holding this temperature for 15 minutes, then slowly cooling the sample over a period of 1-2 hours through the liquid crystal region to the crystal-liquid crystal transition and again holding the temperature for 1 hour before cooling to room temperature, samples with a relatively high degree of orientation could be obtained. The KBr mull produced nonoriented samples. Comparison of spectra from the oriented and nonoriented samples allowed orientational effects to be isolated, since conformational and interactional effects were common to both samples and only the orientational effects were different. An experimental measure of molecular orientation was obtained by comparing the integrated intensity of specific bands from the film cast on the KBr plate with those from the anisotropic mull sample. The C=O stretching vibration at 1780 cm^{-1} and CH stretching region $3000\text{-}2800\text{ cm}^{-1}$ were considered. It was determined that the alkyl chains were oriented almost parallel to the plane of the cores, indicating that the gauche conformation of the C-O-C*O*-C bond was more stable than the trans one. Disordering of the alkyl arms occurred at the solid-solid phase transition with the chain ends disorientating much more readily than the other carbon units nearer the core. Yang *et al* [48] demonstrated that the oriented film / KBr mull technique can be used to identify structural changes at the phase transitions.

A new type of discotic compound (Fig. 1.14.), a hydrocarbon without any heteroatoms, that displayed a nematic discotic phase, was synthesised by Ebert *et al* [49]. This 'star-like' compound was characterised using DSC, X-ray diffraction and Electro-optic (Kerr) relaxation studies.

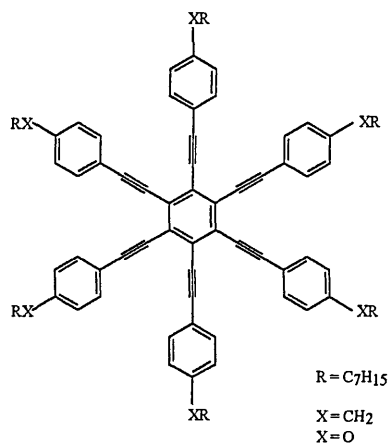


Figure 1.14. A hydrocarbon without any heteroatoms.

Praefcke *et al* [50] went on to synthesise more of the new star-like compounds where $R = C_5H_{11}$, $R = C_6H_{12}$ or $R = C_7H_{15}$. As well as synthesising compounds with longer alkyl arms, another new star-like discotic compound was synthesised where the benzene core of the previous compound [49] was replaced by a triphenylene core with $R = C_5H_{11}$ or $R = C_7H_{15}$ arms. Praefcke *et al* [51] continued the synthetic work and produced a biester based on the hexakis(4-alkylphenylethynyl) benzene sub unit synthesised earlier [49, 50]. This was the first reported example of a liquid crystalline dimer or discotic twin liquid crystal that exhibits a nematic phase, although other dimer or twin liquid crystals containing discotic units had previously been described [52, 53, 54].

1990

Chandrasekhar and Ranganath [55] produced a comprehensive review of the current advances in the discotic liquid crystal field in 1990 describing the two distinct categories of discotic liquid crystals, the columnar phase and the nematic phase. The columnar phase, in its simplest form has long range translational periodicity in two dimensions and liquid like disorder in the third. The second category of discotic compounds, the nematic, is an orientationally ordered arrangement of the molecular discs but does not possess any long range translational order. A number of typical low molecular weight discotic systems were shown, from the hexa-*n*-alkanoates of benzene, triphenylene and truxene, through to the more complex looking octasubstituted phthalocyanine which may

contain a metal atom at the centre of the core. Discotic polymers, both main-chain and side-group polymers, were reported. The extension of Mc Millan's model of smectic A to discotic liquid crystals and application of the continuum theory for columnar liquid crystals were considered. The discotic nematic phase was described in the fifth and final section of the paper, where the similarities and differences of the discotic nematic and the classical nematic of rod-shaped molecules were considered. The director \underline{n} which had previously been defined as the average of the molecular long axis for the rod-like molecules, in contrast represents the average of the preferred orientation of the short molecular axis or the disc normal. The schlieren textures produced when viewed under a polarising microscope are similar for both nematic cases, due to the symmetry of the two kinds of nematics being the same.

The discotic nematic is optically and diamagnetically negative, although the dielectric anisotropy $\Delta\varepsilon = \varepsilon_{\parallel} - \varepsilon_{\perp}$ may be positive or negative and is dependent on the detailed molecular structure of the compound being considered. The Frank constants for splay k_{11} and bend k_{33} were determined using the Freederickz method [34] with values of the same order of magnitude as for nematics of rod-like molecules.

The dielectric anisotropy of a disc-like molecule $[(C_{12}O)_8 Pc]_2Lu$ was measured by Belarbi [56]. An important temperature dependent positive dielectric anisotropy of the columnar mesophase oriented with a magnetic field was observed. The magnetic field was varied from 0 to 0.9T either parallel or perpendicular to the sample cell. It was also found that when slowly cooling the isotropic liquid under a strong magnetic field $> 1.5 T$ a preferred orientation of the columnar phase could be obtained. The molecular planes were aligned parallel to the direction of the magnetic field and therefore the directors are perpendicular to the magnetic field.

Carton *et al* [57], using a theoretical approach, considered the orientational ordering in discotic columnar phases. The different transitions from hexagonal to lower symmetry

phases which resulted from the molecules tilting within the columns were discussed. Several oriented structures were explained and other structures predicted.

Baehr *et al* [58] considered the dendritic-type texture of the hexagonal ordered phase of a hexa-substituted triphenylene derivative doped with trinitrofluorenone. The texture exhibited a six fold symmetry but consisted of a very irregular geometry with rugged boundaries that were self-similar over a certain range of scales. They suggested that the features were reminiscent of fractal geometries, and by use of fractal analysis it should be possible to simulate the growth process. The diffusion limited aggregation approach, a discrete version of a general dendritic growth mode, based on a hexagonal lattice was employed. A seed particle was initially placed at a lattice site, a second particle was added and made to perform random walks on the lattice. When it encountered an empty cell beside an occupied cell it become incorporated into the lattice. A noise reduction parameter was also incorporated into the model. The generated clusters displayed the dendritic like texture, six fold symmetry and irregular geometries of the hexagonal ordered columnar mesophase previously observed with a polarising microscope. It appears that the observed optical texture is conditioned by the hexagonal lattice of the columnar phase and also the growth process of the liquid crystal phase.

^2H NMR was employed by Kranig *et al* [59] to study the molecular motions and alignment processes of a triphenylene based discotic liquid crystal. A 7 T magnetic field was used to align the samples, allowing separation of the side group motions from the motions of the rigid core. A combination of magnetic and mechanical forces allowed the generation of mono domains, where the columns are aligned parallel to each other. ^2H NMR spectroscopy enabled the kinetics of this alignment process to be monitored. ^2H NMR spectroscopy, although it allowed the motions of the cores and side-groups to be separated, was not able to give more detailed conformational information about the side groups.

FTIR spectroscopy was employed by Lee *et al* [60] to study the mesophases of two truxene-based discotic liquid crystals. Pronounced changes in the CH₂ stretching mode frequencies were observed for both compounds at their melting points. Subtle changes in the benzene stretching modes and CH₂ deformation modes were observed at the D_{rd} - N transition for HBTX and at the D_{rd} - D_{hd} transition for HATX. For HATX it was observed that there was a sudden increase in the number of gauche bonds for the alkyl tails 20°C below the melting point. At the melting point the rate of increase of gauche bond density decreased, and only increased slowly through the liquid crystal mesophase. No changes at the N - D_{rd} transition were observed, but a small change in the CH bending frequency at the D_{rd} - D_{hd} transition suggests that this particular transition may primarily involve tail configurations rather than core configurations. Changes in the C=O stretching and CH bending suggest a small change in both the core and tail environments at 150°C. There was no sudden increase in the CH bending frequency intensity at the clearing point.

HBTX showed an increasing number of gauche bonds as the crystalline sample was slowly heated. The increase continues into the columnar phase at a slower rate. The D_{rd} - N transition appears to affect the truxene core only, as the number of gauche bonds of the tails does not significantly increase at this transition.

Rey-Lafon and Hemida [61] conducted vibrational studies on the phase transitions of three hexa-*n*-alkonates C₈HAT, C₁₀HAT and C₁₂HAT using both infrared and Raman spectroscopy. The disordering process was shown to begin in the crystalline state with deformations of the aliphatic carbon skeleton, with a change in the ester plane orientation with respect to the aromatic core appearing at the crystal-mesophase transition. In the crystal phase the chains appear to be mainly in an extended all-trans conformation. As the samples were heated the amount of disorder in the chains increased and existence of all types of conformational defects observed in molten *n*-paraffins such as GTG, GTG' (kink), GG (double gauche) and end gauche were evident in the spectra of these

compounds. In the isotropic phase the number of gauche bonds was slightly higher than in the liquid crystal phase. Rey-Lafon and Hemida considered that the dynamics of the aliphatic groups of the molecules was strongly related to the disordering process.

1.3.4. 1991 - 1995

1991

Lee *et al* [62] studied hexa(hexylthio) triphenylene using FTIR spectroscopy. Spectra over a range of temperatures were recorded, giving information concerning the molecular motions. At the crystal to H transition (the H phase displays long range incommensurate helical order), changes in the CH₃ stretching mode frequencies were observed. The CH₂ stretching mode frequencies showed less temperature variation, indicating that the alkyl chain ends become more easily disordered in the different phases. There was no sudden increase in the number of gauche bonds in the alkyl arms going from one phase to another, and changes in the core environment from the D_{hd} to I phase were very subtle. In the crystal phase, 10°C prior to melting there was an increased motion associated with the tails.

Lawler and Vanhecke [63] carried out dilatometric (density) studies of 2,3,6,7,10,11-hexa-*n*-octanoyloxy triphenylene HAT-C₈ as a function of temperature. It was found that the higher temperature isotropic phase was denser than the lower temperature columnar phase. It was suggested that this peculiar density behaviour may be correlated with the rectangular lattice packing of the columnar phase of HAT-C₈. It was not possible to generalise this suggestion to cover all discotic mesogens with rectangular columnar phases as only one sample was investigated.

Markovitsi and Lecuyer [64] studied the fluorescence properties of 2,3,6,7,10,11-hexa-*n*-hexyloxytriphenylene using steady state and time-resolved spectroscopy. Fluorescence was observed when an energy acceptor, perylene, was added to the liquid crystal in a columnar mesophase.

In 1992 Leisen *et al* [65] using two dimensional nuclear magnetic resonance, studied the molecular dynamics of the core and the alkyl tails of a triphenylene based discotic compound. One of the molecule's six ether side chains was replaced by an ester chain. It was found that the 5 pentoxy side chains were in the plane of the core, whereas the ester bonded chains stuck out of this plane and interfered strongly with the side chains of adjacent discs in the column. This process may stabilize the columnar structure preventing crystallisation, thus allowing the sample on cooling to enter the glass state.

Voigt-Martin *et al* [66] using electron diffraction and high-resolution electron microscopy were able to observe the structure and defects of a discotic liquid crystal in both the crystal and the liquid crystal phase. The most common defects in the crystal samples were grain boundaries, while for the liquid crystals the short range order was disrupted by slight deviations of the molecules from the perfect lattice positions; the quasi long range order was still retained. By use of CERIUS 3.1, a molecular modelling computer package, the crystal structure could be simulated and a diffraction simulation carried out which was compared to the electron diffraction pattern. By modifying the crystal structure it was possible to simulate diffraction patterns identical to those obtained experimentally and the unit cell parameters could be obtained through this simulation method.

Ono and Kondo [67] considered hexakis(pentyloxy) triphenylene (THE 5) using a molecular dynamics atom-atom potential in a canonical (NVT) ensemble. Molecular flexibility in the side chains was investigated and the effects that it had on the profile of the order parameter for the C-H bonds was reported.

Beattie *et al* [68] synthesised a new series of derivatives of hexa-*n*-alkylcyclohexanoates of triphenylene (Fig. 1.15.) which were analogous to the hexa-4-*n*-alkylbenzoates of triphenylene reported by Tinh *et al* [18].

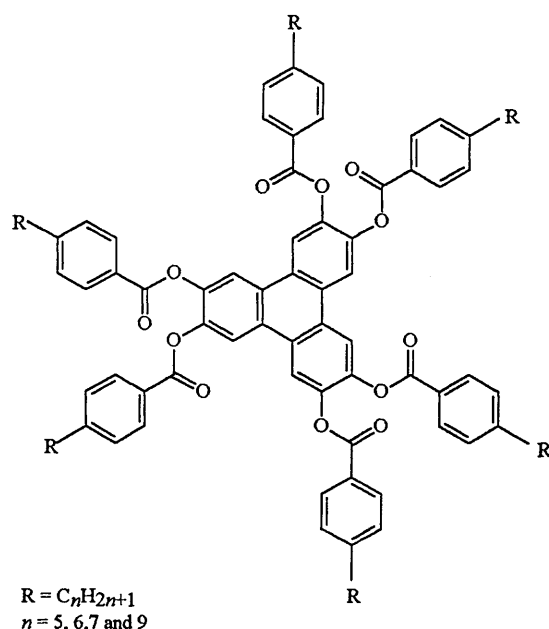


Figure 1.15. hexa-*n*-alkylcyclohexanoates of triphenylene

DSC and thermal optical microscopy were employed to characterise the phase behaviour of these compounds, and columnar mesophases were evident. X-ray powder diffraction showed that the mesophases had hexagonal symmetry, but no long range periodic order. It was found that for the *n*-alkylcyclohexyl series the melting points were lower and the clearing points were approximately 100°C higher than the analogous *n*-alkyl esters and 50-60°C higher than the *n*-alkylbenzoates. It appeared that the cyclohexyl moiety stabilized the columnar phase at the expense of nematic mesophases, and it also increased the mesophase temperature range, in turn stabilizing the liquid-crystalline properties as a whole. The use of cyclohexyl moieties in discotic liquid crystal systems provided a way of preparing materials which exhibited columnar mesophases over a much wider temperature range when compared with the analogous *n*-alkyl benzoates or *n*-alkyl esters.

In 1993 Hindmarsh *et al* [69] investigated the effects of lateral substitution to the phenyl groups of triphenylene-2,3,6,7,10,11-hexayl hexakis(4-alkoxybenzoates) via dimethyl substitution (Fig. 1.16.). Two methyl groups were substituted to the ester benzoate linkage group at the 3,5 or 2,6 positions

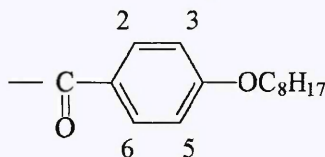


Figure 1.16. Methyl substitution positions.

The 3,5 substituted compounds exhibited both a hexagonal disordered columnar phase and a discotic nematic phase, whereas the analogous 2,6 substituted compounds with the methyl groups pointing towards the core only displayed the nematic mesophase. The methyl substitution in the benzoate rings reduced the transition temperatures of the compounds compared with unsubstituted compounds, the methyl substitutions pointing towards the core having the greatest effect at reducing melting points and the nematic phase stability.

Idziak *et al* [70] through X-ray diffraction and DSC established the phase diagram of a series of hexa-*n*-alkylthiotriphenylenes using mixtures of $C_n + C_{n-1}$ where $n = 5,6,7$. The effective tail length was calculated as the weighted average of the tail lengths from the parent compounds. A range of effective tail lengths from 4 carbon units through to 7 carbon units were investigated. Nine crystal phases were observed, but only three were successfully identified.

The hexa substituted triphenylene nucleus forms the basis of one of the most widely synthesised ranges of discotic mesogens. The synthesis involves the preparation of hexahydroxytriphenylene. The traditional synthesis route, a three step procedure, produces low yields, is difficult to perform on a large scale and purification requires repeated chromatography and repeated recrystallisation.

Boden *et al* [71] suggested a modification to the traditional synthesis route, using iron (III) chloride instead of chloranil, which enabled hexa-alkoxytriphenylenes to be produced in a single step, with a high yield and in a process that can be easily carried out on a larger scale. Previously it was difficult to prepare more than 10g of the pure mesogen in a single batch. This newer route may also provide a better method for synthesising unsymmetrical substituted triphenylenes.

Boden *et al* [72] following from previous work [40] which showed that a discotic liquid crystal, normally an insulator, became a p-type semi-conductor when doped with 1 mol % of the Lewis acid AlCl_3 , reported on the elucidation of the mechanism of quasi-one-dimensional electronic conduction in discotic liquid crystals. For HAT-6 doped with AlCl_3 , in the crystal, liquid crystal and isotropic phases the conductivity at low frequencies was found to be independent of the frequency. At higher frequencies there was a power law dependence, which is characteristic of charge carrier transport by a hopping mechanism. The conductivity measured along the column axis was approximately 10^3 greater than perpendicular to the columns. One-dimensional molecular electronic conductors have the prospect for use as *molecular wires* in molecular device applications.

Transient photo conductivity was observed in a discotic liquid crystal, hexapentyloxytriphenylene, by Adam *et al* [73]. Carrier mobilities of $1 \times 10^{-3} \text{ cm}^2 \text{V}^{-1} \text{s}^{-1}$ were measured, greatly exceeding the mobilities of commonly used organic photo conductors. Further measurements on similar compounds by Adam *et al* [74] suggested that the spontaneous orientation and dynamical fluctuations within the mesophase accounted for mobilities 3 orders of magnitude higher than those observed for conventional amorphous polymers.

Bengs *et al* [75], investigating the photo conductivity in a homologous series of hexa-alkoxytriphenylenes, were only able to detect the photo current in the liquid crystalline

phase of the materials. Higher photo currents were observed during the cooling cycle, arising from the better orientation that the liquid crystal mesophase experiences on cooling. This better orientation reduced the number of defects which act as traps for the charge carriers and also increased the number of columns within the mesophase which carry the charges. As the chain length of the alkyl arms was increased there was a dramatic, nearly exponential decrease in the observed photo current. It appeared that only the triphenylene core was responsible for the photo conducting properties. An increase in photo current was observed with increasing temperature. It was determined that the intensity of the photo current arose from the area covered by the triphenylene core.

Bengs *et al* [76] generated highly oriented discotic elastomers to overcome some of the problems associated with trying to produce single crystals of a discotic compound in order to minimise the defects that reduced charge transport. By utilising mechanical field effects of weakly cross linked polymers, the polymer discotics may achieve a perfect director alignment without enhancing the viscosity too much. Initially the discotic polymer is cross linked and a mechanical field is applied before a second cross linking procedure is carried out. This method of two cross linkings produced highly oriented discotic elastomers, verified by X-ray diffraction.

Atomic force microscopy was applied by Tsukruk *et al* [77] to an ordered monolayer film of a discotic liquid crystalline donor-acceptor twin compound adsorbed at the surface of a silicon wafer. It was shown that columns were formed parallel to the silicon surface, and that the molecules were arranged in an edge-on fashion.

Osipov and Hess [78] produced explicit expressions for the Frank elastic coefficients using a model of perfect local orientational order. The model was valid for nematics composed of rod-like molecules as well as disc-like molecules with the ratios of k_{33}/k_{11} agreeing quite closely with experimental data.

Phillips *et al* [79] measured the dielectric and elastic properties of two compounds synthesised by Beattie *et al* [68]. Homeotropic alignment with the directors perpendicular to the plane of the cell was achieved using either a thin layer of polyimide (PI) or poly-vinyl alcohol (PVA). The Freederickz transition method was used. The capacitance of the empty and full cells was measured as a function of temperature and ϵ_r was calculated by dividing the capacitance of the full cell by the capacitance of the empty cell. A magnetic field parallel to the cell was used to distort the director, enabling ϵ_{\perp} to be extrapolated from the graph of $1/\epsilon_r$ vs $1/B$, where B = magnetic flux density. The elastic constants were found to have similar magnitudes to the calamitics, k_{11} being greater than k_{33} , which contrasted with results obtained from the calamitic range of compounds.

Kruk *et al* [80] studied a hexapentyloxytriphenylene discotic liquid crystal using FTIR spectroscopy. Spectra were recorded over a range of temperatures. By comparison of spectra from the discotic phase with those from the isotropic phase, the order parameter S was determined. The liquid crystal sample was sandwiched between silicon windows, whereas KBr plates are more commonly used for infra-red work. It appears that Kruk *et al* [80] used silicon windows in order to improve the sample alignment in the liquid crystalline phase. It was determined that the molecules were ordered edge-on on the silicon substrate, this deduction arising from the fact that absorption from vibrations parallel to the core were higher in the discotic mesophase than in the isotropic liquid.

The dichroic ratio (R_i) could be calculated from $R_i = I_D/I_I$, I_D is the integrated absorbance for a peak in the discotic phase and I_I is the integrated intensity for the same peak in the isotropic phase. Using the calculations of Neff *et al* [81] for unpolarised radiation, the order parameter may be calculated by $S = 2(R_i - 1)$ for a director parallel to the direction of the infra-red beam e.g. the C-C in plane vibrations of the benzene ring and the C-O-C stretching vibrations. Using $S = 1 - R_i$ the order parameter may be

calculated when the director is perpendicular to the infra-red beam, e.g. the CH out of plane vibrations of the benzene ring.

Using this method the order parameters for the CH aromatic out of plane vibration at 837 cm^{-1} , the C-C aromatic stretching vibration at 1617 cm^{-1} , the C-O-C stretching asymmetric vibration at 1174 cm^{-1} and the C-O-C stretching symmetric vibration at $1000\text{-}1100\text{ cm}^{-1}$ were calculated. All were seen to reduce gradually from the crystal phase through to the liquid crystal phase. No sudden jumps in the order parameters were observed at the crystal-liquid crystal transition. A very large value of S, (approximately 0.85) was determined for the cores in the crystal region from the C-C aromatic stretching vibration. It was concluded that the cores were almost perfectly aligned. Within the nematic discotic phase the order parameter fell gradually to 0.5 with increasing temperature, before falling very sharply to almost 0 at the nematic-isotropic transition. The C-H out of plane vibration was also highly oriented in the crystal phase, with an order parameter of approximately 0.8 falling very slowly to 0.7 in the liquid crystal region before falling rapidly to 0 at the liquid crystal-isotropic transition.

The C-O-C stretching asymmetric vibration at 1174 cm^{-1} and the C-O-C stretching symmetric vibration at $1000\text{-}1100\text{ cm}^{-1}$ had lower order parameters in the crystal phase, 0.4 and 0.6 respectively. Again there was a gradual decrease of about 0.2 in the order parameter as the temperature was increased through the liquid crystal region until the liquid crystal-isotropic transition, where again the order parameter fell rapidly to approximately 0.

Frequency changes were observed for all the bands in the discotic liquid crystal at approximately 3°C below the crystal-liquid crystal transition. Shifts of up to 6 wavenumbers were observed for CH_3 asymmetric stretching vibrations although shifts of the order of 2 wavenumbers were more common for the CH_2 , C-C, C-H and C-O-C

vibrations. The frequency changes were interpreted as changes in the short range order within the sample.

Calculations of the order parameter helped to assign various other vibrations as the molecular structure and molecular alignment were known. This was possible as the core vibrations are more indicative of the order parameter than vibrations from other parts of the molecule. One of the C-O-C stretching symmetric vibrations at 1054 cm^{-1} was found to be highly sensitive to the phase transitions.

Chandrasekhar [82] produced a brief review of discotic liquid crystals, but unlike his previous reviews [23, 55] which emphasised the theoretical developments, this review gave more emphasis to experimental results and reported on the recent progress in the field. There existed to date over 1000 discotic compounds that generally speaking have flat or almost flat cores with six or eight long chain substituents, often with ester or ether benzoate linkage groups.

Examples of discotic mesogens were given, including the complex star-like heptameric triphenylene derivative presented by Diele *et al* [83] in 1992. The compound was based on the triphenylene core, each of the six arms also containing a triphenylene moiety with a further 5 alkyl arms. This gives a massive structure composed of 7 triphenylene units arranged in a hexagonal fashion, 7 ester linkages and 30 alkyl arms in total. As well as various examples of discotic liquid crystalline materials, Chandrasekhar [82] also gave schematic representations of the molecular ordering within the nematic and a number of columnar mesophases. Discotic metalomesogens, discotic liquid crystals containing a metal atom in the centre of the core, were also discussed, with electrical conductivity measurements indicating that these compounds were molecular semiconductors with the conduction direction along the columnar axis.

Discotic polymers of various different types and their mesophases were also discussed. In a discotic polymer, the basic monomer unit is a disc-shaped mesogenic moiety which may either be attached directly to the polymer backbone or as a side group.

Chandrasekhar [82] also noted that the term discotic, first adopted by Billard *et al* [9] to distinguish between disc-shaped and rod-shaped mesogens, has been loosely applied to describe not only the molecules but also the mesophases that they form. Chandrasekhar pointed out that it is the molecule itself that is discotic, not the mesophase which may be columnar or nematic. A number of molecules which are not discotic have been known to form columnar mesophases. Chandrasekhar [82] suggested that it would be useful to redefine the terminology more precisely to prevent ambiguities, now that the realm of discotic liquid crystals was expanding rapidly.

1994

1994 Boden *et al* [84] continued their earlier work [40, 72] concerned with electron transport along the molecular stacks of discotic crystals which exhibited quasi-one-dimensional p-type semiconductor behaviour when doped with 1 mol % of Lewis acid, AlCl_3 . The conductivity measured along the column axis was approximately 10^3 times greater than conductivity in the perpendicular direction. The frequency dependence of the conductivity measured along the columns may be explained in terms of a single charge carrying process, where the charge carriers hop between localised sites associated with radical cations of the Lewis acid. Highly directional charge transport was possible and takes place over relatively large distances of the order of 100 nm.

Boden *et al* [85] expanding on their new route to synthesising hexa-alkoxytriphenylenes, using the iron (III) chloride mediated oxidative coupling reaction [71] developed in 1993, were able to obtain unsymmetrically substituted hexaalkoxytriphenylenes. The high yields and high purities associated with this reaction method have opened a practicable

route for synthesis of reasonably large amounts of polymeric discotic crystals. It was also suggested that it would be possible to extend the synthesis to the case where up to five of the substituents to the triphenylene core could be different, offering great scope and ease with which to synthesise a wide range of different unsymmetrical compounds.

Goodby *et al* [86] developed a novel clean and efficient route for synthesising unsymmetrical triphenylenes using efficient palladium-catalysed cross-coupling reactions. This new method was far superior to that proposed by Boden *et al* [71, 85] using iron (III) chloride which required activating alkoxy substituents, whereas the palladium-catalysed cross-coupling reactions did not. They were interested in preparing unsymmetrical discotic mesogens in order that the boundaries between the traditional calamitic mesophases and the more recent discotic mesophases could be investigated. The unsymmetrical substituted discotic materials are no longer disc-shaped and depending on substitution may appear ellipsoidal or even rod-like. In the region between discs and rods it was expected that the materials would exhibit optical biaxiality. Biaxiality in a liquid crystal sample offers the possibility of extremely fast-switching, as a slight movement of the molecule leads to a large change in the optical response. Goodby *et al* [86] synthesised a number of 2,3,6,7,10,11-hexa-triphenylenes. Although their method would allow for up to five different substituents to the triphenylene core, they chose to use only three different substituents for each compound. The three substituents were placed in pairs at the 2,3 ; 6,7 and 10,11 positions on the triphenylene core respectively. The substituent range included CH₃, C₃H₇, C₆H₁₃, C₈H₁₇ and C₁₂H₂₅ and a number of compounds with differing combinations of the substituents were synthesised. Transition temperatures from a number of the compounds synthesised were reported.

Phillips and Jones [87] working with mixtures of discotic liquid crystals, in order to obtain a more accessible nematic temperature range, measured the refractive indices and found a rather small negative birefringence. The order parameter *S* was also determined. The use of mixtures by Phillips and Jones produced a significant reduction of transition

temperatures. The two compounds mixed by Phillips and Jones were HET 7, triphenylene hexa-*n*-heptanoate originally synthesised by Destrade *et al* [10, 11, 12] in 1979, and DB 126, triphenylene hexa-(2-methyl-4-*n*-decyloxy) benzoate synthesised by Beattie *et al* [68, 88]. The greatest reduction in transition temperature, 80°C compared with the pure DB 126, occurred when 30 wt % of DB 126 was added to HET 7, shown in the phase diagrams produced by Phillips. The clearing point fell from 164°C for the pure DB 126 to $\approx 78^\circ\text{C}$ for the 30 wt % mixture.

Voigt-Martin *et al* [89] used electron diffraction to carefully monitor the transition from crystal to liquid crystal for a discotic liquid crystal. A new high resolution electron microscope technique which allowed direct imaging of molecular positions and defects was also described, enabling quantitative analysis between the defects of the crystal and liquid crystal to be carried out. MOPAC 6.0, a public domain computer program was used to estimate conformational features of the molecules as a prerequisite to the structural modelling from which the diffraction patterns could be simulated and compared with the electron diffraction pattern, indicating if the molecular conformations were correct. The MOPAC 6.0 program which used semi-empirical quantum mechanical methods for energy minimisation was able to produce a minimised structure for the molecule, which was then transferred to CERIUS 3.1, another molecular modelling package that incorporated a number of crystallographic features, which allowed a unit cell of the minimised molecule to be constructed from which the diffraction pattern could be calculated. The model structure could be adjusted and the changing diffraction pattern was observed in real time and compared with the electron diffraction patterns. Good agreement between the calculated diffraction patterns and experimental patterns was obtained and all the lattice parameters could be obtained from the CERIUS 3.1 program. Voigt-Martin *et al* had previously used CERIUS 3.1 to minimise molecular structures of similar discotic liquid crystals before calculating the diffraction pattern [66]. MOPAC 6.0 was used in this later work to optimise the minimum energy conformation for these molecules because of its semi-empirical energy minimising approach which is a

much faster method of minimising larger molecules. The 'medium-high' resolution electron imaging technique showed that the grain boundaries present in the crystal phase were eliminated in the liquid crystal phase, indicating that the ability to act as photoconductors may be related to loss of grain boundaries.

1995

In 1995 Groothues *et al* [90] used broadband dielectric spectroscopy to study the molecular dynamics of various triphenylene and benzene based discotic liquid crystals. They detected two relaxation processes in the columnar mesophase - one process was assigned as a vibrational motion of the ester linkage of the alkyl arms, while the other process was assigned as a hindered rotation of the molecular disc within the columnar axis.

Boden *et al* [91] developed a simple universal rational synthesis for main chain triphenylene-based discotic-liquid-crystalline polymers based on his earlier synthesis work which used the Iron (III) Chloride reaction to produce unsymmetrical substituted triphenylene [71, 85]. This route allows single-isomer, main-chain, polymeric discotic liquid crystal to be prepared on a large scale with defined structures, opening up this field for experimental analysis and characterisation of the material properties of these new compounds.

Henderson *et al* [92] and Plesnivy *et al* [93] reported on a similar synthetic route for unsymmetrical substituted triphenylene and dibenzopyrene derivatives similar to that proposed by Boden *et al* [85]. The intention of this work was to tailor the processability and mesophase behaviour of these materials, specifically the functionalised cores, in order that the charge transport phenomena of the new fast photoconducting materials may be studied at room temperature [73, 74].

1.3.5. 1996 - 1998

1996

Phillips *et al* [94] observed flow-induced order in the isotropic phase of a mixture of methylated triphenylene hexa-alkoxybenzoate DB126 and a doubly-methylated compound PH8. When mixed together there was an observed depression of the transition temperatures with the 75% wt of PH8 mixture, this mixture exhibited the unusual phenomenon of flow induced order. When the mixture was heated a few degrees into the isotropic phase between two glass plates and sheared, a brief flash of light was observed when the sample was viewed between crossed polarisers. This feature was visible up to 10°C above the transition although the duration and magnitude of the effect were reduced further away from the nematic - isotropic transition temperature.

Similar effects have been observed for homeotropically aligned calamitic materials in the nematic phase. Before shearing the sample appears black as it is viewed along the optic axis, during shearing the director is tilted and a bright flash of light appears when viewed by a polarising microscope, after shearing the tilt decays and the sample returns to the homeotropic alignment.

For the discotic mixture the effect is significantly different, transient conoscopy observations suggest that the shear is inducing order, as well as tilting over the director that is created. With calamitic materials the effect is extremely small and needs careful experimentation to detect, while with the discotic materials the effect is clearly visible by the naked eye.

General observation for ordered discotic columnar phases indicates that the one-dimensional order along the columnar axis and the two-dimensional order of the columns

packing together are not correlated [8, 26]. Calamitic mesogens form several smectic mesophases with 3 dimensional positional order [5] but smectic phases are rarely displayed by discotic materials.

Glüsen *et al* [95] observed a novel columnar discotic phase which helps to fill the gap between the ordered columnar phase and the crystalline state. This phase has features in common with the plastic crystalline state and they referred to it as plastic columnar discotic phase. Highly ordered columnar phases are of interest due to their high charge carrier mobility in photoconductivity experiments and the direct transition from the discotic hexagonal ordered phase to the discotic plastic phase with only minor changes in structure, dynamics of the mesophase may prove useful in understanding the nature of photoconductivity. The experiments were carried out on asymmetrically substituted triphenylene 3,6,10,11-pentapentyloxytriphenylenes-2-ylpivaloate(pivaloate). The structure was characterised by a three-dimensional crystal like registry of ordered columns in a hexagonal lattice, the discotic molecules within the columns being able to rotate. It was noted that the intracolumnar repeat distance was twice that found for normal columnar phases, indicating an intracolumnar correlation of pairs of molecules. Photoconductivity measurements showed that the charge-carrier mobility in the plastic columnar discotic phase (D_{hp}) is significantly higher than in the discotic hexagonal ordered phase (D_{ho}).

Calucci *et al* [96] showed that trifluoroacetic acid (TFA) can form 1:1 molar complexes with alkoxy discotic compounds, enhancing mesomorphic properties by inducing a broader thermal stability range and a higher degree of order. The stabilisation of columnar mesophases by these dopants is believed to be due to the formation of intercalated charge transfer complexes similar to the effect of Lewis acid dopants, which although they don't stabilise the mesophases do interact with the molecules forming charge carriers which significantly increase the electrical conductivity. The addition of the trifluoroacetic acid stabilised and even introduced new columnar mesophases for hexa-alkoxytriphenylenes and hexa-alkyl-oxytribenzocyclononenes with a higher degree of ordering than the pure compounds as observed by X-ray diffraction.

Sikharulidze *et al* [97] observed the first optically controlled electro-optic effect in nematic discotic liquid crystals with the so called radical multiynes, Pentakis [(4-pentylphenyl)ethynyl]phenyl-10-carbethoxydecyl ether. This compound was able to be supercooled and the phase is completely stable in a closed cell at ambient temperature for extremely long periods of time. Cells filled more than a year ago still work without losing their characteristics in spite of the frequent application of electric fields and light. The cell consisted of conventional sandwich cells made of glass, coated with a transparent tin oxide conducting layer and an orientations layer. The sample was heated into the isotropic phase and then slowly cooled to room temperature, the sample investigated was able to be super cooled more than 30 K below its melting point. After application of an electric field to the filled cell, a reorientation of the molecules began. At an applied voltage of 6 V a domain structure appeared, illumination of the sample using the conventional white light source of the microscope lead to a local change of colour which was reversible after switching of the light. The process was able to be repeated countless times with no apparent change to the cell.

Wang *et al* [98] used a combination of electron diffraction and molecular simulation studies to investigate 2,3,6,7,10,11-hexakis(pentyloxy)triphenylene. X-ray single crystal analysis is inappropriate for most organic crystalline materials, but Voigt-Martin *et al* [89] have successfully developed electron crystallography using maximum entropy and simulation methods. The first step involves determination of the cell dimensions and lowest space group from the electron diffraction patterns, the second step involves molecular modelling and simulation using the cell parameters.

Three different electron diffraction patterns are required to determine lattice and cell parameters, tilting tiny crystallites is applicable in most cases for electron diffraction and avoids the sophisticated techniques demanded in preparation of samples with different basic faces. Computer modelling was carried out, a semi-empirical quantum mechanical method, MOPAC, could be used but this would only give first estimates of conformational features as the molecular conformation is affected by the crystal field. A force field approach using the Dreiding II force field approach was used to obtain the initial molecular conformation. The initial molecular conformation was obtained by energy minimisation of the molecule with the side chains in the all trans conformation. This energy minimised molecule was then placed in an experimental unit cell and the molecular packing energy was calculated and minimised. The molecule was first considered with all trans chains to speed up the calculations, then proper minimisations were carried out, where the side arms were no longer required to be in the all trans conformation, to give the final crystal conformation. The sample was found to adopt an orthorhombic P_{2212} space group with cell parameters : $a=36.73\text{\AA}$ $b=27.99\text{\AA}$ and $c=4.91\text{\AA}$.

Forget *et al* [99] reported that exposing a uniformly homotropically aligned discotic columnar liquid crystal to an argon ion laser beam, resulted in a reorientation changing the optical properties of a polymer dispersed metallomesogenic compound, they were able to successfully generate an image of 256x256 pixels using a 130mW laser beam.

1.4. Discotic compounds - Hull University.

The liquid crystal materials on which this research programme is based are derivatives of hexa-*n*-alkoxy benzoates of triphenylene (Fig. 1.17.) and unsymmetrical substituted hexa-*n*-alkoxy triphenylenes (Fig. 1.18.).

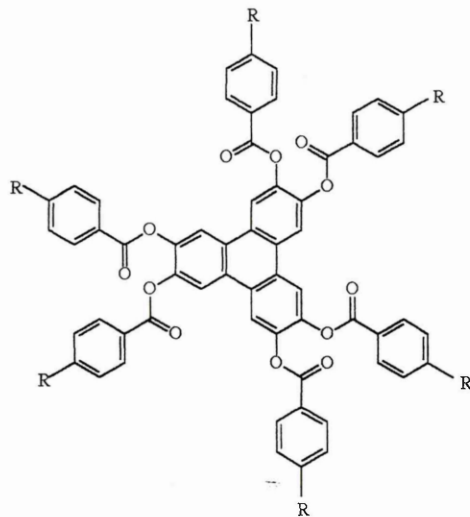


Figure 1.17. Hexa-*n*-alkoxy benzoates of triphenylene.

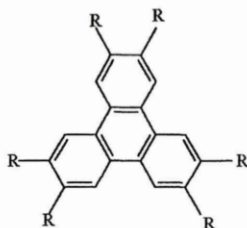


Figure 1.18. Hexa-*n*-alkoxy derivatives of triphenylene.

The first set of compounds are from the DB series, synthesised by Beattie *et al* [68, 88] at Hull University. The temperature data in brackets were obtained by DSC, the other data were obtained through optical microscopy.

The first compound DB26 consisted of a hexa-n-alkoxy core (Fig. 1.18.) with OC_8H_{17} alkoxy chains attached to the benzene linkage group (Fig. 1.19.).

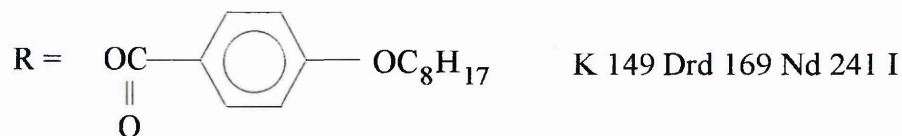


Figure 1.19. DB26.

The second compound DB118 had the same alkoxy chain, but in addition it had a methyl group attached to the benzene link furthest from the core (Fig. 1.20.).

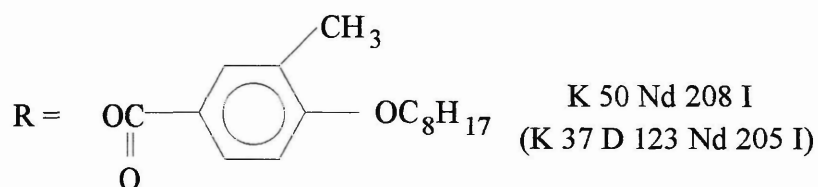


Figure 1.20. DB118.

The third compound DB125 also had the OC_8H_{17} alkoxy chain and a methyl group on the benzene link with the methyl group pointing towards the core (Fig. 1.21.).

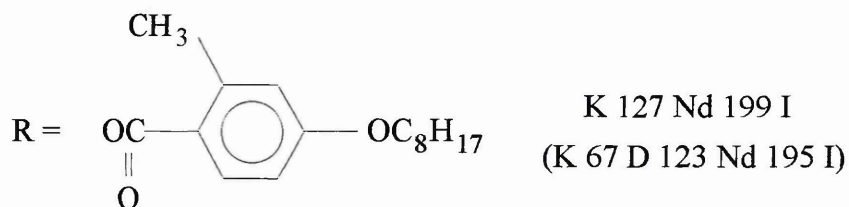


Figure 1.21. DB125.

The second set of compounds, part of the PH series were also synthesised at Hull University, by Hindmarsh *et al* [69]. These were similar in appearance to the DB compounds, but had 2 methyl substituents to the benzene linkage group as opposed to one in the DB series. It was hoped, by the Hull group, that the addition of the methyl groups would disrupt columnar packing and lower the nematic to isotropic transition temperatures.

PH64 had the OC_8H_{17} alkoxy arm with two methyl groups furthest from the core (Fig. 1.22.).

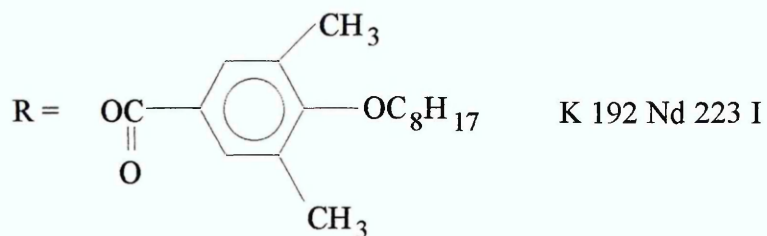


Figure 1.22. PH64.

PH74 also had two methyl groups pointing away from the core, it also had a methyl group attached to the first carbon on the alkoxy arm and an alkoxy arm that was one carbon unit shorter than the other DB and PH compounds (Fig. 1.23.).

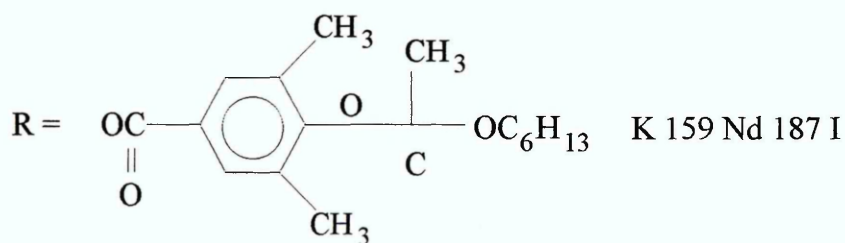


Figure 1.23. PH74.

PH76 had the same OC_8H_{17} alkoxy chain and two methyl groups attached to the benzene link group, both the methyl groups were pointing towards the core of the molecule (Fig. 1.24.).

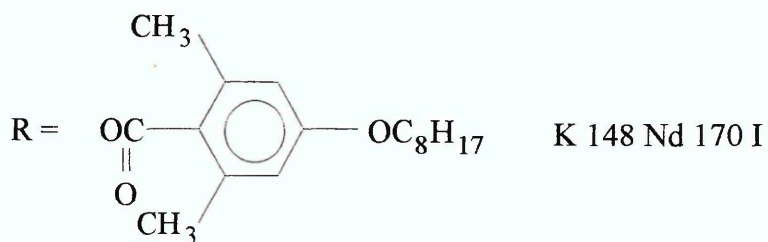


Figure 1.24. PH76.

PH12IME is similar to PH76 except the arms are 12 carbon units long (Fig. 1.25.).

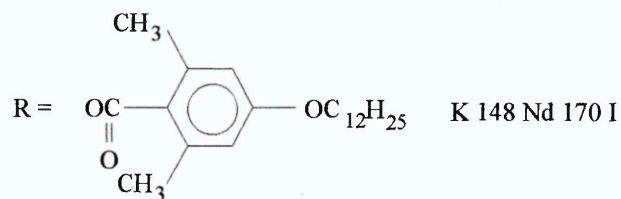


Figure 1.25. PH12IME.

PH12OME again had six arms 12 carbon units long, but the two methyl groups are pointing away from the core (Fig. 1.26.).

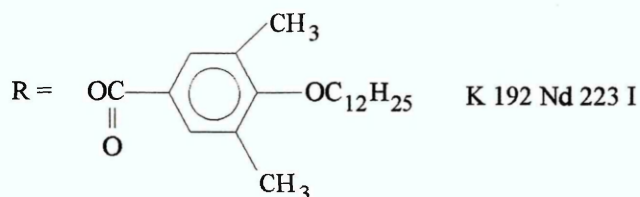


Figure 1.26. PH12OME.

The third set of compounds synthesised by Watson *et al* [86] were based on hexa-*n*-alkoxy derivatives of triphenylene, which had first been synthesised by Destrade *et al* [15] in 1981. The compounds synthesised by Watson *et al* were unsymmetrical in shape, and were based on the basic core molecule (Fig. 1.27.). Due to the simpler molecular structure, the transition temperatures were much lower than those of the hexa-*n*-alkoxy benzoates of triphenylene of the DB and PH series of compounds.

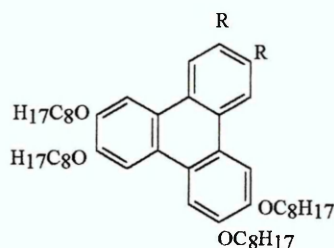


Figure 1.27. Basic core molecule for unsymmetrical substituted compounds.

The substituted arms varied from OC_6H_{13} to $\text{OC}_{12}\text{H}_{25}$.

TW73 was composed of four OC_8H_{17} arms and two OC_6H_{13} arms. TW75 had two $\text{OC}_{10}\text{H}_{21}$ arms and TW77 had two $\text{OC}_{12}\text{H}_{25}$ arms.

Chapter 2. Optical Microscopy.

2.1. Optical Microscopy.

2.1.1. Optical Microscopy and Liquid Crystals.

Early work by Rudolf Virchow who employed optical microscopy between 1850 and 1888 to investigate some biological samples, particularly the outer coatings of nerve fibres which were observed to form soft and flowing forms in water, is discussed in several liquid crystal texts [1,2]. Unusual effects were seen when the samples were viewed between crossed polarisers: light was transmitted, indicating that the samples possessed more than one refractive index and were thus birefringent. These were interesting results as previously only solids had been observed to be birefringent. No liquid had ever shown such peculiar optical properties before. Otto Lehmann, investigating how substances crystallise, built a microscope heating stage allowing control of the cooling process of crystallisation. He is credited as being one of the first physical scientists to utilise polarising optical microscopy, although biologists and physicians had been using this technique for a number of years previously to investigate biological systems. The combination of heating stage, microscope and polarisers was a significant technical advancement, allowing scientists to control the temperature environment of their samples. A polarising microscope equipped with a hot stage has become a standard piece of equipment in liquid crystal laboratories to characterise the phases and determine the phase transition temperatures.

2.1.2. Experimental Set-Up and Sample Preparation.

The liquid crystal samples were investigated orthoscopically using an Olympus BH2 polarising microscope [3] with either an auxiliary 35mm camera or a CCD (charge coupled device) JVC TK-1085E colour video camera with a JVC video recorder and Panasonic colour monitor. The microscope had 20x and 40x objectives allowing total magnifications of 200x and 400x respectively to be achieved. Both the objectives were long working distance lenses approximately 7mm working distance. The necessity for long working distance lenses arose due to the use of a Linkam THMS 600 / HSF 91 hot stage [4]. The hot stage was controlled using a Linkam TMS 92 programmable temperature controller [5] and Linkam LNP 2 cooling pump. Use of liquid nitrogen as a coolant allowed a temperature range from -180°C to $600^{\circ}\text{C} \pm 0.1^{\circ}\text{C}$ to be investigated.

2.1.3. Hot Stage Calibration and Temperature Gradient.

Benzoic acid, with a known melting point of 122°C was used in the calibration of the hot stage. It was observed the factory default settings did not need to be altered though there was a 1°C temperature gradient from the centre of the field of view to the edge with the centre being at a slightly lower temperature. On cooling from the melt the benzoic acid first solidifies in the centre of the field of view and spreads outwards. This behaviour was expected, due to the design of the hot stage: in order to allow light to be transmitted through the silver heating block there is a small hole with a sapphire window in the centre of the block. When the silver block is maintained at a temperature by the heater, the sapphire window is heated by conduction from the silver block. A temperature gradient will thus exist across the sapphire window with the centre of the window being at a fractionally lower temperature. Due to the small dimensions of the heater this temperature gradient amounts to only 1°C temperature difference from the centre of the window to the edge at a $1^{\circ}\text{C}/\text{min}$ cooling rate.

2.1.4. Sample Preparation.

A small quantity of sample was placed on a glass cover slip on top of the heating stage. The sample was heated until it melted. Then a second cover slip was placed on top, in effect sandwiching the sample between two glass plates. The sample could now be viewed over a range of temperatures between crossed polaroids. The camera attachment to the microscope enabled photographs or videos of all the textures viewed to be recorded. The use of a Linkam VTO 232 [6, 7] video text overlay allowed the temperature, heating and cooling rates, date and time and additional text to be superimposed on the video image. Use of a computer equipped with Vidi PC image capture hardware and software also allowed the video signal and superimposed text to be stored digitally. All the samples were heated to the isotropic region, identified by the sample appearing uniformly dark between the crossed polaroids. The samples were initially cooled at a number of rates, 20°C/min, 10°C/min, 5°C/min and 1°C/min and heated at the same rates to identify the phase transitions. The 20°C/min rate allowed a fast first approximation of the transition temperature to be obtained, subsequent lower cooling rates allowing a more accurate measurement of the transition temperatures to be obtained.

2.2. Transition Temperatures Obtained by Optical Microscopy.

2.2.1. Symmetrical Substituted Compounds.

Eleven samples synthesised at University of Hull by Goodby and co-workers [8, 9, 10, 11] were investigated orthoscopically and the transition temperatures recorded during both heating and cooling cycles at a rate of 1°C/min are presented, (Table 2.1). Examples of the optical textures obtained are shown in Appendix A. Values in brackets are DSC results supplied by workers at Hull.

| Sample | Transition temperatures /°C Heating (1°C/min) | | | | Transition temperatures /°C Cooling (1°C/min) | | | |
|---------|--|-------|----------------|----------------|--|-----|-----|-----|
| | C-C | G-N | C-N | N-I | I-N | N-C | N-G | C-C |
| DB26 | (149) | | 171 (169) | 241 (241) | 241 | 169 | | |
| DB118 | (37) | (123) | 150 | 210 (208) | 210 | 150 | | |
| DB125 | (67) | | 126.5 (127) | 199.5 (199) | 199.5 | 108 | | |
| PH64 | (170) | | 197.5 (195) | 217 (215) | 217 | 195 | | |
| PH74 | | | 160 (159) | 186 (187) | 186 | 154 | | |
| PH76 | | 74 | | 171 | 171 | | 74 | |
| PH12IME | | | 172 (170) | 234.7 (231) | 244 | 170 | | 103 |
| PH12OME | | | 143 (143) | 153 (151) | 150 | 137 | | |

Table 2.1 : Transition temperatures obtained through Optical Microscopy and DSC (shown in brackets).

The compounds DB118, DB125, PH64, PH74, PH76, PH12iMe and PH12oMe have methyl additions which interact with the molecular layers above and below preventing the formation of a columnar mesophase. Only the nematic mesophase with its characteristic schlieren texture is observed for these compounds.

2.2.2. Unsymmetrical Substituted Compounds.

The unsymmetrically substituted compounds, based on the triphenylene esters had much lower transition temperatures than the ester benzoates of triphenylene. The unsymmetrically substituted compounds, TW73, TW75 and TW77, all produced a columnar mesophase.

The transition temperatures of these compounds (Table 2.2) were determined using the method described earlier (2.1.4. pg. 52), a heating and cooling rate of 1°C/min was used. All three unsymmetrical compounds showed super-cooling of approximately 20-25°C. In the supercooled region the columnar mesophases were still liquid like in behaviour, this region remaining stable over a number of hours.

| Sample | Transition temperatures /°C Heating (1°C/min) | | | Transition temperatures /°C Cooling (1°C/min) | | |
|--------|--|-------------------|---------------------|--|--------------------|-----|
| | C-C | C-D _{hd} | D _{hd} -I | I-D _{hd} | D _{hd} -C | C-C |
| TW73 | | 50.4 (51) | 53.6-58.8 (61) | 57.1-51.6 | 31 | |
| TW75 | | 45.5 (46) | 84 (84) | 83 | 28 | |
| TW77 | 43.6 | 54.3 (54) | 73.5-77.6 (77.5) | 76.8-74.4 | 29.5-26.5 | |

Table 2.2 : Transition temperatures obtained through Optical Microscopy and DSC (shown in brackets).

Comparing the transition temperatures of the unsymmetrical compounds with results of a symmetrical compound from the classification by Destrade [12] the effects of the alteration to alkyl arm lengths can be clearly seen. The samples were based on the basic core molecule (Fig. 2.1.).

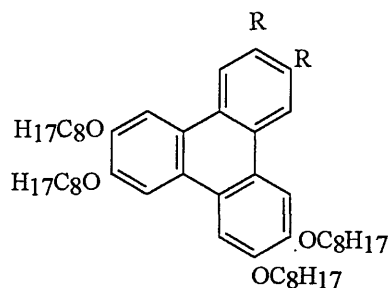


Figure 2.1. Basic core molecule for unsymmetrical substituted compounds.

| | | | | | | | | |
|-----------|----------------------------------|---|------|---|------|---|---------------|---------------|
| R group = | OC ₆ H ₁₃ | C | 46 | D | 84 | I | unsymmetrical | TW75 |
| | OC ₈ H ₁₇ | C | 66.8 | D | 85.6 | I | symmetrical | Destrade [12] |
| | OC ₁₀ H ₂₁ | C | 54 | D | 77.5 | I | unsymmetrical | TW77 |
| | OC ₁₂ H ₂₅ | C | 51 | D | 61 | I | unsymmetrical | TW73 |

As the alkyl chain length is increased from OC₈H₁₇ to OC₁₂H₂₅ the isotropic transition temperature is reduced, the crystal - liquid crystal transition is also reduced. This has been observed many times before for calamitic materials and it is a well known and reported effect. As the alkyl component of a molecule is increased in length, the transition temperatures reduce and the temperature range of the liquid crystal phase is also seen to reduce, e.g. for the above compounds where R = OC₁₀H₂₁ the range was 23.5°C but with R = OC₁₂H₂₅ the range was now only 13°C.

The most interesting point to consider is the effect of reducing the length of the alkyl arm substitution. In the case where the two arms are OC₆H₁₃ the isotropic transition is reduced slightly when compared with the symmetrical molecule OC₈H₁₇, but the crystal - liquid crystal transition temperature is reduced from 66.8°C to 46°C, increasing the liquid crystalline range from 18.8°C to 38°C, in effect doubling the liquid crystal temperature range.

2.3. Accidental Alignment

On cooling from the isotropic to the liquid crystal phase it was observed that some of the samples aligned on the untreated glass cover slips, in particular DB118 and PH76. Appendix A pg. A - II, A - VII. The samples initially exhibited a schlieren nematic texture and then aligned immediately upon entering the liquid crystal phase. The samples remained aligned during further cooling of up to 10 - 15°C, but eventually the alignment was lost and the nematic schlieren texture returned. Here the sample disorder increases on cooling as opposed to decreasing. A possible mechanism for this increase in disorder may arise from loss of liquid like fluidity of the flexible arms as the sample is cooled, as the arms begin to solidify steric hindrance effects from the arms will play a more important role and cause disruption of the molecular alignment. In this case the sample was aligned homeotropically, with the director perpendicular to the glass surface. This was verified by rotating the sample relative to the polaroids. The sample remained uniformly dark during this rotation, indicating that there was no change in the direction of the director \underline{n} . Thus the director \underline{n} must have been perpendicular to the glass surface, resulting in the plane of the molecular discs being parallel to the plane of the glass surface (Fig. 2.2.).

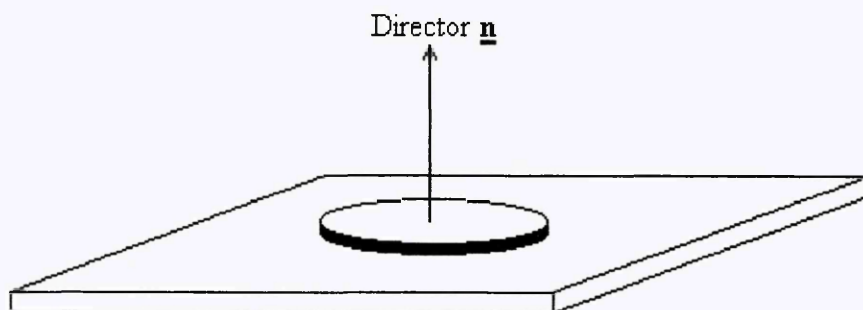


Figure 2.2. Homeotropic alignment of a discotic molecule.

2.4. Intentional Alignment.

Traditional methods of aligning calamitic liquid crystals have utilised various surface treatments. Rubbed polymer layers, polyimide or poly vinyl alcohol (PVA), have proved to successfully induce alignment in rod like liquid crystals where the director aligns parallel to the rubbing direction. Use of obliquely evaporated films of silicon monoxide SiO by Janning [13] of 100Å thickness or less onto substrates inclined at an angle of 5° to the vertical causes the deposited film to "grow" in a preferred direction. Liquid crystals become aligned in the direction of film growth. These deposited films and evaporated layers have been extensively used to align the calamitic or rod like molecules.

Another method of aligning calamitic liquid crystals is to use either magnetic or electric fields, the molecules aligning themselves parallel to the field direction. This forms the basis of the nematic display where an applied electric field realigns the molecules within the display.

2.4.1. Alignment by Magnetic and Electric Fields.

Belarbi [14] successfully orientated a discotic molecule, octasubstituted bis(phthalocyaninato)lutetium $[(C_{12}O)_8Pc]_2Lu$, using an electromagnet with a magnetic flux density, $B > 1.5T$. The sample was slowly cooled from the isotropic liquid and a preferential orientation of the columnar phase was obtained which depended on the field strength. Bengs *et al* [15] used an electric field of 900 kV m⁻¹ applied across a sample cell to align hexa-alkoxytriphenylene based liquid crystals. They again achieved much better alignment when the sample was allowed to slowly cool from the isotropic liquid to the nematic phase with the field applied to the cell.

Alignment of the discotic liquid crystals described in this report was attempted using an electric field across a sample cell and also using a magnetic flux density of $\approx 1 T$

generated by 2 BreMag rare earth magnets. Unfortunately neither of these methods was able to align the discotic compounds in the field direction, probably because a high enough magnetic flux density could not be achieved.

2.4.2. Alignment by Surface Treatments.

Vauchier *et al* [16] used a number of surface treatments to align 2,3,6,7,10,11-hexa substituted triphenylenes. Homeotropic alignment with the directors perpendicular to the glass surface was achieved by coating the glass surfaces with a sheet of flat molecules with their directors parallel to the surface. Flat molecules with six polar side-functions which give good anchorage to the glass substrate e.g. hexaphenol, mellitic acid, 2,3,6,7,10,11-hexahydroxytriphenylene and rufigallol were used. Using conoscopic microscopy it was established that the samples were uniaxial and negative, the optic axis being perpendicular to the substrate and the orientation of the liquid crystals homeotropic. Orientation on crystalline surfaces, the perfect cleavage (001) of apophyllite (a lamellar tetragonal silicate) and the perfect cleavage of muscovite (a monoclinic mica), were also investigated but these only yielded homeotropic alignment with the director perpendicular to the crystal surface.

Partial parallel alignment was achieved between glass slides scratched with diamond powder. Use of silicon oxide deposited at an oblique angle of 20° also resulted in partial parallel alignment : a mosaic like texture was observed with most of the grains orientated in the same direction with their directors parallel to the glass surface. Raughunathan *et al* [17] obtained homeotropic alignment by placing hexa-*n*-dodecanoylox truxene (C₁₂HATX) between clean glass plates of ITO-coated plates. They were unable to obtain homogeneous alignment using the SiO treatment described by Vauchier *et al* [16], and instead they could only obtain homeotropic alignment. The aromatic cores of the molecules had a strong affinity for the SiO surface. By treating the SiO coated plates with octadecyl triethoxy silane an aliphatic surface was obtained which

was expected to have the undulations from the underlying SiO coating. This combination of surface treatments resulted in homogeneous alignment of C₁₂HATX.

Warmerdam *et al* [18, 19] homeotropically aligned samples of 2,3,6,7,10,11-hexakis (*p*-alkoxybenzoyloxy) triphenylenes using a thin polyimide coating (Dupont, P12566). Almost perfect alignment, determined by polarising optical microscopy, was achieved. Phillips *et al* [20] obtained homeotropic alignment of two hexa-*n*-alkylcyclohexanoates of triphenylene, synthesised by Beattie *et al* [21], using the polyimide coating method described by Warmerdam *et al* [18, 19]. Phillips *et al* [20] also obtained homeotropic alignment using poly-vinyl alcohol (PVA).

2.4.3. Alignment of Discotic Mesophases.

Alignment of the discotic mesophases of the liquid crystal samples under investigation was achieved by use of a rubbed poly-vinyl alcohol (PVA) layer. 3% by weight of PVA was dissolved in water. Microscope glass cover slips were then dipped into the PVA solution and allowed to dry for 24 hours in a dust free environment. After drying a thin film of PVA remained on the cover slips. At the bottom of each glass slide there was a drop of PVA that was much thicker than the rest of the film covering the slide, and this drop was removed using a razor blade (Fig. 2.3.).

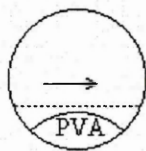


Figure 2.3. Removal of PVA drop from the bottom of the cover slip .

After removal of the PVA drop the rest of the PVA film appeared uniformly thick. The cover slip was then rubbed with a lens tissue along the direction shown in (Fig. 2.3.).

Rubbing the coated slide produces fine grooves along which the liquid crystal molecules align.

Due to the relatively high nematic - isotropic transition temperatures of some of the discotic compounds it was necessary to determine if the PVA layer would withstand these temperatures or if it would degrade. A glass slide coated with PVA was placed on the microscope hot stage and heated to 250°C for 6 hours, after which there were no obvious signs of degradation of the PVA layer, the layer was intact and was not discoloured by the heating process. With the rubbing directions of the two plates parallel most of the liquid crystal samples aligned when in the nematic phase. The best sample alignment occurred on cooling from the isotropic liquid to the nematic phase. Using glass slides with perpendicular rubbing directions alignment of the samples was also achieved on cooling from the isotropic liquid. Through the polarising microscope the aligned sample appeared uniformly dark, indicating that a very high degree of alignment was achieved. Rotating the aligned sample between the crossed polaroids of the microscope the sample remained uniformly dark, indicating that the samples were homeotropically aligned with their optic axes perpendicular to the glass cover slips. The PVA induces homeotropic alignment for disc-like molecules, which is the opposite of that observed for rod-like molecules. Therefore it may be possible to obtain homogenous or parallel alignment with the discotics if a method which produces homeotropic or perpendicular alignment for rods is used. Treatments which produce homeotropic alignment for rod-like molecules include ultra clean glass surfaces, cleaned with chromic acid, coating with hexadecyl trimethyl ammonium bromide (HTAB) or obliquely evaporated SiO.

A 5% solution of HTAB was prepared. At room temperature the HTAB crystallised out of the water, heating the solution caused the HTAB to re dissolve. The solution was heated to 30°C and glass cover slips were dipped into it. The slides were allowed to dry in a dust free environment for 24 hours. When a liquid crystal sample was placed

between 2 HTAB coated plates which had been rubbed and viewed using a polarising microscope, poor alignment of the liquid crystal sample was observed. When the sample was rotated between the crossed polars of the microscope it remained uniformly dark indicating that the sample was homeotropically aligned. This was a similar result as was obtained for the PVA coated plates, although the PVA treated plates produced much better more uniform alignment.

SiO₂, supplied in granular form was ground to a fine powder for use in the evaporator. A tungsten evaporating boat was required to hold the SiO₂ powder as the SiO₂ has a high melting point of 2150°C. The SiO₂ was evaporated using resistive d.c. heating under low vacuum of approximately 10⁻⁵ - 10⁻⁶ torr using the configuration below (Fig. 2.4.).

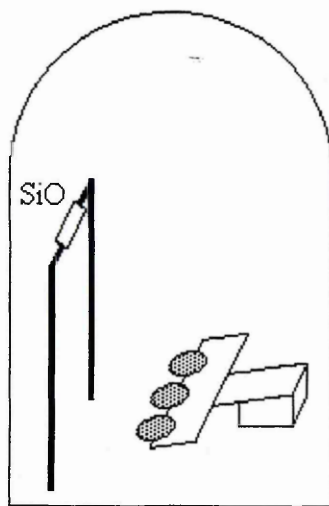


Figure 2.4. Configuration for SiO₂ evaporation.

The above configuration allowed the evaporation angle to be adjusted, but a uniform coating of SiO₂ was not able to be obtained. The glass cover slips showed interference fringes (Fig. 2.5.) indicating that the thickness of the SiO₂ layer varied across the glass cover slip.

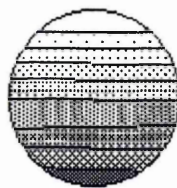


Figure 2.5. Interference fringes observed on the glass cover slip.

As well as interference fringes large grains and droplets of SiO that had jumped out of the boat were present in the film. To improve the quality of the SiO evaporated layer, the configuration within the evaporating chamber was adjusted to the configuration in (Fig. 2.6.). The plates to be coated were placed above the evaporating boat reducing the possibility of droplets forming. The use of a retort stand and clamp allowed the angle of the plates relative to the evaporating boat to be adjusted. When SiO was evaporated an uneven coating on the glass slides was obtained, the interference pattern resembling a rainbow (Fig. 2.7.).

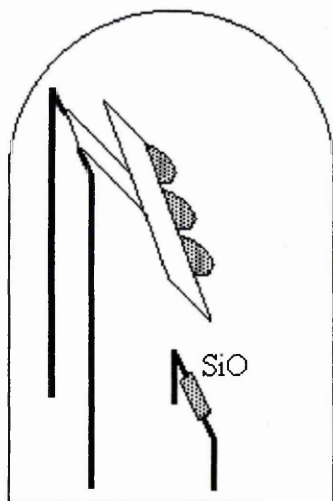


Figure 2.6. Modified evaporator configuration.

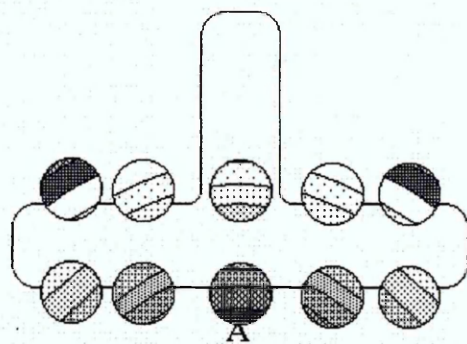


Figure 2.7. Uneven SiO coating.

The coating in region A (Fig. 2.7.) started to flake off indicating that it had been deposited too quickly. Increasing the distance between the glass plates and the SiO evaporation source would reduce the rate of deposition and produce a more robust coating. From the appearance of the interference pattern on the glass slides it seemed that the SiO evaporation was acting as though it was coming from a point source. A point source produces a uniform coating at a distance r from the source, whereas a number of point sources interfere with the deposition of each other producing a more even coating (Fig. 2.8.).

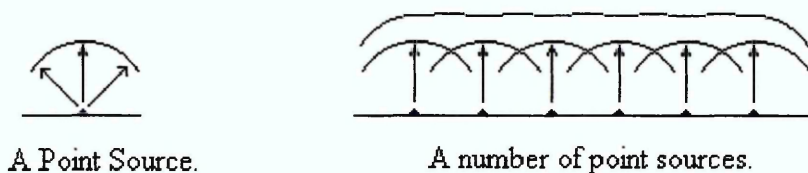


Figure 2.8. Coatings produced by a point and a number of point sources.

An old tungsten boat was punctured with a fine needle producing a number of holes less than 1mm^2 , resulting in a lid which could be placed over the SiO powder in the evaporating boat (Fig. 2.9.).

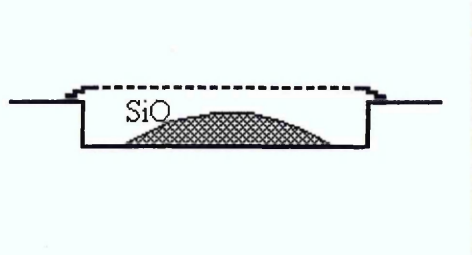


Figure 2.9. Tungsten boat with perforated lid.

The new tungsten boat and lid configuration were placed in the evaporator and a test evaporation was carried out to determine the effect of the perforated lid. The coating formed uniformly and only one interference colour was observed across all the glass slides. The SiO was evaporated onto a number of glass slides at varying angles of deposition from 5° to 55° in 5° steps. When the liquid crystal was placed between the slides in the range 5° - 35° it appeared uniformly dark when rotated under the polarising microscope, indicating homeotropic alignment.

The 40° coated slide had some regions of parallel aligned sample, the slide coated at 45° showing the best homogeneous or parallel alignment achieved. This was determined by rotating the sample in the polarising microscope, at 0° the sample appeared uniformly dark. Rotating to 45° the sample appeared bright, further rotation to 90° resulted in the sample appearing uniformly dark. Homogeneous alignment with the director parallel to the surface of the glass slide was obtained.

Chapter 3. X-Ray Diffraction.

3.1. Discovery of X-rays.

Several books give a useful introduction to the generation and origin of X-rays, for example [1 - 5]. X-rays incident to a crystal may be diffracted, the diffracted waves appearing as a reflection of the incident wave from one of the sets of crystal planes (Fig 3.1.). The equation giving the angle at which diffraction takes place is the well-known Bragg equation :

$$n\lambda = 2d \sin \theta$$

Where n , an integer, is the order of the diffraction wave, d is the spacing of the crystal planes, θ is the angle of incidence of the X-rays on the crystal planes and λ is the wavelength of the radiation used.

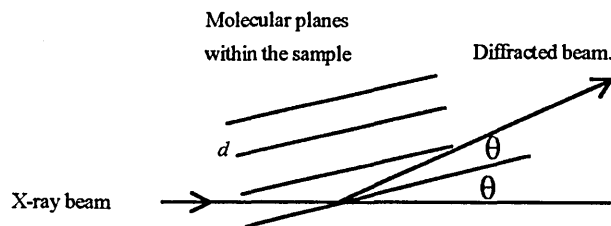


Figure 3.1. Reflection of X-rays from Crystal Planes.

Knowing the wavelength λ it is possible to calculate the value of d that gives a particular diffraction angle.

When X-rays are produced a background spectrum with a continuous distribution is produced and superimposed upon this are two strong lines referred to as the K_{α} and K_{β} lines (Fig 3.2).

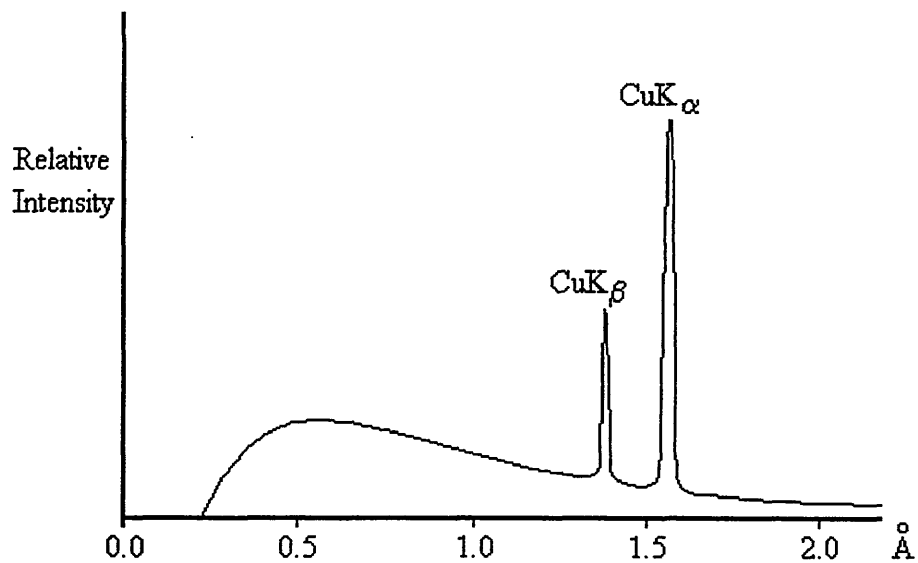


Figure 3.2. Typical spectrum from Cu.

Both the K_{α} and K_{β} lines are complicated but to a first approximation the K_{β} line can be regarded as single while the stronger K_{α} line has two components α_1 and α_2 with intensities in the approximate ratio 2:1.

A nickel filter was used to filter the radiation, nickel (Ni) has absorption characteristics shown below such that it is effectively transparent to Cu K_{α} radiation but strongly absorbs Cu K_{β} (Fig 3.3.).

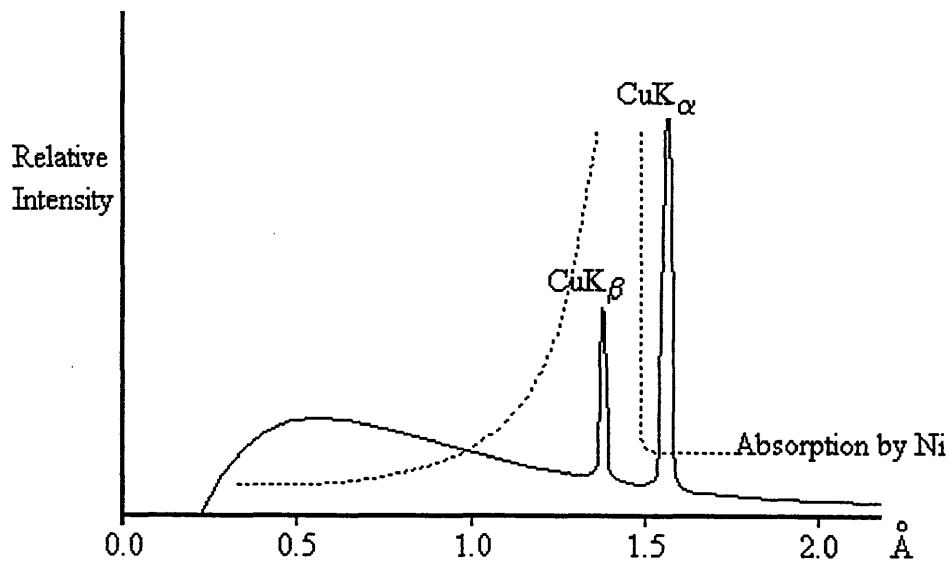


Figure 3.3. Absorption of Nickel.

Nickel is one atomic number lower than copper in the periodic table and the absorption characteristics of all materials one atomic number lower than the target show a similar absorption spectrum. Therefore for any particular X-ray radiation a suitable filter can be found.

The use of the filter slightly reduces the intensity of the K_{α} line, but the K_{β} and background are both reduced to almost zero and the X-ray beam may be considered to consist of only the K_{α} component. The commonly accepted value for the wavelength of the Cu K_{α} component is the weighted average of the Cu $K_{\alpha 1}$ (1.5405Å) and Cu $K_{\alpha 2}$ (1.5443Å) components and this value is agreed upon as 1.5418Å [5,6].

The production of X-rays is an extremely wasteful process, only a fraction of < 1% of the energy input being converted into X-rays and only a small fraction of the X-rays produced, the K_{α} , providing the characteristic radiation that is used in X-ray analytical methods.

3.2. X-ray Analysis.

3.2.1. Powder Diffraction Camera.

X-ray diffraction has been employed as an analytical tool to examine the crystal structure of a sample and the use of a powder diffraction camera to record the plane spacings is common throughout X-ray laboratories.

The X-ray camera used was a powder diffraction type camera (Fig. 3.4.). The camera consisted of a metal box with a small pinhole at the front to allow an X-ray beam to enter. The incident X-ray beam then passed through a narrow metal tube, a collimator, to ensure that the beam was parallel. The powder sample to be investigated was held in a small glass tube, a Lindemann tube, which in turn was placed in a sample stage in the line of the X-ray beam. There was also a lead beam stop in front of the film holder. This was necessary in order to stop the very intense direct beam that would fog the film and end up obscuring some of the diffraction lines.

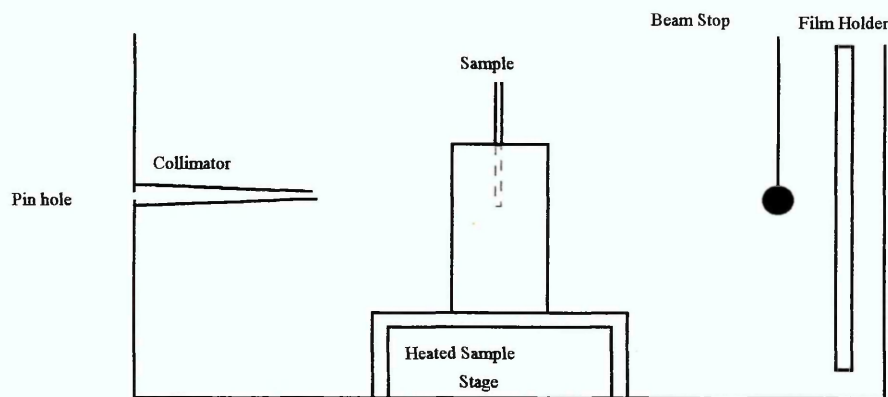


Figure 3.4. X-ray Camera.

The sample stage consisted of a brass block that could be heated up to a maximum of 260°C (Fig. 3.5.), allowing for different thermotropic mesophases to be investigated. The X-ray beam when hitting the sample will be diffracted by the specimen according to Bragg's law.

$$n\lambda = 2d \sin \theta$$

As we are only concerned with the first order diffracted beam, $n = 1$. The diffraction pattern is then captured on a flat plate film, which is held in a film holder at the back of the camera. The specimen to film distance may be varied, enabling wide angle or small angle diffraction peaks to be recorded. The sample will influence the choice of film position, large planar spacings requiring the film further from the sample, while small planar spacings may be recorded with a smaller specimen to film separation.

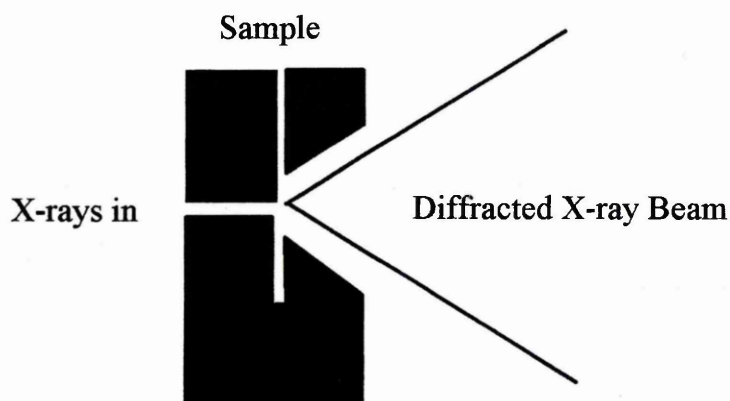


Figure 3.5. Sample stage Cross Section.

The camera was situated on a Philips PW1100/60 generator set equipped with a Philips fine focus copper tube, which produced a narrow beam of Cu radiation. The Cu K_{β} part of the spectrum was filtered out by the use of a nickel filter at the exit of the X-ray tube.

Due to the fact that the sample was unaligned, the molecular planes were not usually highly oriented. Planes of molecules existed at many different orientations within the sample relative to the plane of the X-ray beam. This gives the sample a polycrystalline like texture which, instead of producing sharp diffraction spots for allowed reflections, gives rise to circular diffraction rings arising from the differently oriented planes.

3.2.2. Combining Bragg's Law and Camera Geometry.

Using the geometric set-up within the camera (Fig. 3.6.) and Bragg's law it is possible to determine the planar spacing within the sample by measuring the diameter of the diffraction rings.

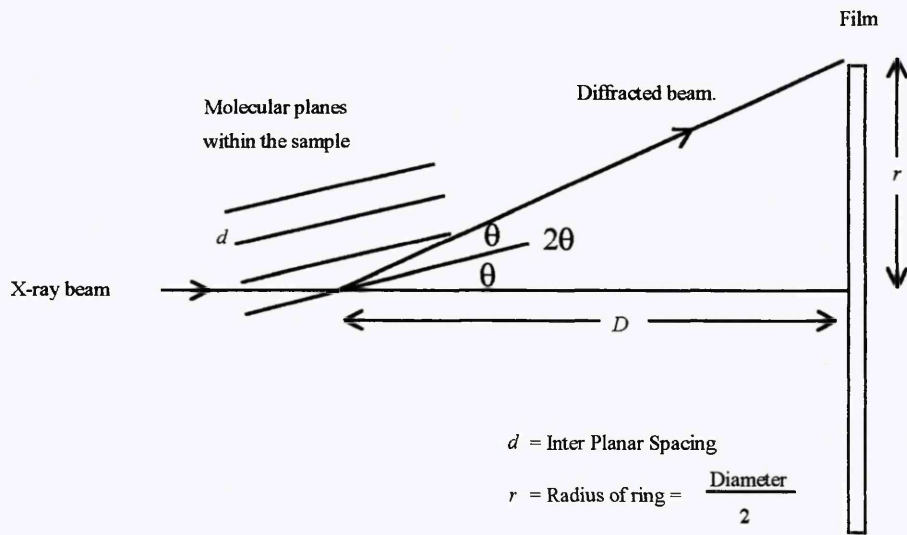


Figure 3.6. Geometric setup within the camera.

Camera Geometry $\tan 2\theta = r/D$ Braggs law $\lambda = 2d \sin \theta$

reorganise for θ .
 Equation 1. $\frac{\tan^{-1} r/D}{2} = \theta$

reorganise for d .
 Equation 2. $d = \frac{\lambda}{2 \sin \theta}$

Considering equation 1, D is the sample to film separation, (94mm for this particular set-up), and r can be measured from the X-ray photographs allowing θ to be calculated. Once θ has been calculated it may then be substituted into equation 2. As λ is known, (the wavelength of Cu K_{α} radiation = 1.5418Å), the planar spacing d may then be calculated. A computer program was written using Pascal in order to carry out this calculation as it would have to be repeated for every X-ray diffraction photograph,

typical photographs are included in [Appendix B.]. The program takes as input a number of ring diameter measurements in millimetres, which are averaged and the average ring diameter measurement is used in the calculation of the planar spacing d which is then output along with the relevant camera parameters (i.e. sample to film separation and wavelength of the radiation used).

3.2.3. Sample Preparation and Determination of Exposure Time.

3.2.3.1. Sample Preparation.

The samples were prepared for the X-ray diffraction by placing a small amount of each sample in the neck of a Lindemann tube. This was then heated on a hot plate until the liquid crystal sample started to melt. The liquid was then drawn into the body of the Lindemann tube by capillary action. When the sample had flowed into the tube it was allowed to cool before the end of the capillary was sealed in a Bunsen flame. All the samples were prepared in this manner and labelled for identification purposes.

3.2.3.2. Determination of Exposure Time.

In order to determine the correct exposure time and power settings for the diffraction camera a number of different values were used. With the X-ray set the total power should not exceed 1500kW and for long X-ray tube life it was recommended that powers between 500-1000kW be used [6]. It was found that 35kV, 20mA (700W) and a 3 hour exposure yielded photographs with suitable contrast between the diffraction rings and the background to be detected by a microdensitometer.

3.3. Ring Diameter Measurements

3.3.1. Use of Vernier Callipers and a Light Box.

It was possible to measure the ring diameters directly from the X-ray diffraction photographs using vernier callipers and a light box, but the peaks were rather broad and diffuse and this method of measurement had high uncertainties associated with it, due to the difficulty in determining the exact position of the centre of the diffraction peak. Considering two diffraction rings with approximately 6mm and 37mm radii respectively, there was approximately ± 0.5 mm uncertainty in the measurement of the ring radius. When these values and uncertainties were converted to plane spacings the following measurements were obtained (Table 3.1.):

| Wavelength | | Camera Length | | Radius | | Plane Spacing | |
|----------------------|----------------------------|---------------|----------------------|---------------|----------------------|----------------|-----------------------|
| $\lambda/\text{\AA}$ | $\delta\lambda/\text{\AA}$ | D/mm | $\delta D/\text{mm}$ | r/mm | $\delta r/\text{mm}$ | $d/\text{\AA}$ | $\delta d/\text{\AA}$ |
| 1.5418 | 0.00005 | 94 | ± 0.5 | 6 | ± 0.5 | 24.163 | ± 1.006 |
| 1.5418 | 0.00005 | 94 | ± 0.5 | 37 | ± 0.5 | 4.0810 | ± 0.025 |

Table 3.1. Uncertainties in planar spacing measurements.

$$d = \frac{\lambda}{2\sin\theta}$$

$$\theta = \frac{\tan^{-1} r/D}{2}$$

$$\left(\frac{\delta d}{d}\right)^2 = \left(\frac{\delta\lambda}{\lambda}\right)^2 + \left(\frac{\delta\theta}{\theta}\right)^2$$

$$\left(\frac{\delta\theta}{\theta}\right)^2 = \left(\frac{\delta r}{r}\right)^2 + \left(\frac{\delta D}{D}\right)^2$$

$$\frac{\delta d}{d} = \sqrt{\left(\frac{\delta\lambda}{\lambda}\right)^2 + \left(\frac{\delta D}{D}\right)^2 + \left(\frac{\delta r}{r}\right)^2}$$

The first two terms in the above equation are constant and depend on the accuracy of the measurement of λ and D . The third term comes from the measurement of the diameter and the uncertainty is smaller if the diameter is larger.

Uncertainties associated with the planar spacings when using vernier callipers to measure the radius of the diffraction rings.

The uncertainty in the planar spacing from a 6mm radius ring

$$\frac{\delta d}{d} = 4.7\%.$$

The uncertainty in the planar spacing from a 37mm radius ring

$$\frac{\delta d}{d} = 1.2\%.$$

By increasing the diameter of the ring the associated uncertainties of the planar spacing are reduced. Also if the centre position of the ring could be determined then the uncertainty in this measurement would be reduced giving an overall reduction in the plane spacing uncertainty.

3.3.2. Use of Wooster Mark III Mod III Microdensitometer.

The microdensitometer enables an intensity profile across the X-ray diffraction pattern to be recorded on a paper roll (Fig 3.7). From the intensity profile it is very easy to determine the position of the centre of the peak. By varying the speed of the chart recorder it is also possible to increase the range of the trace helping to reduce uncertainties in the measurement of peaks that are close together.

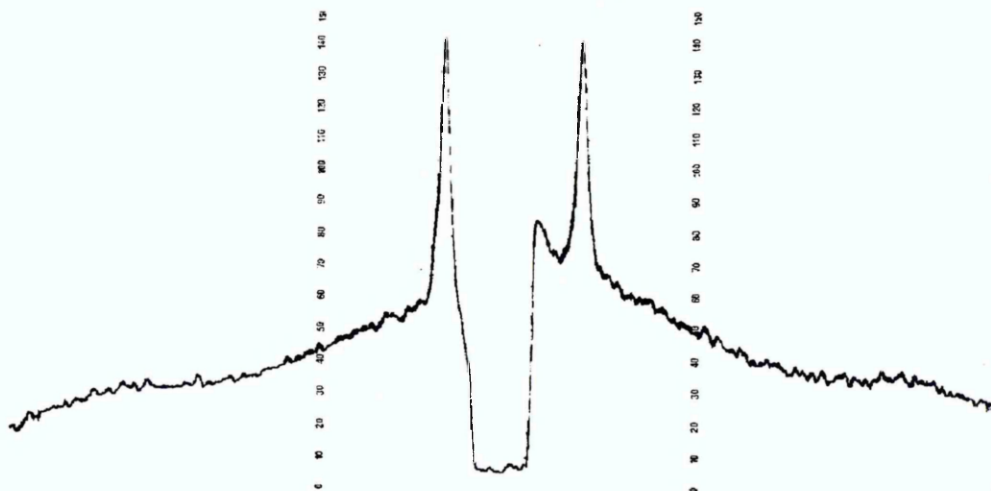


Figure 3.7. Microdensitometer trace.

3.3.3. Mode of Operation of the Microdensitometer.

In the microdensitometer there are two optical paths, the main beam and the reference beam. The main beam passes through a series of focusing lenses and apertures before being focused to produce a sharp image of the photograph being viewed before it is detected by a photomultiplier.

The reference beam passes through two optical wedges which are connected to a pen on the chart recorder. The optical wedges consist of a piece of neutral filter glass ground so as to be thinner at one end than at the other and bonded to a clear glass prism, resulting in a parallelepiped having a greater optical density at one end than at the other. The upper wedge can be moved through the light beam manually by use of a control disc. It can also be exchanged for a number of different density wedges enabling a large intensity contrast range to be investigated by use of the appropriate wedge. The zero on the chart recorder is adjusted by looking at the lowest intensity region of the X-ray photo and moving the pen so that it is recording on the chart. It is necessary to ensure that the correct density wedge has been chosen, and to prevent the pen going off scale the most intense region is first investigated. If the pen goes off scale or only moves to less than half of the full scale deflection the upper wedge can be changed to a darker or lighter one as required.

When an X-ray photograph is scanned, the lower wedge is moved through the beam by the action of a servomotor adjusting the intensity of the reference beam so that it is the same as the main beam which is transmitted through the photograph. As the wedge moves, the pen on the chart recorder traces out the intensity profile. The speed of the scan and the chart recorder can be adjusted, a slow scan and a fast chart recorder speed giving the greatest accuracy in the measurement of the diffraction rings. Settings were used on the densitometer that effectively magnified the ring diameters by a factor of 10. Thus a diameter of 12mm on the photograph effectively became 120mm on the chart

recorder. This greatly reduced the uncertainty in r by a factor of 10 resulting in much smaller uncertainties in d the plane spacing.

The new uncertainty in the planar spacing from a 6mm radius ring $\frac{\delta d}{d} = 0.95\%$.

The uncertainty in the planar spacing from a 37mm radius ring $\frac{\delta d}{d} = 0.6\%$.

3.3.4. Planar Spacings.

A computer program was written in Pascal which took as input a number of ring diameter measurements in mm, either directly from the X-ray film using the vernier callipers or from the measurement of the separation of the two peaks on the densitometer trace. The program took an average value to calculate the planar spacing d which was displayed in Å along with other relevant camera parameters i.e. sample to film separation and wavelength of radiation used.

3.4. Planar Spacings.

The X-ray diffraction photographs recorded a diffuse broad ring in the liquid crystal phase, some samples produced a number of sharp rings in the crystal phase [Appendix B - III]. The planar spacings measured are shown in below (Table 3.2.).

| Sample | Temperature / °C | Planar Spacing / Å |
|--------|------------------|--------------------|
| DB26 | 20.0 | 23.5 |
| DB26 | 155.2 | 24.1 |
| DB26 | 163.3 | 24.1 |
| DB26 | 164.4 | 25.4 |
| DB26 | 203.8 | 25.1 |
| DB26 | 209.8 | 26.3 |
| DB26 | 214.2 | 23.1 |
| DB118 | 25.0 | 30.5 |
| DB118 | 84.3 | 28.4 |
| DB118 | 107.0 | 22.3 |
| DB118 | 164.0 | 22.7 |
| DB118 | 169.0 | 22.2 |
| DB118 | 203.8 | 21.7 |
| DB118 | 223.5 | 23.1 |
| DB118 | 244.0 | 24.0 |
| DB125 | 20.0 | 22.4 |
| DB125 | 74.6 | 23.5 |
| DB125 | 171.2 | 22.7 |
| DB125 | 184.8 | 23.1 |
| DB125 | 244.0 | 22.3 |
| PH64 | 20.0 | 25.0 |
| PH64 | 194.7 | 25.1 |
| PH64 | 202.3 | 26.0 |
| PH64 | 210.5 | 24.5 |
| PH64 | 212.8 | 23.8 |
| PH64 | 220.5 | 26.5 |
| PH74 | 20.0 | 20.4 |
| PH74 | 166.4 | 25.5 |
| PH74 | 172.2 | 23.5 |

| Sample | Temperature / °C | Planar Spacing / Å |
|---------|------------------|--------------------|
| PH12IME | 20.0 | 28.3 |
| PH12IME | 57.0 | 28.7 |
| PH12IME | 86.6 | 29.5 |
| PH12IME | 105.0 | 25.7 |
| PH12OME | 20.0 | 29.4 |
| PH12OME | 127.0 | 31.0 |
| PH12OME | 148.0 | 28.6 |
| PH12OME | 167.0 | 27.2 |
| TW73 | 52.0 | 21.0 |
| TW73 | 57.7 | 21.5 |
| TW73 | 65.0 | 21.5 |
| TW75 | 58.0 | 21.7 |
| TW75 | 68.1 | 19.4 |
| TW75 | 95.0 | 18.6 |
| TW77 | 56.0 | 20.4 |
| TW77 | 58.1 | 20.3 |
| TW77 | 81.0 | 20.6 |

Table 3.2. Planar spacings at different temperatures for the discotic compounds.

(Uncertainty $\pm 0.5\text{Å}$)

Considering the DB series of compounds, the only difference between the 3 DB compounds was the addition and position of a single methyl group on the benzene ring of the ester benzoate linkage of the arm.

DB26 had no methyl additions and the molecules had a planar spacing of between 24-26Å depending on the temperature.

DB118 had a methyl group pointing away from the core. It would be expected that the planar spacing would be larger than for DB26 due to the increase of steric hindrance around the core region resulting in the arms of adjacent molecules not being able to fully interdigitate. At room temperature and throughout the crystal phase this is observed to be the case, the sample has a planar spacing of 30.5-28.4Å. However as the sample enters the liquid crystal phase the planar spacing decreases sharply to 21.7-24Å, which is smaller than the values measured for DB26 in the liquid crystal phase.

One possible explanation as to why this should occur may be that in the crystal phase the benzene linkage of the arm is locked in a planar orientation parallel with the plane of the triphenylene core. The methyl group causes a lot of steric hindrance in this region and the arms of adjacent molecules are not able to interdigitate as much as in the case of DB26 - leading to larger planar separations in the crystal phase.

As the sample melts into the liquid crystal phase, the ester benzoate linkage becomes freer and due to steric hindrance effects of the methyl group, the plane of the benzene group in the arm is rotated with respect to the plane of the triphenylene core. The methyl group will no longer be in the plane of the alkyl arms and adjacent molecular arms can interdigitate further before experiencing steric hindrance effects from the triphenylene core resulting in the lower planar spacings observed in the liquid crystal phase.

DB125 has a methyl addition to the ester benzoate linkage, the methyl group is attached so that it is pointing towards the central triphenylene core of the molecule. There are only small variations between the planar spacings observed from DB125 in the crystal phase, the liquid crystal phase and the isotropic liquid. This may be accounted for by the fact that the methyl group which is pointing towards the core experiences a lot of steric hindrance due to the close proximity of the core and other molecular units from adjacent alkyl arms. The plane of the benzene ring in the ester benzoate linkage is rotated with respect to the plane of the triphenylene core, allowing the arms of adjacent molecules to interdigitate more than in the case of DB26.

As the sample enters the liquid crystal phase and the flexibility of the arms increases the benzene ring will still remain rotated with respect to the central core, the methyl group will prevent it rotating further and the planar spacings remain approximately the same as the environment around the central core of the molecule does not alter much with temperature.

The planar spacings for PH64 vary from 25Å at 20°C and decrease to 23.8Å as the sample is heated to the liquid crystal phase. PH64 has 2 methyl groups attached to the benzene ring pointing away from the core. These methyl groups cause the plane of the benzene ring to be rotated with respect to the plane of the central triphenylene core. As the sample enters the liquid crystal phase, increased flexibility in the alkyl arms increases interactions with the methyl groups, initially causing the planar spacing to increase. As the temperature increases further the ester benzoate linkage becomes more mobile and with increased steric hindrance from disordered interdigitated arms is able to rotate slightly away from the plane of the triphenylene core, reducing steric hindrance in this region and thus causing the planar spacing to decrease at higher temperatures. In the isotropic phase, completely disordered arms and freely rotating ester benzoate linkage causes a large amount of steric hindrance around the core region, dramatically increasing planar spacings.

PH74 contained two methyl groups pointing away from the core and also a methyl group attached directly to the alkyl arm. The PH74 samples also had alkyl arms that were one carbon unit shorter than the other DB and PH compounds. At room temperature the planar spacing was 20.4Å, but as the sample was heated into the liquid crystal phase the planar spacing increased to 25.5Å and on further heating dropped to 23.5Å. A mechanism that explains this behaviour is that at room temperature the benzene ring on the arm is rotated with respect to the plane of the triphenylene core, this would cause the methyl group attached to the alkyl arm to be rotated as well. Adjacent molecules would be able to interdigitate fully and due to the shorter alkyl arms pack closer resulting in a planar spacing of 20.4Å. As the temperature increases the alkyl arm flexibility will increase and due to steric hindrance from the two methyl groups on the benzene linkage the methyl group on the arm may be rotated causing increased steric hindrance for the interdigitated arms resulting in a dramatic increase in the planar spacing. Further heating increases disorder within the alkyl arm and closer packing becomes possible.

The PH12IME compound had much longer alkyl arms than the other compounds, instead of OC₈H₁₇ they were OC₁₂H₂₅. PH12IME also has two methyl groups pointing towards the core. The planar spacing at room temperature was measured as 28.3Å as the sample entered the liquid crystal phase the spacing increased to 29.8Å. In the isotropic phase when the arms are most flexible the planar spacing reduced to 25.7Å.

The PH12OME compound was similar in structure to PH12IME except the two methyl units on the benzene linkage were pointing away from the core. This caused steric hindrance around the core region which resulted in the room temperature planar spacing of 29.4Å being slightly larger than the equivalent room temperature measurement for PH12IME. When the sample entered the liquid crystal phase the planar spacing increased to 31Å, as the temperature was increased this spacing decreased to 27.2Å in the isotropic liquid.

PH12OME had a planar spacing of 27.2Å in the isotropic liquid, whereas PH12IME has a planar spacing of 25.7Å. The two methyl groups pointing away from the core caused an increase in steric hindrance further away from the core, reducing adjacent molecular arm interdigitation and thus causing the planar spacing to increase.

The TW series of compounds are the unsymmetrically substituted hexa-*n*-alkoxy derivatives of triphenylene, the alkoxy arms are connected directly to the triphenylene core, due to the simpler molecular structure the transition temperatures are much lower than the other compounds and the planar spacings are smaller as the molecular diameters are much smaller.

TW73 had four OC₈H₁₇ and two OC₆H₁₃ arms and had a planar spacing of between 21-21.5Å in the crystal, liquid crystal phase and isotropic liquid.

TW75 with two longer OC₁₀H₂₁ arms had a larger planar spacing of 21.7Å in the crystal phase, but only 19.4Å in the liquid crystal phase and 18.6Å in the isotropic liquid, smaller values than measured for TW73 even though TW75 is a larger molecule. A possible mechanism which helps to explain this arises from the fact that the OC₁₀H₂₁ arms have a larger number of possible sites for gauche and gauche' conformers than the shorter OC₆H₁₃ arms and subsequently may become more distorted and bend back on themselves, while the OC₆H₁₃ arms are more unlikely to take on this particular conformation. This would result in effectively shorter alkyl arms, increasing the packing and reducing the planar spacing.

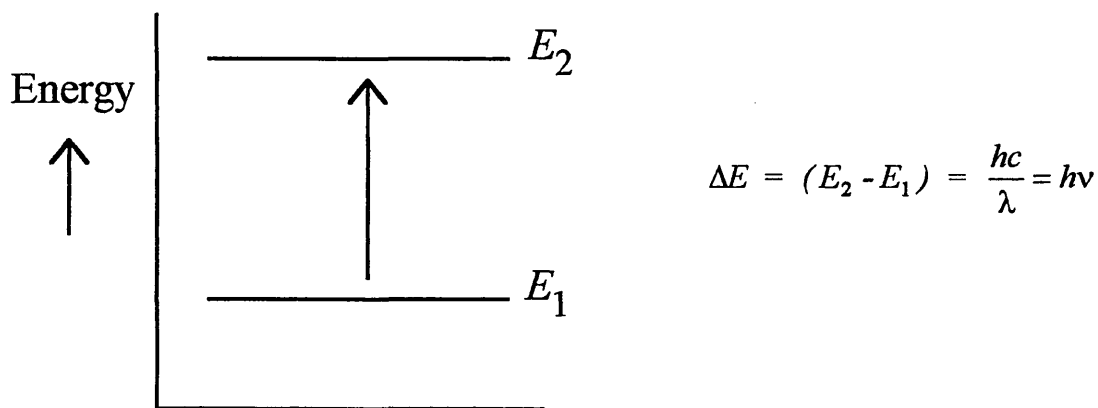
TW77 with two OC₁₂H₂₅ arms had a planar spacing of 20.3-20.6Å in the crystal, liquid crystal phase and the isotropic liquid. In the liquid crystal phase and the isotropic liquid the planar spacings were larger than the equivalent TW75 spacings, this difference arose from the fact that TW77 had two longer arms than TW75.

Chapter 4. Infra Red Analysis.

4.1. Background

A number of books cover spectrometer development and usage [1-5]. The basic principle arises from the fact that when light is passed through a sample some of the wavelengths are absorbed, while others are transmitted. At room temperature molecules are constantly vibrating, each bond in the molecule having for example a characteristic stretching or bending frequency, such that the bond is capable of absorbing energy from electromagnetic radiation at that frequency.

When a molecule absorbs energy in the ultraviolet - visible region its electrons become excited and jump into higher energy levels (Fig 4.1.). The change in energy corresponds to an absorption of energy exactly equivalent to the energy of the photon absorbed.



h = Planck's constant.

λ = Wavelength.

c = Velocity of light.

ν = Frequency.

Figure 4.1. Electron jumping into a higher energy state.

"A molecule can only absorb a particular frequency, if there exists within the molecule an energy transition of magnitude $\Delta E = h\nu$." [1].

By studying the absorption of radiation it is possible to deduce information about the molecule. In the ultraviolet - visible absorption region information about changes in the electronic energy levels of the molecule can be deduced, while for the infrared region changes in the vibrational and rotational movements of the molecule can be determined.

In the infrared region ($\lambda = 2.5 - 25\mu\text{m}$, $\bar{\nu} = \nu/c = 4000 - 400 \text{ cm}^{-1}$), it is possible to detect vibrational and rotational movements of the molecule, and also to detect functional groups that have specific vibrational frequencies e.g. C=O. The particular position of an absorption band can be expressed by a number of different units; frequency ν (Hz), wavelength λ (μm) or wavenumber $\bar{\nu}$ (cm^{-1}) where $\bar{\nu} = \nu/c$. The wavenumber expressed in cm^{-1} is defined as the inverse of the wavelength measured in cm. It is used by spectroscopists to avoid using large numbers and is a measurement of the number of waves per cm.

The majority of spectroscopists use wavenumbers and organic spectroscopy is almost entirely concerned with the range $4000 - 650 \text{ cm}^{-1}$. For example a particular stretching vibration of the C-H bond occurs at 3000 cm^{-1} , corresponding to a frequency of $9.3 \times 10^{13} \text{ Hz}$ and a wavelength of $3.3\mu\text{m}$.

4.1.1. Normal modes of vibration.

At room temperature molecules are constantly vibrating, with each bond having a characteristic stretching or bending frequency and being capable of absorbing electromagnetic energy of that frequency. Using an analogue of three balls joined by springs to represent atoms joined by a chemical bonds, it can be seen that more energy is required to stretch the spring than to bend it. Therefore the stretching energy of a bond is greater than the bending energy. This in turn leads to the stretching absorptions of a bond appearing at higher wavenumbers than the corresponding bending absorptions of the same bond (Fig 4.2.).

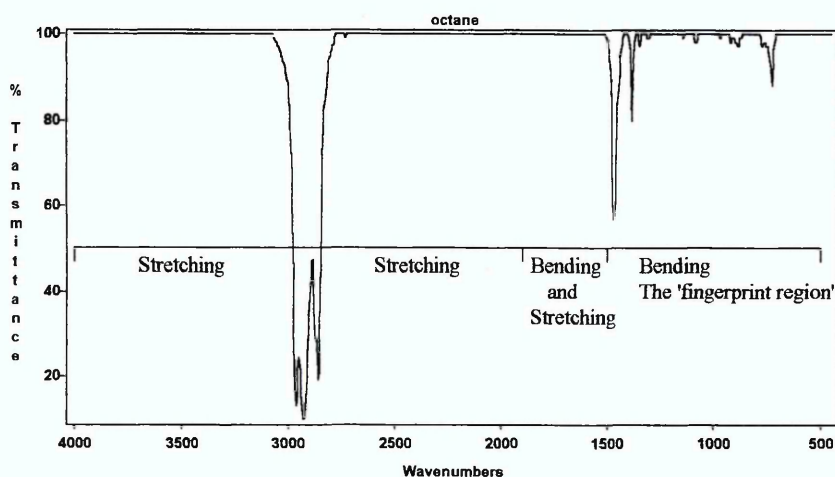


Figure 4.2. Stretching and bending regions of a spectrum.

The vibrational frequency of a bond can be calculated reasonably accurately in the same way that the vibrational frequency of a ball spring system can be calculated using using the following equation which correlates frequency with bond strength and atomic mass.

$$\nu \propto \sqrt{\frac{\text{bond strength}}{\text{reduced mass}}} \qquad \nu = \frac{1}{2\pi} \sqrt{\frac{k \cdot 10^{-5}}{m_1 m_2 / (m_1 + m_2)}}$$

ν = frequency

k = force constant of the bond (N/m)

m_1, m_2 = masses of the two atoms

$\bar{\nu} = \nu/c$ to convert the frequency to wavenumbers

$m_1 m_2 / (m_1 + m_2)$ = reduced mass

For single bonds k is approximately $5 \times 10^{-2} \text{ N m}^{-1}$ and approximately 2 to 3 times this value for double and triple bonds respectively. This equation is not highly accurate for calculating the vibrational frequencies, due to the fact that accurate data for all force constant possibilities are not available. Also effects arising from the environment of the vibrating unit are not considered. The force constants of the bonds are usually calculated using the experimental frequency of the IR absorption and they are usually refined using normal mode calculations to try to reproduce the experimental data.

As the bond strength increases, the frequency will increase and the frequency will also increase if the reduced mass of the system decreases. Changing the reduced mass of the system through deuteration (and thus inducing a frequency shift in vibrations) is often employed to help assign particular vibrations.

There are two basic types of molecular vibrations, stretching and bending. The stretching vibration is a rhythmical movement along the bond axis, causing the interatomic distance to increase and decrease. Bending vibrations result from a change in the bond angle between bonds with a common atom, or movement of a group of atoms with respect to the rest of the molecule. Twisting, rocking and torsional vibrations are forms of bending vibration where the bond angles change with reference to an arbitrary set of co-ordinates within the molecule.

Only vibrations that result in a rhythmical change in the dipole moment of a molecule are observed through IR spectroscopy. The changing charge distribution produces an alternating electric field allowing the molecular vibrations to be coupled to the oscillating electric field of the electromagnetic radiation.

The number of observed vibrations is dependent upon how many degrees of freedom the molecule has. A molecule has as many degrees of freedom as the sum of the degrees of freedom of the individual atoms. Each atom has three degrees of freedom,

corresponding to the Cartesian coordinates (x , y , z) necessary to describe its position relative to the other atoms in the molecule. Therefore for a molecule with n atoms there are $3n$ degrees of freedom. For non linear molecules three degrees of freedom are necessary to describe the rotation of the whole molecule and three degrees of freedom are necessary to describe the translation of the molecule; therefore the remaining $3n-6$ degrees of freedom are vibrational degrees of freedom. In the case of linear molecules only two degrees of freedom are necessary to describe the rotation resulting in $3n-5$ vibrational degrees of freedom. These fundamental vibrations involve no change in the centre of gravity of the molecule.

In theory each degree of freedom will produce an absorption band in the IR spectrum, but the theoretical number of fundamental vibrations is seldom seen due to various factors that increase and decrease the number of bands observed.

The number of observed bands may increase through :

- Overtones (harmonics) - multiples of a given frequency.
- Combination tones (beats)- sum or difference of two other vibrations.

Reduction of the number of observed bands arises through :

- Fundamental bands that are too weak to be observed.
- Fundamental bands that are so close they coalesce.
- Fundamental bands that fall outside the range investigated $4000 - 700 \text{ cm}^{-1}$.
- Degenerate bands - several absorptions of the same frequency - occur in highly symmetrical molecules.
- Centrosymmetric stretching vibrations of symmetrically substituted bonds about the centre of symmetry which produce no overall change in the electric dipole moment and are thus inactive in infra red.

- Quantum restrictions apply to chemical bonds imposing certain limitations - the vibrational energy can only increase by quantum jumps such that the energy difference between successive vibration levels is $\Delta E = h\nu$.

The immediate environment of the atom also affects the frequency and intensity of the vibrations. Sterically hindered atoms will have different fundamental frequencies of vibration than those from a correspondingly free atom.

4.1.2. Coupled interactions.

When two bond oscillations share a common atom, they seldom behave as individual oscillators but are mechanically coupled resulting in symmetrical ($\bar{\nu}_{\text{sym}}$) and asymmetrical ($\bar{\nu}_{\text{asym}}$) modes of vibrations. In the case of CH_2 groups the two stretching modes appear as (Fig 4.3.) and the bending modes appear as (Fig 4.4.).

Vibrational coupling takes place between two bonds vibrating with the same frequency provided that the bonds are reasonably close in the molecule.

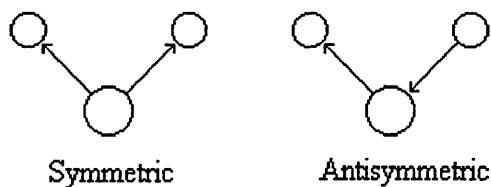


Figure 4.3. Stretching modes for CH_2

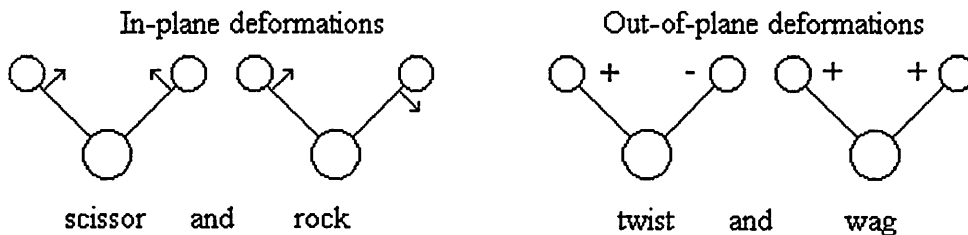


Figure 4.4. Bending or deformation modes of CH_2 .

4.2. FTIR spectrometer development.

Infra red spectrometers were used in the early 1900s, but only after the development of the optical null dispersive spectrometer in the 1940s did chemical IR spectroscopy soon become a familiar tool in organic characterisation laboratories. These spectrometers consisted of an IR source, detector and a complicated array of moving optical components, lenses, slits, diffraction gratings or prisms, filters and mirrors. The diffraction grating or prism was necessary in order to separate the IR signal into its constituent wavelengths. The other components directed the signal through the sample and then to the analyser.

The discoveries that lead to the development of the FTIR occurred in the 1950s and 1960s.

- The first major discovery was the realisation by Fellgett [6] that information from all the spectral components in a signal is simultaneously measured in a Michelson interferometer. The variation in intensity (voltage \propto Intensity) with time for such an interferometer is known as an interferogram.
- The second was the rediscovery of the Fast Fourier Transform (FFT) by Cooley and Tukey [7] in 1965. A spectrum could now be computed from an interferogram in a matter of minutes as opposed to hours when using conventional Fourier transform routines.

Other significant developments were the minicomputer and small reliable HeNe lasers; the mini-computer was required in order to carry out the mathematics of the FFT allowing spectra to be directly computed after measurement of the interferogram. The HeNe laser is used to monitor the moving mirror which in turn gives an internal wavelength standard for all measurements.

By the early 1970s IR spectroscopy was being surpassed as an analytical tool by NMR and mass spectrometry, but by the mid 1980s IR spectrometry was the most rapidly growing instrumental technique [3]. This change was due to the commercial development of the Fourier-Transform Infra red (FTIR) spectrometer.

4.2.1. Michelson interferometer.

In 1892 Albert Michelson devised this instrument (Fig 4.5.), involving monochromatic light striking a half silvered mirror, known as a beamsplitter. In the case of an IR spectrometer the beam splitter is made from KBr coated with germanium. Approximately half the light is transmitted to the stationary mirror M2, while the rest is reflected to the moving mirror M1. These beams are reflected back and recombine as beam A. If the path difference between the two beams is an integral number of wavelengths, they will combine with constructive interference.

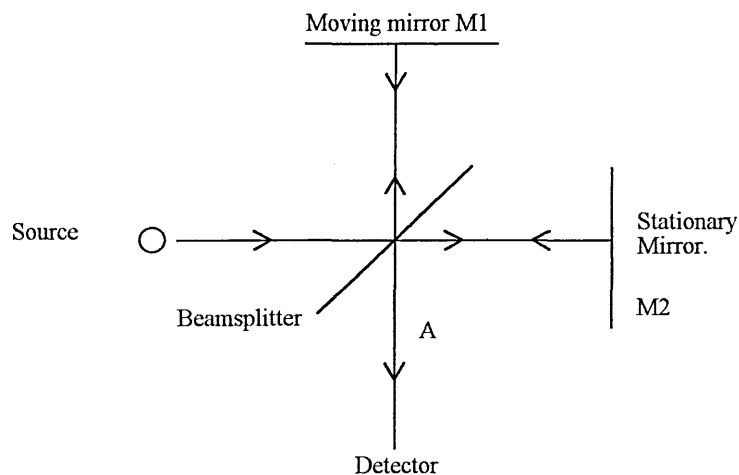


Figure 4.5. Michelson Interferometer.

If the mirror M1 is moved $\lambda/4$ from the 'in phase' position, the two beams will be half a wavelength out of phase and will combine with destructive interference. As the mirror moves back and forwards a series of light and dark bands are seen.

For the more complicated case of using polychromatic light sources, a more complex interferogram is produced (Fig 4.6.).

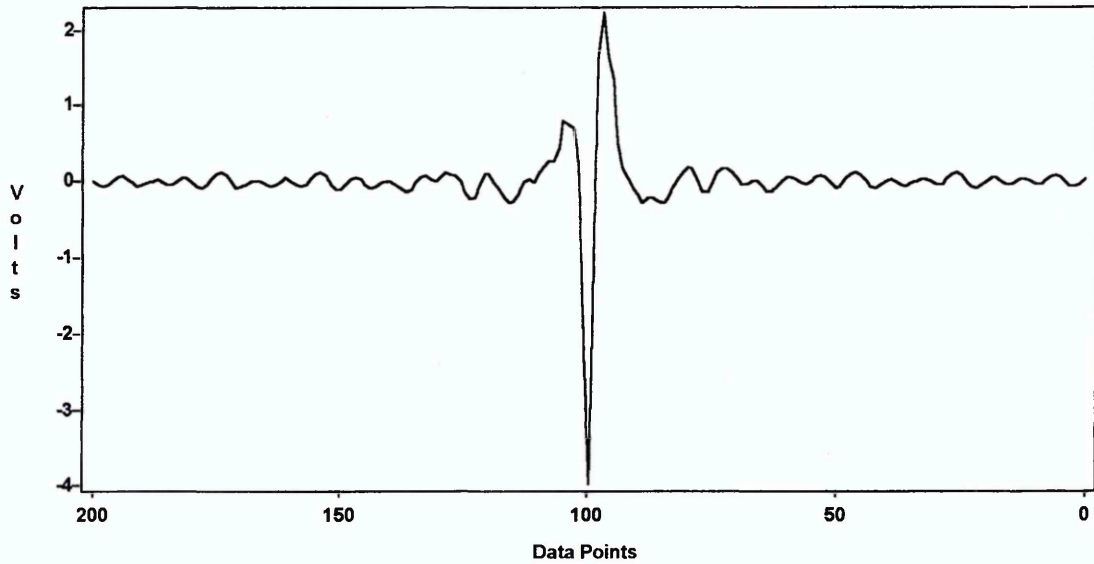


Figure 4.6. Galaxy Interferogram.

The Mattson Galaxy spectrometer utilises corner cube optics that eliminate misalignment of the beam if the mirrors are slightly misaligned (Fig 4.7.).



Figure 4.7. Comparison of plane and corner cube optics.

4.2.2. Interferograms.

Interferograms are records of intensity vs time and are relatively simple to record but are visually complex. Simpler to comprehend and compare directly are plots of intensity vs frequency. Changes against time are referred to as being in the time domain, while changes against frequency are in the frequency domain. Time is measured in s, while frequency is recorded in HZ or s^{-1} .

An Interferogram may be described by a set of sine and cosine functions, each with a unique frequency. The conversion of an interferogram to an intensity versus frequency plot is done by Fourier transforming it. Consider the simple interferometer (Fig 4.8.)

[3, 4, 5]

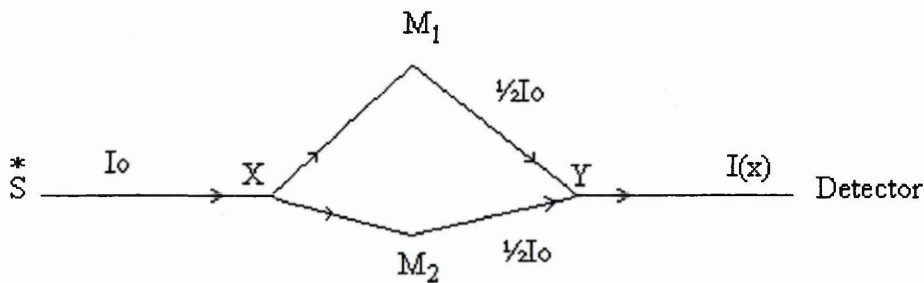


Figure 4.8. Simplified interferometer.

The partial beam travelling along the path XM_1Y to the detector has travelled a greater distance, x , than the beam taking the XM_2Y path. This difference in distance, x , is called the path difference. Because of this the beams arrive at the detector with a phase delay of $2\pi\bar{\nu}x$.

Intensity at the detector = Intensity along path 1 + Intensity along path 2

For zero path difference $I_0 = B(\bar{\nu})d\bar{\nu} + B(\bar{\nu})d\bar{\nu}$

Where $B(\bar{\nu})d\bar{\nu}$ = spectral component of power. In practice, power rather than intensity is detected, but assuming uniform illumination across the beam the power is directly proportional to the intensity.

For path difference (x) $I(x) = B(\bar{\nu})d\bar{\nu} + B(\bar{\nu})\cos 2\pi\bar{\nu}xd\bar{\nu}$

The above equation is for monochromatic light. For polychromatic light all the components from different wavenumbers ($\bar{\nu}$) must be summed.

$$I(x) = \int_0^{\infty} B(\bar{\nu})d\bar{\nu} + \int_0^{\infty} B(\bar{\nu})\cos 2\pi\bar{\nu}xd\bar{\nu}$$

The first term $B(\bar{\nu})d\bar{\nu}$ does not depend upon the path difference (x), whereas the second term varies as a function of x . This variable term is referred to as the interferogram $F(x)$

$$F(x) \propto \int_0^{\infty} B(\bar{\nu})\cos 2\pi\bar{\nu}xd\bar{\nu}$$

The interferogram depends on the spectrum according to a cosine Fourier integral and by application of the inversion theorem, applicable to such integrals, it may be rewritten as :

$$B(\bar{\nu}) \propto \int_0^{\infty} F(x)\cos 2\pi\bar{\nu}xdx$$

This allows the spectrum $B(\bar{\nu})$ to be calculated by Fourier transforming the measured interferogram $F(x)$.

4.2.3. Fourier transformation and the fast Fourier transformation.

The interferometer allows changes in intensity against time, interferograms, to be recorded. Interferograms are visually complex, but there is a relationship between the complex interferogram and the set of sine and cosine functions that produce it. The conversion from one to the other is called the Fourier transform. The interferogram is recorded in the time domain and Fourier transforming it converts it to the frequency domain.

The Fourier transformation of the data is usually carried out by a digital computer, the integral in the calculation being replaced by the summation over a total of M interferogram samples:-

$$B(\bar{\nu}) = \Delta x \sum_{m=(-M/2)}^{m=(M/2-1)} F(m\Delta x) \cos 2\pi\bar{\nu}m\Delta x$$

If the function $F(x)$ is symmetrical about $x = 0$ then $F(x) = F(-x)$ and the summation can be rewritten:

$$B(\bar{\nu}) = 2\Delta x \left[\frac{1}{2}F(0) + \sum_{m=1}^{m=(M/2-1)} F(m\Delta x) \cos 2\pi\bar{\nu}m\Delta x + \frac{1}{2}F(M/2.\Delta x) \cos 2\pi\bar{\nu}M/2.\Delta x \right]$$

The total number of multiplications using this method is $\approx 3/2M^2$ and this approach is referred to as the *slow Fourier transform*. It was found that the calculation time using the slow Fourier transform could be reduced by restricting the number of points to be transformed to a power of two. Cooley and Tukey [10] showed that this technique was not restricted to base two calculations but could be expressed in any base. They described an algorithm by which a full complex Fourier transformation could be rapidly carried out by an electronic computer, the number of operations required being reduced from $\approx 3/2M^2$ to $M \log_2 M$ for base 2. This represents an enormous saving in time when M is large and forms the basis of all the FFT algorithms used today.

4.2.4. Apodization.

In practice it is not possible to record the interferogram over the entire range $0 \leq x \leq \infty$ [2, 5, 8]. Instead a finite data set is recorded, the data collection period corresponding to what is known as a box car function. By cutting off the interferogram at x_{\max} we are effectively multiplying the interferogram by a box car function $D(x)$ (Fig 4.9.).

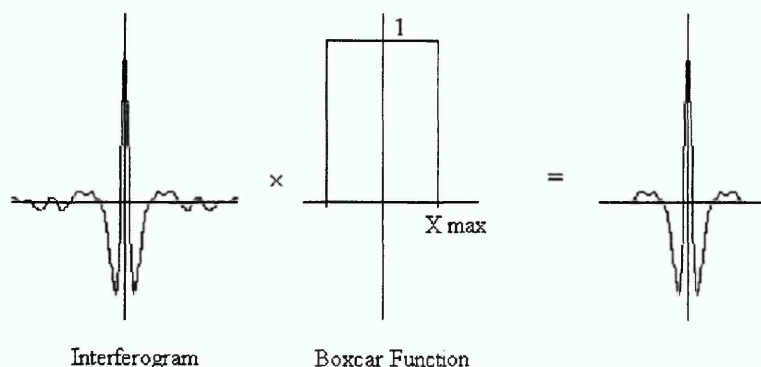


Figure 4.9. Interferogram multiplied by a box car function.

This box car function is part of the collected data and is transformed along with the spectral information in the interferogram. The transformation of the box car (top hat) function is a $\text{sinc}(x)$ function. One problem arises when this $\text{sinc}(x)$ function is convoluted with the spectra data by the fast Fourier transform: there is ringing at the edges of the spectral absorption bands. An improvement is to use a modified apodizing function which assigns less weight to the data set start and end, e.g. a triangular function. This results in less ringing in the baseline, but there is a trade off in that there is a reduction in the resolution of the spectrum when triangle apodization is used.

The interferogram is now :

$$F(x) = \int_0^{\infty} B(\bar{\nu}) \cos 2\pi \bar{\nu} x d\bar{\nu} D(\bar{\nu})$$

Where $D(x)$ is the boxcar function.

$$\begin{aligned} \text{FT } [F(x)] &= \text{FT } [I(x).D(x)] \\ &= \text{FT } [I(x)] * \text{FT } [D(x)] && [* = \text{convolution}] \\ &= B(\bar{\nu}) * D(\bar{\nu}) \end{aligned}$$

4.2.5.

FTIR advantages.

A FTIR spectrometer has many advantages over a conventional dispersive type IR spectrometer, which are discussed in a number of IR books [1-5, 9].

1. *Jacquinot's advantage* - also known as throughput advantage. The FTIR spectrometer has a much simpler optical path than a dispersive IR, with fewer optical components and no slits. Therefore all the energy of the source passes through circular apertures rather than slits and is available for obtaining the spectrum. About 40 times more energy reaches the sample and therefore the detector in a FTIR spectrometer compared with a dispersive IR, thus greatly increasing the signal-to-noise ratio.
2. *Fellgett's advantage* - or multiplex advantage. An interferometer does not separate light into individual frequencies for measurement. Each point on the interferogram contains information from each wavelength present. Therefore if the interferogram is sampled 4000 times each wavelength is thus sampled 4000 times also. For a dispersive instrument, if the spectrum is sampled at 4000 points, then each wavelength is sampled only once. The interferograms can also be acquired in a very short time, as short as a few milliseconds. The spectroscopic data can therefore be collected rapidly, and multiple scans are usually used, typically 250 scans.
3. *Connes advantage* - frequency precision for dispersive instruments depends on calibration with external standards and the use of high quality, high precision electromechanics to move gratings, mirrors and slits. The FTIR has its own internal frequency standard, a HeNe laser with a wavelength = 632.8nm or $15\ 804\text{cm}^{-1}$ and the only moving part is the moving mirror in the interferometer. This greatly increases the accuracy of the system. The wavelength accuracy depends only upon the precision with which the mirror can be moved and resolutions of $0.1\ \text{cm}^{-1}$ can easily be obtained.

4.2.6. FTIR disadvantages.

1. The spectrum cannot be seen during data collection as the interferogram is recorded and must be Fourier transformed to produce the spectrum. The time involved to complete this operation has been greatly reduced by use of digital computers and the fast Fourier transform algorithm.
2. If the source is noisy the detector sees all the noise all the time because the signal is integrated over all frequencies.
3. The FTIR spectrometer is a single beam instrument. As the background and sample spectra are sampled at different times, H₂O vapour and CO₂ concentrations can cause problems. Purging the system with dry air producing a stable environment usually rectifies these problems.

4.3. Software.

The standard Mattson software ACQ was used for the data acquisition, while the FIRST software [9] was used to analyse the data. The FIRST software contained a number of powerful routines in the advanced FIRST menu that allowed peak identification, deconvolution, second derivative and curve fitting to be applied to the data set. These standard features were all employed in the analysis of the infra red data of the samples. The advanced FIRST features employed in the analysis of the data were deconvolution, second derivative and curve fitting.

4.3.1. Advanced FIRST feature - second derivative.

The second derivative function available in FIRST simply takes the second derivative of a data set and then inverts the result and with a combination of linear regression analysis allows peaks to be accentuated, thus enabling peaks close together to be differentiated allowing peak positions and approximate shapes to be determined for use with latter curve fitting routines.

4.3.2. Advanced FIRST feature - curve fitting.

The curve fitting routine available in the advanced FIRST suite of programs [9] allows the user to fit curves to a section of the spectrum. A wavenumber range for fitting is chosen. A number of curves can be placed in order to produce a fit for the spectral region of interest, height, width and peak centre can be adjusted separately. The curve type can be altered to 100% Lorentzian, 100% Gaussian, a Gaussian Lorentzian combination or a linear baseline. All parameters can be adjusted manually until a fairly good fit is obtained. The variable parameters can then either be fixed at their present value or allowed to be optimised by the automatic optimisation fitting routine.

The optimisation routine uses a least squares fitting algorithm, the variable parameters being adjusted automatically along with the percentage of Gaussian to Lorentzian components of the curves if this curve type was initially chosen. The optimisation routine uses 10 iterations in the fitting and displays a parameter derived from the least squares difference routine which indicates how good the fit is. The smaller this value, the better the fit. For the curve fitting used later, values as low as 0.005 were typically obtained.

Care must be taken with curve fitting routines, as it is possible to improve the quality of the fit by simply increasing the number of peaks used to fit to the data, introducing extra curves without evidence of their existence in the vibrational spectra of the molecule. The minimum number of curves required to explain the various vibrational modes should be used when fitting to a data set.

Due to the nature of the curve fitting algorithms and the mathematical complexity of the operation, it is only possible to fit curves to a small region of the sample spectrum at a time. Each curve can have 4 variables that need to be simultaneously optimised: as the number of curves increases the number of mathematical steps required by the optimisation routine greatly increase resulting in very long optimisation times.

4.4. Experimental set up and sample preparation.

4.4.1. Experimental Set-up.

The Infra-red spectra were recorded using a Mattson Galaxy 6021 Fourier transform infra red spectrometer [2], equipped with a liquid nitrogen cooled mercury cadmium telluride (MCT) mid infra red (MIR) detector. A resolution of 1 cm^{-1} was used and typically 250 scans for both background and sample were recorded. The region scanned was the mid infra red region from 4000 cm^{-1} to 700 cm^{-1} . Triangular apodization and zero filling were employed and absorbance data were recorded. To overcome the problems of CO_2 and water vapour absorption inherent in single beam instruments the entire sample compartment was purged with dry air for 40 minutes before taking readings. The sample temperature was controlled to within $\pm 0.5^\circ\text{C}$ using a Graseby Specac heated cell [10] with the sample compartment of the heated cell evacuated, reducing the CO_2 and water vapour content and also reducing possible oxidation damage to the samples at higher temperatures.

4.4.2. Sample preparation.

The liquid crystal sample must be placed on a plate in order to be investigated. The plates may be made from a number of infra red transmitting materials with potassium bromide (KBr) and silver chloride (AgCl) being frequently used. These materials are transparent to infra red radiation over a large range: for KBr the range is from $40,000 - 400\text{ cm}^{-1}$ and AgCl has a range of $10,000 - 400\text{ cm}^{-1}$.

KBr is hygroscopic, meaning that it absorbs water readily and will dissolve if enough water is absorbed. It has to be kept in an environment free from water vapour. KBr is also susceptible to both mechanical and thermal shock, so care must be taken in sample

preparation and plate handling. The silver chloride is more robust and has the advantage of being insoluble in water, but it is more expensive than KBr.

Before use the plates are cleaned and polished using diamond paste and ethanol. The majority of experiments were carried out with samples on KBr, although AgCl plates were tried at one point during aligned sample studies (Section 4.6.)

A few mg of sample were dissolved in dichloromethane (DCM). The dissolved liquid crystal was then cast onto a 13mm diameter KBr plate on a hot stage at 40°C. The DCM immediately evaporated leaving the liquid crystal sample confined to the centre of the KBr plate (Fig 4.10.).

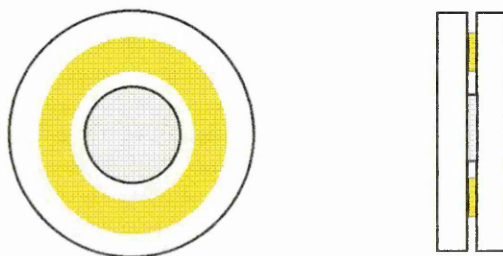


Figure 4.10. Sample preparation on KBr.

A thin teflon spacer (0.05mm) was added before a second KBr plate was placed on top, sandwiching the liquid crystal film and sealing it in place. The two KBr plates were then placed in the IR sample holder and the sample was heated into the isotropic region and allowed to cool.

For each sample run a background was required for the FTIR spectrometer. The background reading was taken with only the sample holder and two KBr plates in the instrument. The detector had to be cooled by liquid nitrogen to -176°C in order to operate. The entire sample chamber was pumped with dry air that had CO₂ removed, this process requiring about 40 - 45 minutes to ensure that CO₂ and H₂O levels had

reached a sufficiently low stable concentration. CO_2 and H_2O have strong absorption bands in the region of the absorption spectra of interest. Fig 4.11. shows a spectrum after a dry air purge.

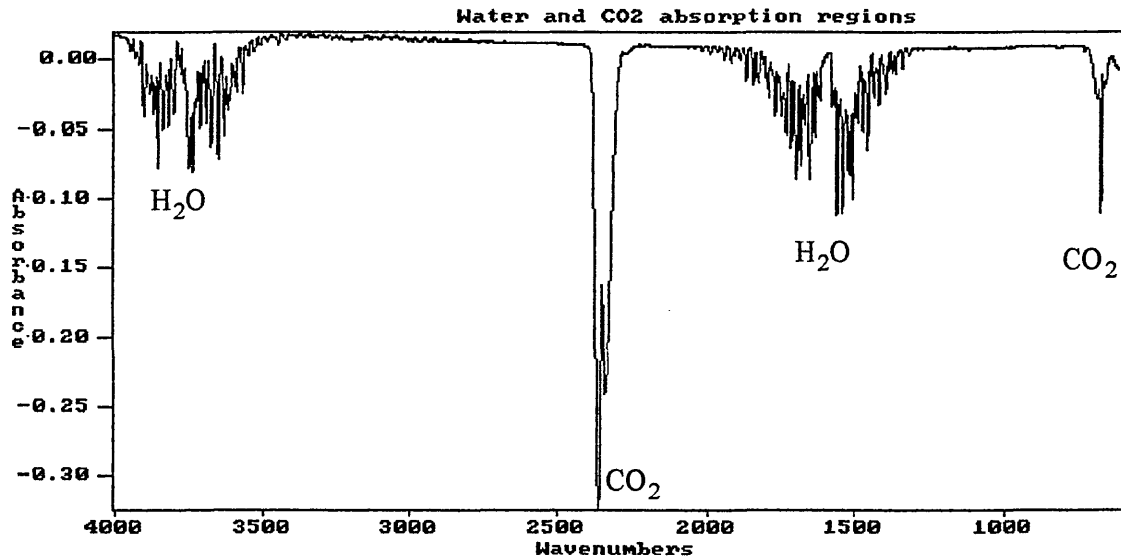


Figure 4.11. Absorption spectra of air (unpurged background, purged sample run).

These absorptions are much stronger than other molecular vibrations, so their reduction is essential to ensure that the CO_2 and H_2O concentrations are the same for the background and the sample data runs.

Once a background had been established it was then possible to take a sample run. Again the machine required purging for about 40 - 45 minutes. The sample stage, a RIIC hot stage controlled by a RS controller, was able to be heated up to 200°C with 0.1°C accuracy or to 400°C with 1°C accuracy [10]. This enabled investigation of the different liquid crystal phases. The interferograms for each sample and temperature were recorded and converted to plots of absorbance versus wavenumber.

4.5. IR. analysis.

4.5.1. Peak identification.

The first stage of analysis is identification of the peaks, to determine exactly where each vibration has come from. The samples studied had not previously been analysed using vibrational spectroscopy, so a strategy was required for their analysis. As the samples being investigated were all triphenylene based derivatives, the first logical step of identification was to compare the FTIR results of the samples with the spectra produced by the unsubstituted triphenylene (Fig 4.12.) and thus identify the C=C and C-H vibrations arising from the triphenylene core. Only a few of the peaks were identified this way.

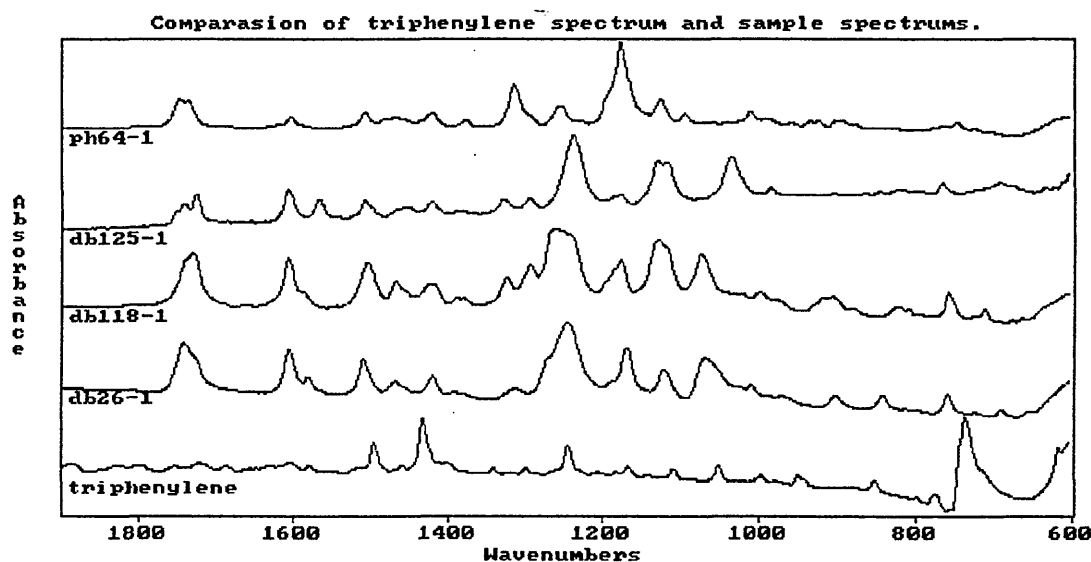


Figure 4.12. Samples and Triphenylene graph.

By consulting various IR correlation charts and tables [11-15] and also cross referencing results for CH₃ vibrations and deducing possible steric hindrance effects, all the major peaks have been assigned (Table 4.1.).

FTIR peak assignments.

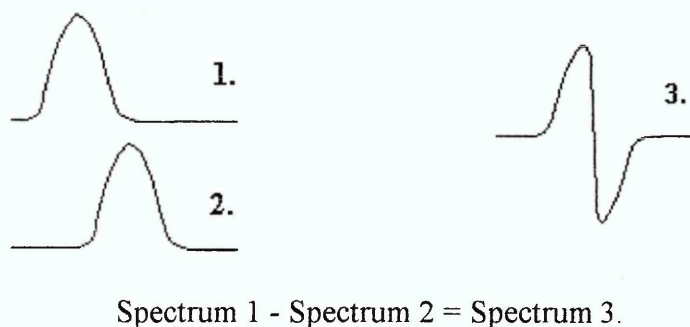
| Wavenumber cm ⁻¹ | | | | Vibration assignment |
|-----------------------------|---------|--------|--------|--|
| DB26 | DB118 | DB125 | PH64 | |
| 1007.7 | 1 023.2 | 1033.8 | 1009.7 | Aromatic in plane deformation C-H. |
| 1068.5 | 1074.3 | | 1096.5 | Aromatic in plane deformation C-H. |
| | | 1117.7 | | Ester stretching vibration C-O. |
| 1122.5 | 1129.3 | 1130.2 | 1126.4 | Ester stretching vibration C-O. |
| 1168.8 | 1176.5 | 1177.5 | 1177.5 | Ester stretching vibration C-O. |
| | | 1186.2 | | Ester stretching vibration C-O. |
| 1245.0 | 1240.2 | 1237.3 | | Alkane skeletal vibration. |
| 1269.1 | 1259.4 | | 1253.7 | Ester stretching vibration C-O. |
| | 1293.2 | 1295.1 | | Ester stretching vibration C-O. |
| 1312.5 | 1324.1 | 1327.9 | 1315.4 | CH ₂ wagging. |
| 1379.0 | 1379.0 | 1381.0 | 1377.1 | Alkane C-H deformation, CH ₃ mode. |
| 1390.6 | 1387.7 | 1387.7 | | Alkane C-H deformation. |
| 1418.6 | 1416.6 | 1420.5 | 1419.5 | Ionised carboxyl. |
| 1467.7 | 1466.8 | 1465.8 | 1466.8 | Alkane -CH ₂ - methylene deformation. |
| 1510.2 | 1504.4 | 1507.3 | 1508.2 | Aromatic C=C stretching. |
| 1580.6 | 1588.3 | 1568.0 | | Aromatic C=C stretching. |
| 1605.6 | 1606.6 | 1606.6 | 1603.7 | Aromatic C=C stretching. |
| 1730.1 | 1728.1 | 1725.2 | 1735.8 | Ester C=O stretching. |
| 1740.7 | | 1740.7 | 1745.5 | Ester C=O stretching. |
| 2854.5 | 2855.4 | 2854.5 | 2854.5 | Alkane -CH ₂ - methylene stretching. |
| 2868.0 | 2868.0 | 2868.0 | 2868.0 | Alkane -CH ₃ - stretching. |
| 2923.9 | 2925.8 | 2924.9 | 2925.8 | Alkane -CH ₂ - methylene stretching. |
| 2950.9 | 2950.9 | 2951.9 | 2951.0 | Alkane -CH ₃ - stretching. |

Table 4.1. IR peak assignment.

4.5.2. Peak shifts from subtraction spectra.

By comparison of different liquid crystal samples at room temperature (Fig 4.12.), concerning ourselves with the region $2000 - 800 \text{ cm}^{-1}$, it can be clearly seen that the different samples contain many vibrations that are the same, occasionally shifted by a few wavenumbers.

Differences in the spectra have arisen due to the different methyl substitution positions, either causing a vibration to shift a few wavenumbers, altering the intensity of an already present vibration or by introducing a completely different vibration. The shifts show up clearly in the subtraction spectra as peaks that take the shape shown in Fig 4.13. (Spectrum 3).



Spectrum 1 - Spectrum 2 = Spectrum 3.

Figure 4.13. Result of subtracting spectra frequency shifted relative to each other.

The subtraction spectra were generated by subtracting the spectrum produced by DB26 from the other spectra. The reason behind doing this was to determine the effect of addition of methyl groups to the phenyl link group. The DB26 molecule has an unsubstituted phenyl link and a similar molecular formula to the other molecules, the only difference being the addition of one or two methyl groups pointing towards or away from the triphenylene core.

Thus by subtracting the spectrum of the simpler DB26 molecule from the more complex molecular spectra (Fig 4.14.), the effects of the methyl addition are more easily observed.

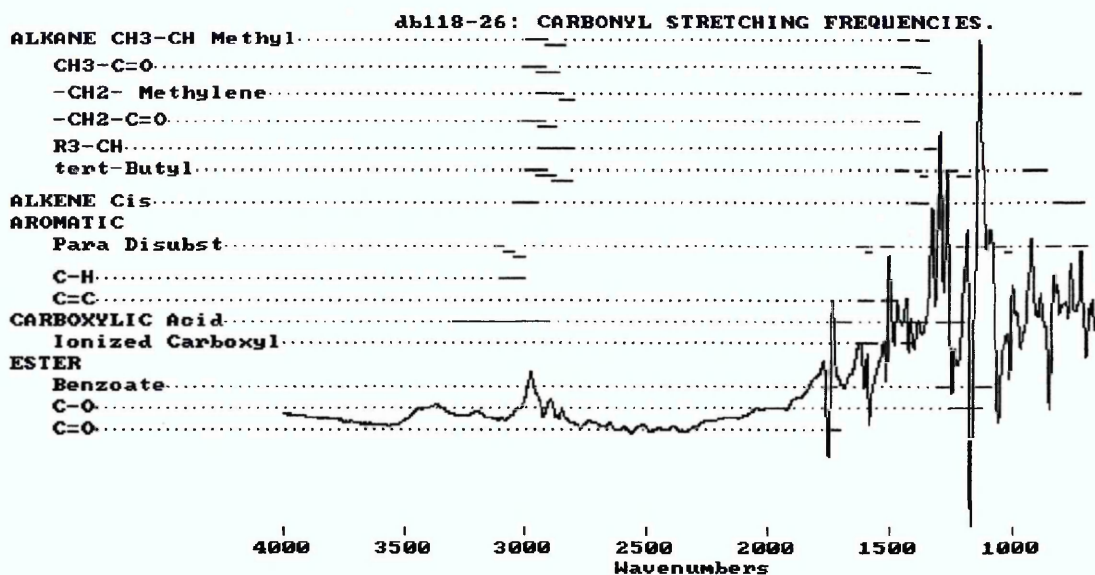


Figure 4.14. Subtraction spectrum, DB118 - DB26.

The effects of CH₃ addition to the ester benzoate linkage will affect the vibrational characteristics of bonds in the immediate vicinity. The addition of the CH₃ group will cause the intensity of some vibrations to increase i.e. there are double or triple the number of CH₃ groups and the corresponding CH₃ vibrations will increase in intensity. The CH₃ addition will also cause the intensity of other vibrations to decrease. Interdigitated arms from adjacent molecules will also be affected due to the increase in steric hindrance around the benzene group caused by the addition of a bulky methyl group reducing the space available for other groups. When the DB26 spectrum was subtracted from the other spectra the stretching vibrations in the region $\approx 3000 \text{ cm}^{-1}$ arising from CH₂ and CH₂-CH₃ vibrations were used to determine the subtraction factor necessary to reduce the intensity of these vibrations to approximately zero. The vibrations in this region are relatively unaffected by the methyl additions to the ester benzoate linkage.

4.5.3.1. Effect of the addition of methyl groups pointing away from the core.

The DB26 spectrum with no additional methyl groups was subtracted from the DB118 spectrum. This resulted in the following changes:

1. Shift of 2 cm^{-1} from 1726 cm^{-1} to 1728 cm^{-1} for the ester C=O vibration.
2. Shift of 9 cm^{-1} from 1167 cm^{-1} to 1176 cm^{-1} for the ester C-O vibration.
3. Increases in ester benzoate absorbances at 1730 cm^{-1} , 1295 cm^{-1} , 1270 cm^{-1} , 1132 cm^{-1} and 1117 cm^{-1} .
4. Absorbance increase of benzene aromatic C=C vibrations at 1590 cm^{-1} and 1500 cm^{-1} .
5. Change in the vibration at 800 cm^{-1} corresponding to a change from disubstituted to a trisubstituted aromatic out of plane deformation.

4.5.3.2. Effect of the addition of a methyl group pointing towards the core.

Subtracting the spectrum of the unsubstituted DB26 from DB125 which contains a methyl group attached to the benzene ring pointing towards the triphenylene core of the molecule resulted in :

1. C=O vibration at 1723 cm^{-1} relatively unchanged.
2. Small shift of 2 cm^{-1} to a larger wavenumber for the C=C aromatic benzene vibration.
3. Small shift of approximately 1 cm^{-1} and an increase in amplitude of the ester benzoate vibrations at 1730 cm^{-1} , 1295 cm^{-1} , 1270 cm^{-1} , 1132 cm^{-1} , and 1117 cm^{-1} .
4. Increase in absorbance of the CH_2 wagging vibrations at 1331 cm^{-1} .
5. Increase in absorbance of the alkene cis vibrations at 1383 cm^{-1} and 770 cm^{-1} .
6. Increase in absorbance of the methyl vibrations at 1450 cm^{-1} and 1383 cm^{-1} .

4.5.3.3. Addition of two methyl groups pointing away from the core.

The DB26 spectrum was subtracted from that of PH64, resulting in:

1. C=O vibration at 1723 cm^{-1} unchanged.
2. Ester benzoate vibrations at 1279 cm^{-1} and 1124 cm^{-1} increased in intensity.
3. Increase in alkane CH_3 vibrational intensity at 1317 cm^{-1} .

4.6. CH₂ wagging vibration analysis.

4.6.1. CH₂ wagging vibrations.

The intention was to obtain conformational information about the molecules' alkyl arms by use of CH₂ wagging vibrations [16]. There are distinct localised CH₂ wagging vibrations in the region 1400 - 1300 cm⁻¹.

When an alkyl chain is fully extended it is said to be in the "all - trans" configuration (Fig 4.16.a.) and has no IR active CH₂ wagging vibrations. The gauche state is where one of the C-C bonds on the alkyl arm is rotated 120° clockwise relative to the trans state position of the alkyl arm, while the gauche prime state occurs when the rotation is 120° anticlockwise. In the gauche and gauche prime positions, the chemical bond is at a local low energy conformation, but it is not in the lowest energy conformation possible (Fig 4.15.).

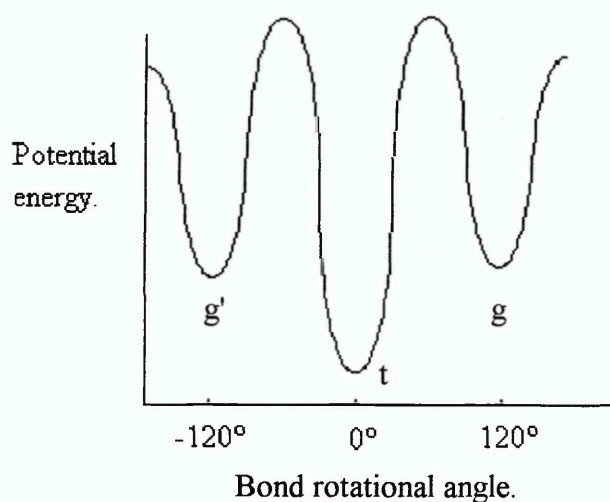


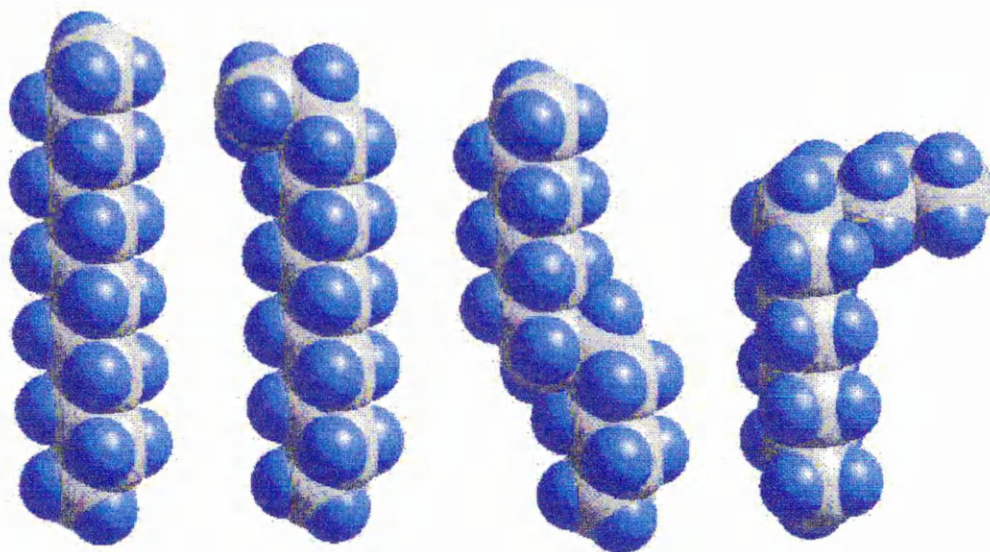
Figure 4.15. Energy plot of C-C bond rotation.

An end gauche conformation (Fig 4.16.b.) may occur when the last bond of the all trans alkyl chain is in either a gauche or gauche prime position, resulting in a CH₂ wagging

vibration at 1341 cm^{-1} . The vibrations due to specific non-trans bond conformers were assigned by Maroncelli and co-workers [16].

If the alkyl system has a kink, where the chain bends twice and then continues in the original direction (Fig 4.16.c.), then the all-trans conformation is altered by a gauche, trans, gauche prime sequence of bonds (gtg'). This results in a CH_2 wagging vibration at 1366 cm^{-1} and also one at 1306 cm^{-1} . These vibrations also involve contributions from gtg conformers although the exact composition of the latter peak is not altogether clear. Other bond sequences are possible e.g. ggtggt, which would contribute to gg bands.

The final conformation which gives rise to an I.R. peak is the double gauche. This causes approximately a 90° bend in the molecule (Fig 4.16.d.). The double gauche conformation results in a CH_2 wagging vibration at 1353 cm^{-1} .



A. All-trans

B. End gauche

C. Kink

D. Double Gauche

Figure 4.16. Structures of the planar conformer and non-planar conformations in alkyl chains.

When the IR spectrum from the DB26 sample was investigated closely in the region 1400-1300 cm^{-1} , the CH_2 wagging vibrations present in pure alkanes at 1366, 1353, 1341 and 1306 cm^{-1} were not easily observed (Fig 4.17.), they only become apparent after curve fitting.

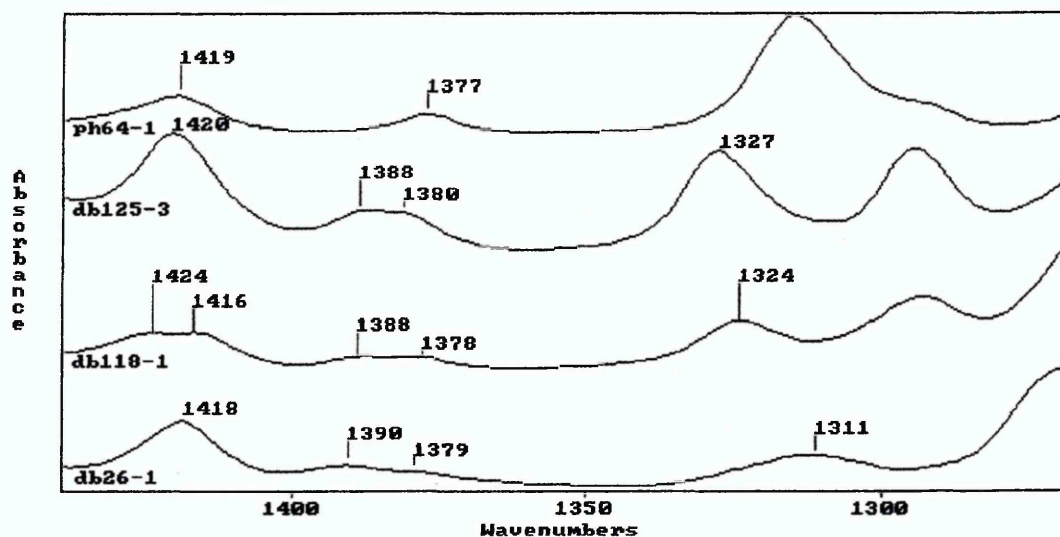


Figure 4.17. CH_2 wagging region.

Maroncelli [16] observed these bands in the odd n -alkanes $n\text{C}_{17}\text{H}_{36}$ through to $n\text{C}_{29}\text{H}_{60}$. These alkanes are at least three times longer than the alkyl chains of the discotic liquid crystals investigated, and therefore it would be expected that for these wagging vibrations the intensity ratio $I_{\text{CH}_2 \text{ wag}} / I_{\text{CH}_3 \text{ deformation}}$ would be smaller. Also Maroncelli investigated pure alkanes, whereas in our system one end of the alkane is joined to the triphenylene core. This would reduce the probability of an end gauche formation at this end. Another important point for the case of the discotic liquid crystals is that the C-O and C=O stretching vibrations are rather intense and overlapping. The CH_2 wagging vibrations are therefore relatively weak and difficult to detect when compared with stronger vibrations from the other chemical groups and it was necessary to use deconvolution, 2nd derivative and the curve fitting routines available with advanced FIRST [9] to extract this information (Section 4.6.3.).

4.6.2. Rotational isometric state model (RIS).

Senak *et al* [17] working with n alkanes fitted a cubic polynomial as a function of temperature to the calculated percentages of kink, double gauche and end gauche conformers. The percentages, which are independent of chain length except for the percentage of end gauche which is a function of chain length, were calculated in accord with the rotational isometric state (RIS) model. This model assumes that only one of the t, g or g' states is occupied for each bond. Additional equations to convert the percentages to number of bonds in a particular type of conformation for a particular alkane molecule were also given.

$$P_{gg} = \% \text{ double gauche} = -7.364 + 8.859 \times 10^{-2} T - 1.388 \times 10^{-4} T^2 + 8.741 \times 10^{-8} T^3$$

$$P_{eg} = \% \text{ end gauche} = -4.522 + 1.620 \times 10^{-1} T - 3.486 \times 10^{-4} T^2 + 2.855 \times 10^{-7} T^3$$

$$P_k = \% \text{ kink (gtg + gtg')} = -9.092 + 12.49 \times 10^{-2} T - 2.732 \times 10^{-4} T^2 + 2.176 \times 10^{-7} T^3$$

T = Temperature (K)

The equations to convert the percentages to numbers of bonds are :

$$N_{gg} = \text{No. of double gauche} = P_{gg}(N_{C-C} - 3)/100$$

$$N_{eg} = \text{No. of end gauche} = 4P_{eg}/(100(1 + P_{eg}))$$

$$N_k = \text{No. of kinks (gtg + gtg')} = P_k(N_{C-C} - 4)/100$$

N_{C-C} is the number of C-C bonds in the alkane.

The equations, although derived from 100% alkane liquids were used to determine the maximum possible number of CH₂ conformations in the alkane arms of the discotic

compounds in the isotropic phase. The equation for P_{eg} assumes that the alkane chain is free and has two ends where an end gauche conformation can occur. With the discotic liquid crystals one end of the alkane arm is attached to the central core, so the number of possible end gauche positions is halved. The numbers of the various conformations were calculated at 200°C, the isotropic region, for one alkyl arm and then multiplied by 6 for all the arms in the molecule. The following results were obtained :

$$N_{gg} = 0.51 \text{ per arm} = 3.06 \text{ per molecule}$$

$$N_{eg} = 0.36 \text{ per arm} = 2.16 \text{ per molecule}$$

$$N_k = 0.04 \text{ per arm} = 0.24 \text{ per molecule}$$

Senak's model computes the number of conformations per molecule for isotropic liquid alkanes very accurately: there is very good agreement with experimental values. However, the model constantly overestimates the numbers for bilayers: for the end gauche this is 2-3 times too much and for the double gauche there is an over estimation factor of 3-5 times. The model is only valid for free $C_nH_{2(n+1)}$ systems in the isotropic phase and becomes inadequate for other systems due to bilayer lateral pressure which reduces the number of conformations through steric hindrance effects.

In the case of the discotic liquid crystals the alkyl arms are interdigitated and this interdigitation may resemble a partial bilayer structure. Thus the numbers calculated earlier are probably over estimates, although they give an idea of the maximum number of conformers to expect.

4.6.3. Curve fitting.

Graphs of absorbance versus wavenumber for temperatures are displayed as a superimposed spectra graph (Fig 4.18.) from 250°C to 210°C in 10°C steps.

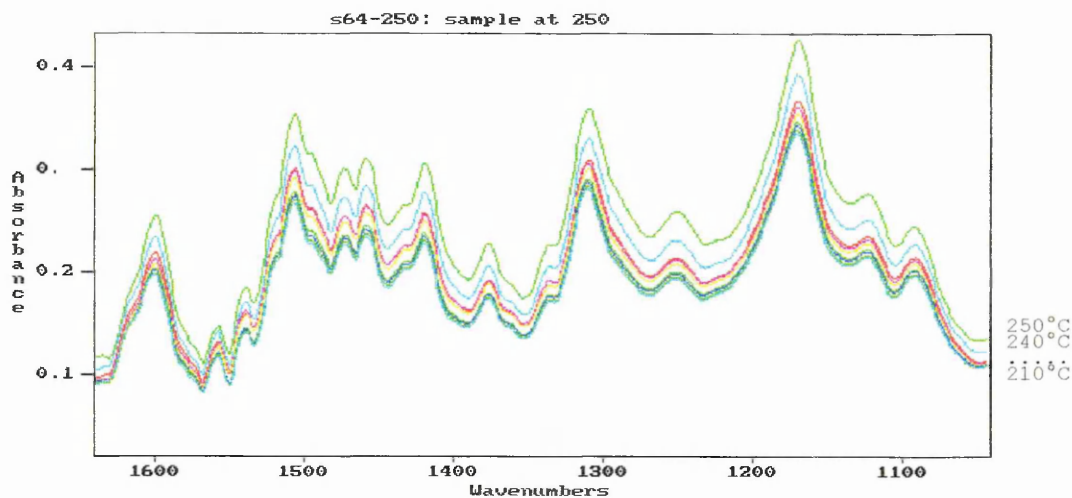


Figure 4.18. Superimposed spectra

The transitions from isotropic to nematic and nematic to crystal can be seen as reductions in the sample baseline and a decrease in peak intensity, which is accounted for by the fact that as the material changes from a clear isotropic liquid to a cloudy nematic liquid the reflectance of the sample alters and correspondingly the baseline of the absorbance spectra will change, the molecules are also in a different environment and therefore the intensity of the I.R. vibrations will alter.

Looking closely at the region from 1420 cm^{-1} to 1200 cm^{-1} , (the CH_2 wagging region), there are small peaks and shoulders that correspond to the CH_2 wagging modes of the end gauche, double gauche and kink conformations.

Curve fitting was used in order that the area of a particular peak could be determined at a particular temperature, plotting a graph of peak areas verses temperature allowed the behaviour of a particular vibration to be observed within the liquid, liquid crystal and solid phases and also observed during phase transition. Curve fitting is a complicated

process, although the software somewhat eased this process and allowed curves to be fitted to the data with a high precision and allowed various curve fitting combinations to be relatively quickly analysed.

Fitting a curve to the data, the following parameters were able to be individually set and adjusted: peak position, peak height, full width at half height, gaussian-lorentzian component, number of peaks and an additional base line could also be chosen.

Once the peak positions were identified curves were fitted to the spectra. The curves were initially optimised manually, the various parameters being adjusted until a reasonable fit was achieved. The initial manual adjustment of the parameters greatly increased the ability of the automatic optimisation to successfully fit the peaks to the data. Only the region from 1400 cm^{-1} to 1300 cm^{-1} was optimised. The two peaks at 1396 cm^{-1} and 1302 cm^{-1} (Fig 4.19.) were not used in the analysis: they were simply present to allow a better fit at the two extremes of the data set to be achieved.

It should be stressed here again that great care should be taken when fitting peaks to a data set. The minimum number of peaks required to fit the data should be used. It is possible to obtain an exact fit to the data by continually adding additional smaller peaks, this fit can no longer be classed as a realistic representation of the spectra as many of the additional peaks bear absolutely no relationship to actual molecular vibrations. Limiting the peaks to only those that were clearly identified using deconvolution and 2nd derivative and those that were expected to appear in the region (based on information from I.R. correlation charts), the number of peaks used are then kept to a minimum and all peaks can be justified as valid.

Even when the peaks used by the curve fitting are all justifiable it is still possible to obtain a number of different possible fits, all of which optimise equally well and give similar "good fit criterion". The "good fit criterion" was determined using the

summation of the square of the differences between the actual data and the fitted curve, the smaller this value, the better the fit. Due to the large number of adjustable parameters e.g. peak height, position, width etc. it is clearly possible that adjustment of the parameters for one peak and modification of the parameters for another peak could result in an equally good fit, although the results from both fits are different.

To reduce the possibility of this occurring fits with unrealistic peak shapes and fits where the area of one peak in relation to the area of another peak did not agree with results from Maroncelli^[16] and Senak^[17], who observed the I.R. vibrations of alkanes in detail were rejected. This still resulted in a number of probable fits. Taking a fit optimised at one temperature and then re-optimising it at a slightly lower temperature allowed some more fits to be rejected. During the second optimisation stage fits that caused the optimisation routine to fail through "numerical instability" were rejected. At phase transitions the I.R. spectrum was expected to change. Also, the solid phase and the liquid crystalline phase are two completely different environments for molecular vibrations, but within a particular phase it was not expected that the environment and molecular conformations would differ greatly from one temperature to the next temperature, especially if the temperature change is relatively small. Therefore the I.R. vibrations were expected to change only slightly. This was indeed the case, observable when two I.R. spectra were superimposed on top of one another, the general spectra shape remained the same with only a small change in intensity. Therefore it was valid to assume that a curve fit at one temperature should only require minor adjustments to the curve parameters in order to fit at the new temperature. Curve fits that optimised quickly at the new temperature were then classed as good approximations to the actual I.R. vibration intensities, curve fits that required a large number of optimisations to fit to the new data were rejected on the basis that there existed other fits which optimised quicker and were therefore assumed to be better fits. Fits with poor "good fit criteria" were also rejected and only the fits with small "good fit criterion" values which optimised quickly from one temperature to the next were accepted and used as the basis for further

detailed analysis. It could be argued that when a number of possible fits existed that satisfied the good fit-optimisation criteria, then they could be considered equally valid and it is difficult to say if any in particular is the exact representation of the areas of the molecular vibrations. Averaging the results from the various fits and plotting the graphs with the averaged results give the best possible results from the curve fitting data Fig 4.21.

This curve fitting optimisation procedure combined with 2nd derivative was used both with the CH₂ wagging vibration data and the C-O-C, C-O, C=O and ester benzoate vibrations used later to determine the order parameter of various molecular components.

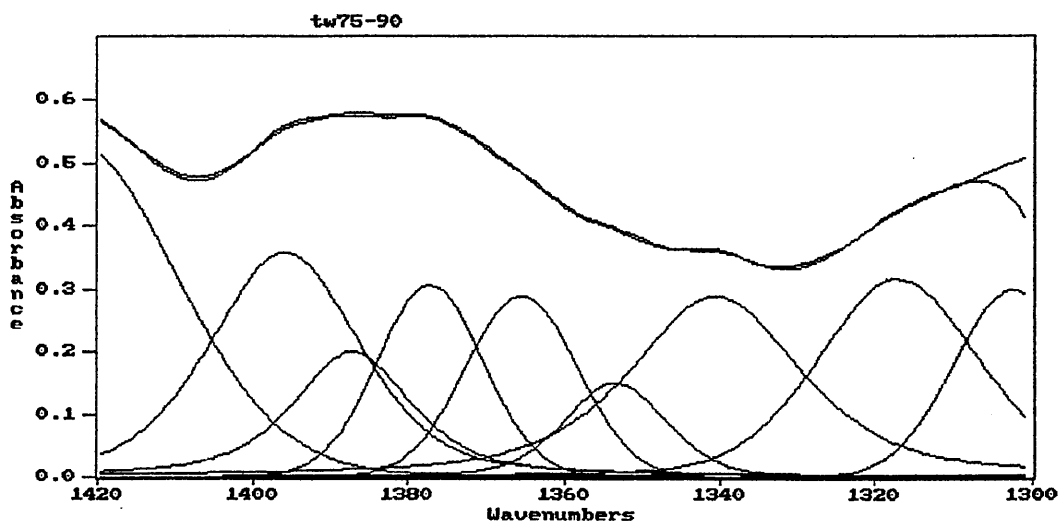


Figure 4.19. Curve fit from 1420 - 1300 cm⁻¹

The average areas of the kink (1366 cm⁻¹), end gauche (1341 cm⁻¹) and double gauche (1354 cm⁻¹) peaks were ratioed against the average area of the methyl peak fitted at 1378 cm⁻¹. Use of area ratios compensates for variable sample thickness or variations in the intensity of the infra red source between different sample runs.

From the work of Senak [17] it was shown that the ratioed areas for end gauche, kink and double gauche occurred in the ranges shown in the diagram below (Fig 4.20.). The ratioed area range for DB26 and TW75 are also shown for comparison, while the actual variation of number of conformations vs temperature is shown in (Fig 4.21.). The range

of the values shown corresponds to the variation in the number of conformers with temperature.

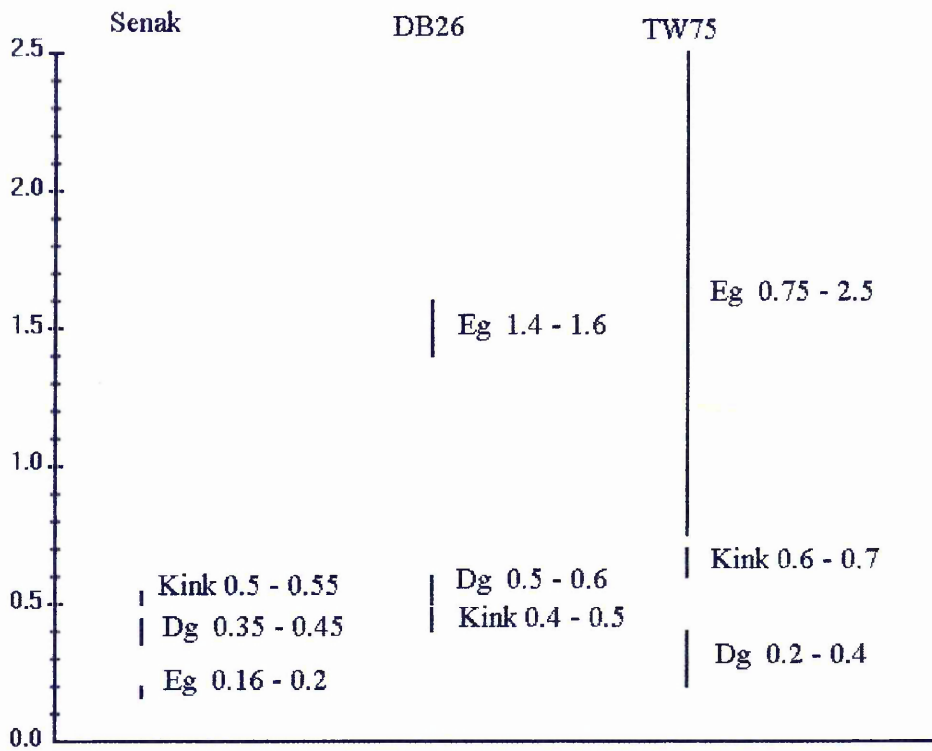
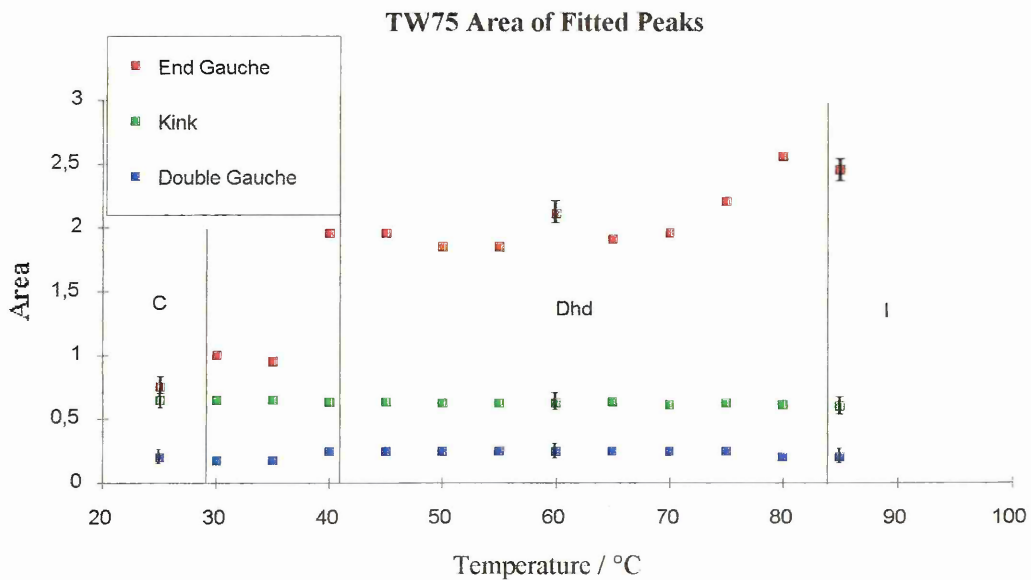


Figure 4.20. Numbers of various conformers per molecule.



DB26 Area of Fitted Peaks

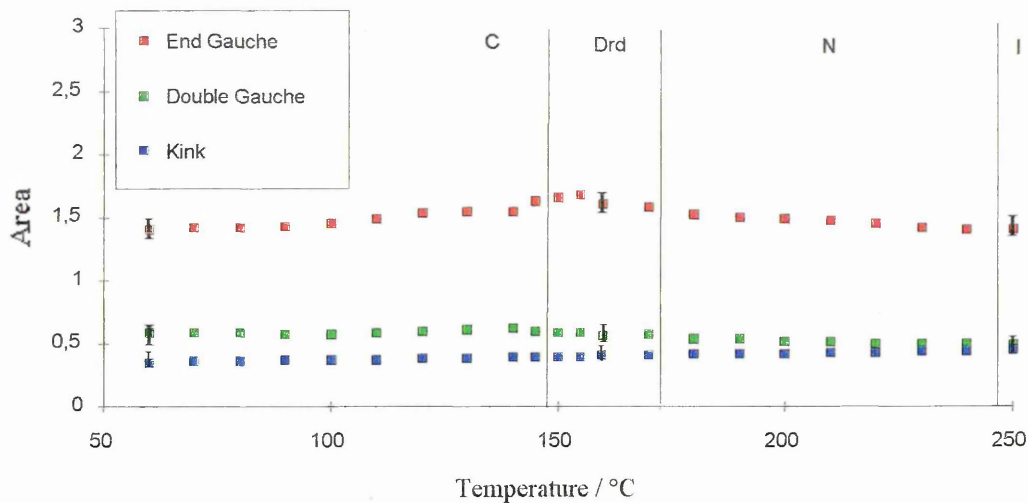


Figure 4.21. Comparison of ratioed areas for TW75 and DB26.

Comparing the DB26 and TW75 samples (Fig 4.21.) it was found that :

- The ratioed areas for kink conformations for DB26 give similar values when compared with values calculated using the rotational isometric state (RIS) model, although the double gauche number was slightly larger than the calculation (Fig 4.20.).
- There was a marked decrease in the end gauche intensity for TW75 when cooled from the liquid crystal mesophase to the crystal phase (Fig 4.21.).
- The ratioed areas for the end gauche vibrations for both DB26 and TW75 were much larger than values from the RIS model [17].

RIS $eg = 0.18$

Expt $eg = 1.4 - 1.6$ for DB26

Expt $eg = 1 - 2.5$ for TW75

There are significantly more end gauche vibrations in the discotic liquid crystals than the RIS model calculates. The end gauche conformation appears to be favoured more by these discotic liquid crystal molecules than for the alkanes, with the vibrational intensity for TW75 being greater than DB26.

With the arms interdigitated, steric hindrance from the central triphenylene core of the molecule may cause the last carbon unit in the arm to assume an end gauche conformation, increasing the arm interdigitation and increasing the molecular packing density.

- For DB26 the double gauche conformation is favoured over the kink, while for TW75 the kink is favoured more than the double gauche.

The reason why this is so may be explained by the fact that the alkyl arms of TW75 are planar with respect to the core. A double gauche conformation therefore results in an approximately 90° bend in the arm perpendicular to the plane of the triphenylene core. This will obviously cause interference with adjacent molecules and produce large steric hindrance effects. The kink conformation maintains the planarity of the alkyl arm and is thus easier to accommodate.

In the case of DB26 the ester benzoate linkage causes the plane of the alkyl arms to be rotated by about 56° relative to the plane of the core (Section 5.3. Computer modelling). A 90° bend in the alkyl arm is no longer perpendicular to the plane of the central core and this conformation is more easily accommodated.

The kink conformation still remains in the plane of the alkyl arm, but because this plane is now rotated it will interfere with molecules in the layer above. Thus it occurs slightly less frequently than the double gauche conformation in DB26.

4.7. FTIR studies on aligned samples.

Using the alignment methods described earlier (Chapter 2.4.3.), namely a rubbed PVA layer and vacuum deposited SiO films it was hoped that FTIR investigation of the vibrations in the plane of the cell could be carried out. The in plane vibrations would thus cause a larger absorbance in the aligned sample, while out of plane vibrational intensities should reduce. The two alignment methods orientate the liquid crystal in different (perpendicular) directions.

4.7.1. Use of PVA alignment.

Due to the fact that the PVA was dissolved in water, it was not possible to coat the KBr plates with PVA as they would be dissolved. Calcium Fluoride (CaF₂) plates were used instead. Large CaF₂ plates were taken and cleaved to the required size of 5mm x 15mm. The plates were cleaned with DCM and ethanol before being dipped in the PVA solution and allowed to dry for 24 hours. The PVA coated both surfaces of the plates, so one coating was carefully removed from the CaF₂ plates and the other layer was gently rubbed with a lens tissue along the plate long axis to produce the grooves that would induce alignment within the liquid crystal.

A sample cell containing only 2 CaF₂ plates coated on their inside surfaces was placed in the spectrometer to determine the absorbance of the PVA layer. Unfortunately the PVA layers were too thick and reduced the intensity of the transmitted beam to such a point that subtracting the background spectrum from a sample spectrum would have left virtually nothing. The PVA film also contained a large amount of water which resulted in a complex spectrum that proved too difficult to subtract from the sample spectrum (Fig 4.22.).

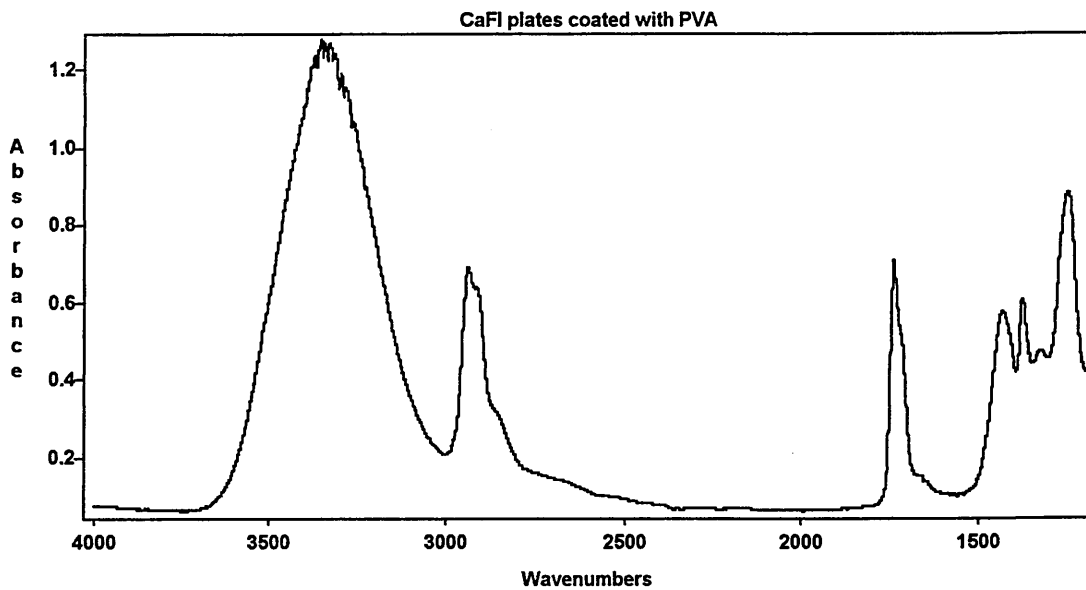


Figure 4.22. PVA I.R. absorbance.

Use of the PVA aligning layer was not feasible for FTIR analysis.

4.7.2. Use of SiO alignment.

13mm KBr plates were coated with a thin layer of evaporated SiO using the procedure described earlier (Chapter 2.4.3.).

SiO is relatively transparent to infra red radiation from 10 000 - 1500 cm^{-1} , while at approximately 1500 cm^{-1} there is a very strong absorbance. The SiO layers were very thin evaporated films of between 70 - 100 Å. It was hoped that due to the thinness of the film the majority of the infra red radiation could be transmitted through the layers.

KBr plates coated with SiO were investigated using IR spectroscopy. There was evidence of absorbance below 1500 cm^{-1} but the spectra had a fairly low intensity and a simple structure (Fig 4.23.) which proved easy to subtract from sample spectra.

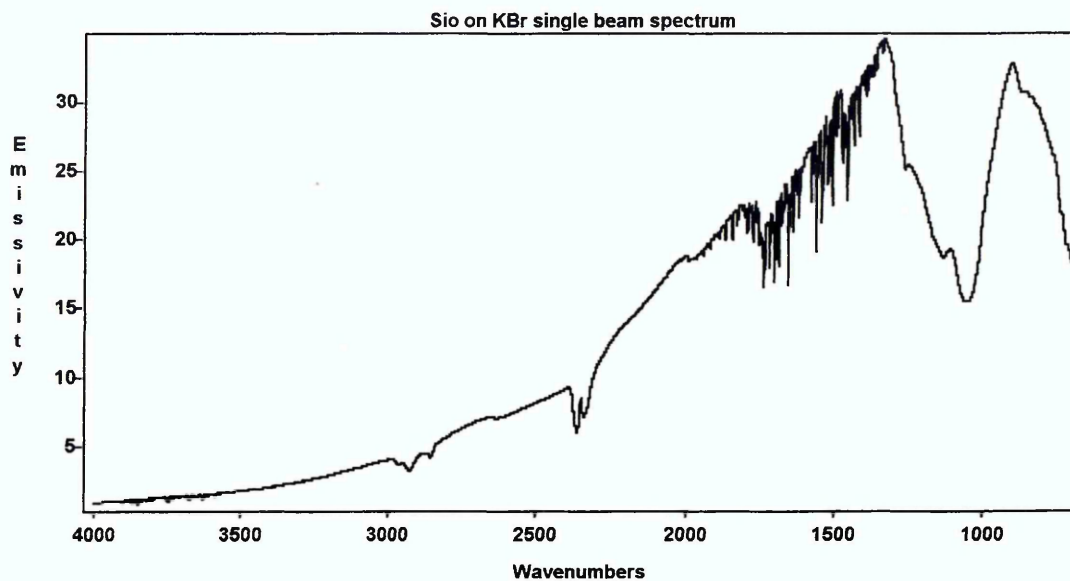


Figure 4.23. SiO evaporated film - single beam spectrum.

The KBr plates coated with SiO were heated to 250°C to determine the effect of temperature on the SiO spectra: no obvious changes were observed. Samples were prepared and investigated in the aligned nematic phase using FTIR spectroscopy.

4.7.3. Effect of SiO layer on sample alignment.

Evaporated SiO films produced alignment of discotic liquid crystals between glass cover slips (Chapter 2.4.3.). The same coating on KBr should also align the liquid crystal. If the aligned sample is then investigated using I.R. spectroscopy certain vibrations in the plane of the radiation will increase in intensity, whilst other out of plane vibrations should decrease. Comparison of the spectra of aligned and unaligned samples will highlight these vibrations which may be identified.

The major I.R. peaks have already been assigned (Chapter 4.5.1. Page 103). By comparing two I.R. spectra at the same temperature, one from the unaligned sample and the other from the SiO aligned sample, the changes in peak intensities could be clearly observed (Fig 4.24.).

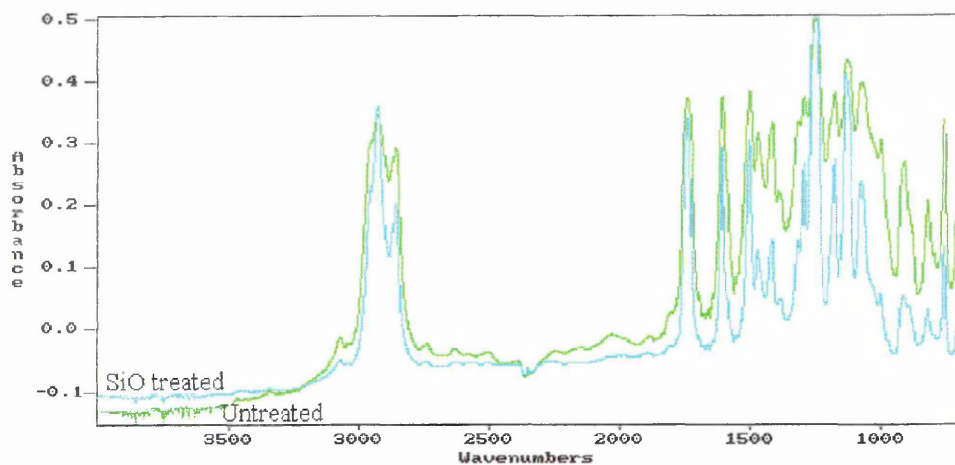


Figure 4.24. SiO aligned and unaligned samples of DB118 at 190°C.

The following table of results was produced (Table 4.3.).

| cm ⁻¹ | ABS | | |
|------------------|------|----------------------------------|------------------------------|
| 1072.62 | 0.45 | Aromatic in plane C-H | Decrease intensity |
| 1128.39 | 0.50 | Ester benzoate C-O | Increase intensity + sharper |
| 1173.99 | 0.44 | Ester C-O + C=O | No Change |
| 1244.89 | 0.56 | Alkane skeletal | Increase intensity |
| 1291.13 | 0.43 | Ester benzoate C-O | No Change |
| 1314.78 | 0.39 | CH ₂ wagging | Decrease intensity |
| 1380.01 | 0.25 | Alkane C-H | Decrease intensity |
| 1384.27 | 0.25 | Alkane C-H | Decrease intensity |
| 1388.54 | 0.25 | Alkane C-H Methyl | Decrease intensity |
| 1453.73 | 0.31 | Aromatic /Alkane methyl | Decrease intensity |
| 1467.84 | 0.36 | Alkane -CH ₂ - | Decrease intensity |
| 1501.38 | 0.44 | Aromatic C=C | No Change |
| 1604.55 | 0.43 | Aromatic C=C | No Change |
| 1731.09 | 0.40 | Ester C=O | Increase intensity |
| 1736.25 | 0.42 | Ester C=O | Increase intensity |
| 1741.07 | 0.42 | Ester benzoate C=O | Increase intensity |
| 2856.81 | 0.33 | Alkane CH ₂ methylene | No Change |
| 2927.75 | 0.39 | Alkane CH ₂ methylene | Increase intensity |

Table 4.3. Effect of SiO alignment on vibrational intensity.

The most obvious difference between the two spectra is to be observed in the peak at 1244.9 cm^{-1} . This peak arises from vibrations along the alkane skeleton. In the SiO aligned sample these vibrations are the most intense, having the largest absorbance. There is approximately a 50% increase in intensity comparing the aligned sample with the unaligned sample.

The peak at 1128.4 cm^{-1} shows a similarly large increase of approximately 50% in absorbance. The 1128.4 cm^{-1} vibration is associated with the C-O ester benzoate bending vibrations.

The increase in intensity of these vibrations would indicate that the plane of the alkane skeleton is orientated perpendicular to the plane of the I.R. cell and the C-O-C component of the ester benzoate linkage is also perpendicular to the plane of the cell. This situation can occur if the plane of the triphenylene core is perpendicular to the SiO treated surface and the plane of the benzene ring of the ester benzoate linkage is also perpendicular to the surface. Rotation of the plane of the benzene ring will increase the molecule's internal energy, but the total energy of the molecule and the SiO surface will be a minimum.

The two peaks either side of the alkane skeleton (1244 cm^{-1}) both arose from ester vibrations, 1291.1 cm^{-1} ester benzoate C-O and 1174.0 cm^{-1} ester C-O-C stretching antisymmetric vibration. Both increased in intensity by approximately 20% in the aligned sample. As well as increasing in intensity both these peaks also sharpened, narrowing in width.

4.8. Order parameter determination.

4.8.1. Background theory.

The order parameter of a liquid crystal sample may be determined using FTIR, by ratioing the areas of certain specific peaks. Kurk *et al* [19] determined the order parameter of various components of hexapentyloxytriphenylene (H5T) using this method. They used aligned samples, the alignment being achieved by using silicon windows and repeated heating and cooling cycles to give good alignment. The area of the peak being investigated was calculated and ratioed against the area of the same peak in the isotropic phase, allowing the dichroism ratio to be calculated, from which the order parameter could then be determined.

Kurk *et al* [19] were able to determine the order parameter for the C-C aromatic stretching vibration near 1617 cm^{-1} , the CH aromatic out of plane vibration at 837 cm^{-1} , the C-O-C stretching symmetric vibration near $1000\text{-}1100\text{ cm}^{-1}$.

4.8.2. Neff's method of analysis.

Using Neff's method of analysis [20] (Fig 4.25.) shows the interaction of an unpolarised beam with a discotic material.

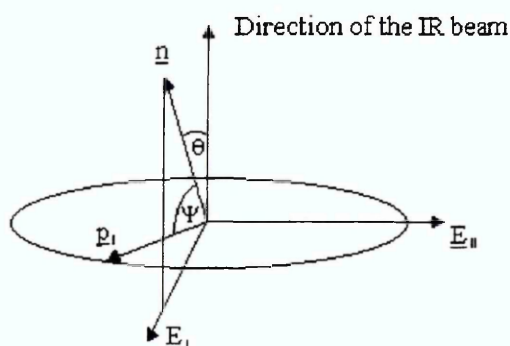


Figure 4.25. Interaction of an unpolarised I.R. beam with a discotic material.

θ is the angle between the normal to the plane of the aromatic core the director \underline{n} and the direction of the incident I.R. beam.

Ψ is the angle between the normal to the plane of the core and the direction of the dipole moment vector \underline{P}_i .

Ψ depends on the conformation of the alkyl tails for CH_2 and CH_3 vibrations and is approximately the same for core vibrations of different molecules.

θ is different for different molecules and its average value determines the order parameter of the central part of the core.

The dichroism ratio R_i for an unpolarised beam is defined as follows :

$$R_i = \frac{I_D}{I_I}$$

I_D = integrated absorbance for the peak in the discotic phase.

I_I = integrated absorbance for the peak in the isotropic phase.

The order parameter is defined as :

$$S = 1 - \frac{3}{2} \langle \sin^2 \theta \rangle$$

Rearranging, $\langle \sin^2 \theta \rangle = \frac{2}{3}(1 - S)$

Using Neff's calculations for unpolarised radiation :

$$I_D = \cos^2 \Psi \langle \sin^2 \theta \rangle + \frac{1}{2} \sin^2 \Psi \langle 1 + \cos^2 \theta \rangle$$

$$I_I = \cos^2 \Psi \langle \sin^2 \theta \rangle_I + \frac{1}{2} \sin^2 \Psi \langle 1 + \cos^2 \theta \rangle_I$$

I_D - Discotic Phase, I_I - Isotropic phase.

In the isotropic phase :

$$\langle \sin^2 \theta \rangle_I = \frac{2}{3} \quad \langle \cos^2 \theta \rangle_I = \frac{1}{3}$$

Substituting into the equation for I_I , one obtains

$$I_I = \frac{2}{3}(\cos^2 \Psi + \sin^2 \Psi)$$
$$I_I = \frac{2}{3}$$

Therefore

$$R_i = \frac{I_D}{I_I} = \frac{\cos^2 \Psi \langle \sin^2 \theta \rangle + \frac{1}{2} \sin^2 \Psi \langle 1 + \cos^2 \theta \rangle}{\frac{2}{3}}$$

Assuming $\Psi = 90^\circ$, and using the previous expression for the order parameter leads to

$$R_i = 1 + \frac{1}{2}S$$
$$S = 2(R_i - 1)$$

This order parameter expression for $\Psi = 90^\circ$ can be used for calculating the order parameter of C-C in plane vibrations of a benzene ring (1617 cm^{-1}) and the C-O-C stretching vibrations of the ester benzoate linkage (1174 cm^{-1} and $1000\text{-}1100 \text{ cm}^{-1}$)

If the calculations are repeated for the case of $\Psi = 0^\circ$ the order parameter becomes $S = 1 - R_i$. This result can reasonably be applied to CH out of plane vibrations of the benzene ring (837 cm^{-1}).

4.8.3. Order parameter results

A number of spectra were collected for DB118 between untreated KBr plates and SiO treated KBr plates. The samples were heated and spectra were taken at 5°C intervals during the cooling cycle. The samples were cooled slowly, at approximately 1 °C min⁻¹. The KBr cell was allowed to stabilise at the desired temperature for 15 minutes before the IR absorbance spectrum was recorded.

A comparison of the sample spectrum from the isotropic phases and spectra from the discotic phase allowed peaks that changed from one phase to the other phase to be identified.

Comparing the different results at each temperature it was obvious which peaks had increased or decreased.

From these results the order parameter for various molecular components could be calculated. The calculations for the order parameter required the dichroism ratio R_i to be calculated. The integrated absorbances of each of the peaks at each temperature were calculated and then ratioed against the integrated absorbance of the isotropic phase yielding the dichroism ratio from which the order parameter was then calculated. Plots of order parameter against temperature were determined for compounds from the DB and PH series.

Order parameters for the TW series of compounds could not be determined using this method as these compounds aligned poorly or not at all on the SiO treated KBr plates, suggesting that the ester benzoate linkage plays a major role in the alignment process.

From Neff's model [20] (Fig 4.25) when the angle $\Psi = 0^\circ$ the director \underline{n} is perpendicular to the direction of the IR beam the order parameter $S = 1 - R_i$. When $\Psi = 90^\circ$ the

director \underline{n} is parallel to the IR beam direction and the order parameter $S = 2(R, -1)$ (Fig 4.26)

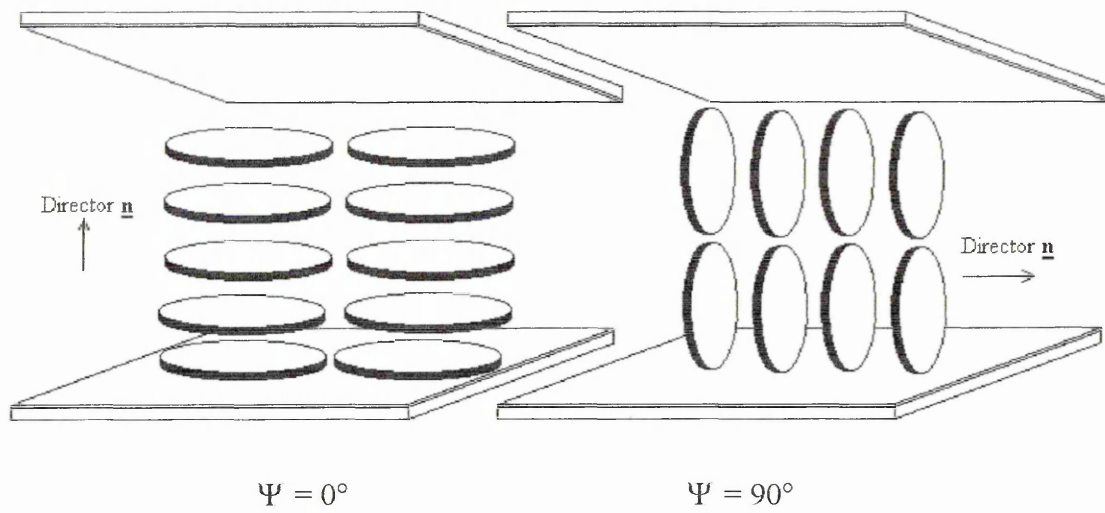


Figure 4.26 Order Parameter variation with the angle Ψ

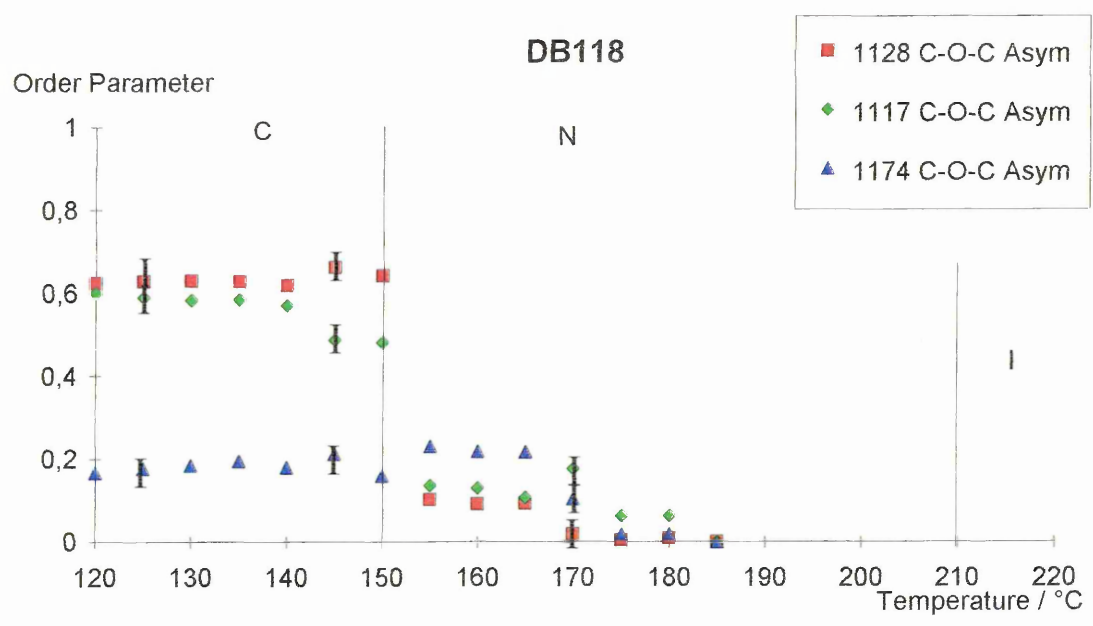


Figure 4.27.a Order Parameters for DB118

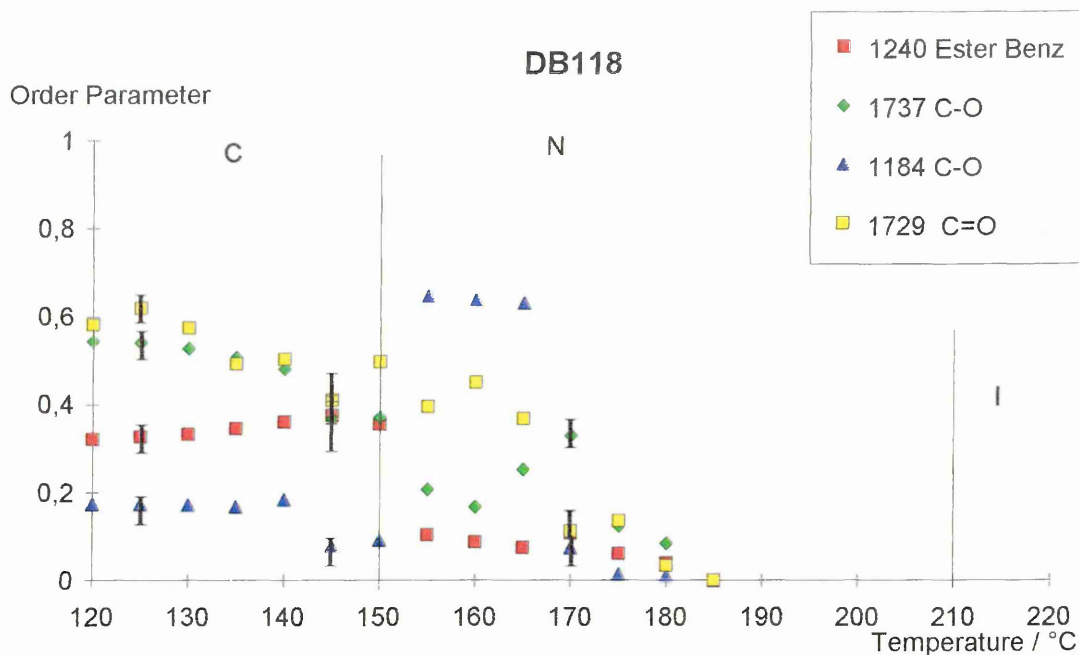


Figure 4.27.b Order Parameters for DB118

Figure 4.27.a shows the C-O-C antisymmetric vibration for DB118. Although the C-O-C bonds are connected directly to the triphenylene core, the direction of the dipole moment for these vibrations is not exactly parallel to the plane of the core and varies with molecular conformations. Therefore the order parameter measured for these vibrations will actually be smaller than the order parameter from the core. The order parameters for the C-O-C antisymmetric vibrations 1117 cm^{-1} , 1128 cm^{-1} and 1174 cm^{-1} were approximately 0.2 in the liquid crystal phase, indicating a poorly ordered structure. The C-C aromatic stretching vibration at 1617 cm^{-1} which would allow the order parameter of the core to be directly determined could not be analysed separately due to the large intensity of this band and the neighbouring aromatic C=C vibration at 1604 cm^{-1} . The two bands overlapped greatly, making curve fitting of this region of the spectrum quite difficult.

A number of different curve fits in this region were possible, each resulting in different values for the areas of the C-C and C=C components. It was impossible to determine which of these curve fitting models was an accurate representation of the actual bands to be used in the further analysis.

It should be noted that the C-C band around 1617 cm^{-1} not only contains information from the triphenylene core of the molecule, but also information about the conformation of the benzene ring in the ester benzoate linkage and is the average of components from these to molecular regions.

From the graph (Fig 4.27.a) for the C-O-C asymmetric vibrations, the nematic to crystal transition at $\approx 150^\circ\text{C}$ can be clearly seen as an increase in the order parameter from the 1117 cm^{-1} and 1128 cm^{-1} peaks. One component of the C-O-C asymmetric vibration at 1174 cm^{-1} shows less disorder, while the other C-O-C vibrations at 1117 cm^{-1} and 1128 cm^{-1} show enhanced order on cooling, especially after the liquid crystal to crystal phase transition. This may indicate reduced rotation of the benzene on the ester benzoate linkage as the sample cools. The loss of flexibility in the molecular arms begins first by fixing the bulky ester benzoate components, indicated by the relatively high value for the C-O-C order parameters (0.6).

This increase in the order parameter at 170°C is also observed for the other vibrations, namely, 1184 cm^{-1} C-O, 1737 cm^{-1} C-O and 1729 cm^{-1} C=O vibrations (Fig 4.24.b). The transition from nematic to crystal is also clearly observable on this graph, the C-O 1737 cm^{-1} and ester benzoate 1240 cm^{-1} vibrations each showed an increase in the order parameter from approximately 0.2 to 0.4 and 0.5 respectively in the crystal phase, indicating short range order.

For DB125 the C=C and C-C vibrations at 1506 cm^{-1} , 1607 cm^{-1} and 1623 cm^{-1} were not as intense as the DB118 sample, probably arising from steric hindrance effects of the methyl groups on the ester benzoate linkage of DB125 which points towards the triphenylene core. The spectra were able to be easily fitted, allowing the areas of each vibration to be determined and in turn the order parameter for these vibrations calculated (Fig 4.28.a).

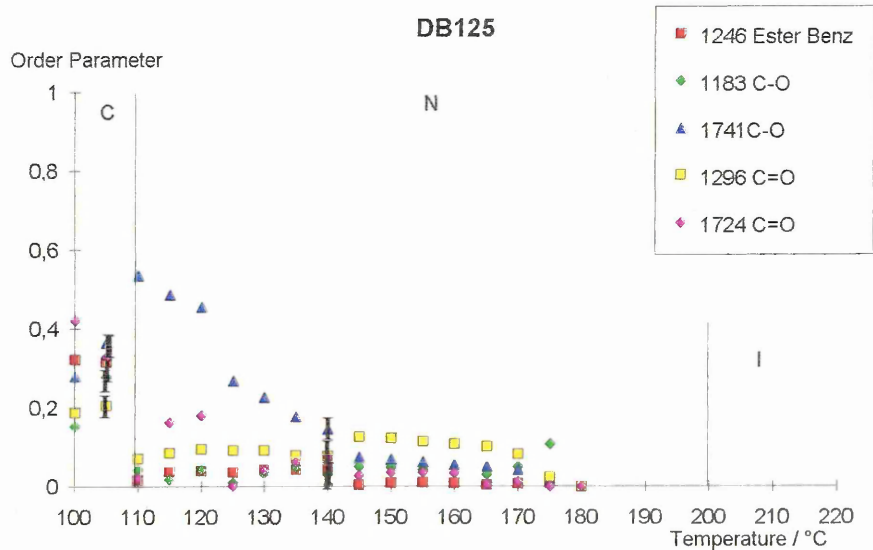
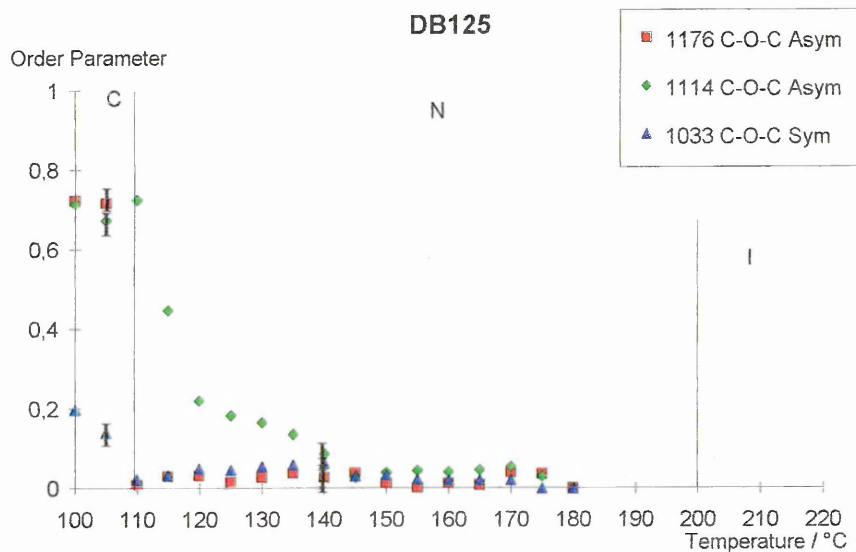
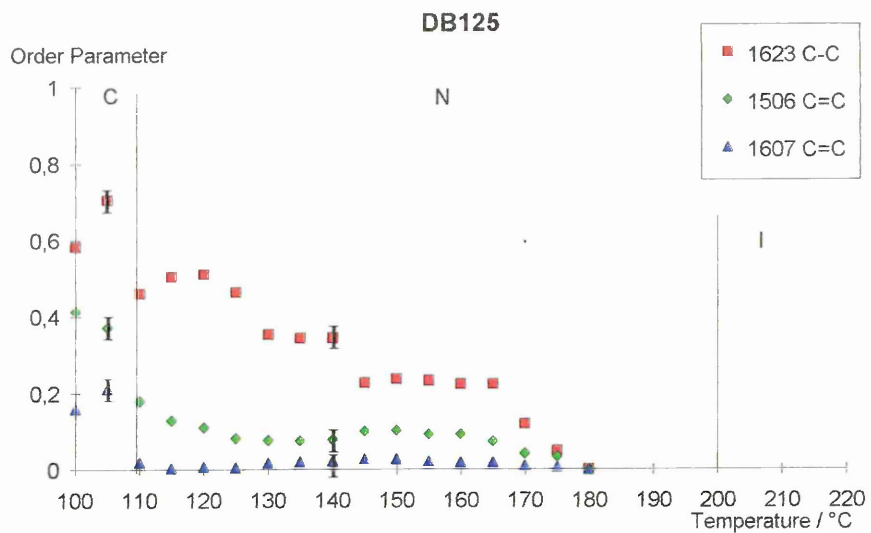


Figure 4.28 Order Parameters for DB125

The C-C 1623 cm^{-1} vibration gives an order parameter of 0.7 - 0.8 in the crystal phase, although the C=C vibrations only resulted in order parameters of 0.2 and 0.4 in the crystal phase.

The C=C vibrations observed in the sample arise from both C=C vibrations of the triphenylene core of the molecule and from the C=C vibrations in the benzene ring of the ester benzoate linkage. Order parameters from other components from the molecule indicated that the structure is highly ordered in the crystal phase, with order parameters greater than 0.7 for C-C 1623 cm^{-1} , C-O-C antisymmetric 1176 cm^{-1} and antisymmetric 1114 cm^{-1} vibrations, while the C-O-C antisymmetric 1114 cm^{-1} (Fig 4.28 - 2 and 3).

This indicates that while the triphenylene core of the molecule may be highly ordered, indicated by the high order parameter for the C-O-C vibrations, the benzene rings of the ester benzoate linkages are not so highly ordered and are able to take up a number of conformations, indicated by the lower order parameters for the C=C and C=O vibrations. The ester benzoate linkage of DB125 has a methyl group attached, which points towards the core region of the molecule (Fig 4.29).

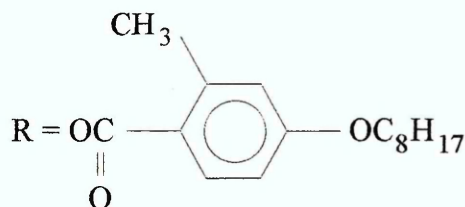


Figure 4.29 DB125

As the sample crystallised this ester benzoate linkage, due to steric hindrance between the CH₃ group and the triphenylene core, may take two possible conformations relative to the plane of the triphenylene core, approximately 53° above the plane of the core or 53° below the plane of the core (Fig 4.30), the angle having been determined using the Cerius 3.2 computational chemistry software (Chapter 6).

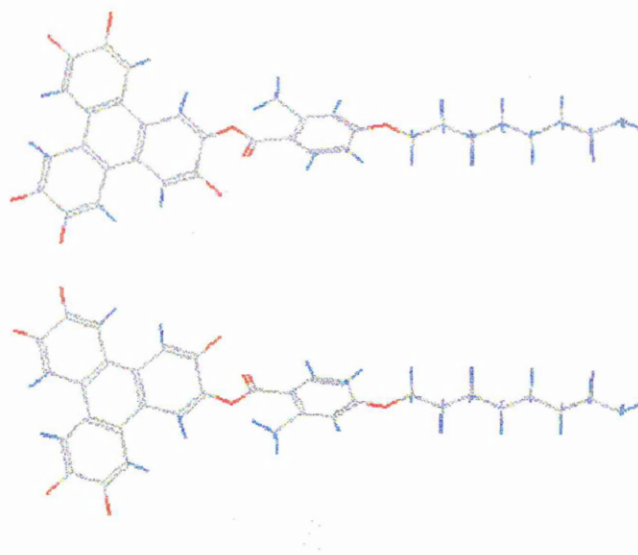


Figure 4.30 The two possible conformations of the DB125 ester benzoate linkage

The different possible conformations of the benzene ring in the ester benzoate linkage relative to the plane of the triphenylene core results in a reduced order parameter for the C=C vibrations. As the sample was cooled from the isotropic phase the order parameter for the C=C vibrations increased gradually, although between 110°C and 105°C, the nematic to crystal phase transition, there was a sudden increase in the order parameter. This increase is also observed for the C-O-C antisymmetric vibrations at 1033 cm⁻¹ and 1176 cm⁻¹, the ester benzoate vibration at 1246 cm⁻¹ and the C-O, C=O vibrations at 1183 cm⁻¹, 1296 cm⁻¹ and 1724 cm⁻¹ (Fig 4.28 Graphs 2 and 3).

The C-O-C antisymmetric vibration at 1176 cm⁻¹ showed the greatest increase in the order parameter at the nematic to crystal phase transition, an increase from an order parameter of less than 0.1, highly disordered, to an order parameter of 0.7, highly ordered. For the C-O-C antisymmetric vibrations (Fig 4.28 Graph 2) the order parameter was measured as 0.7 for the 1176 cm⁻¹ vibration and 0.7 for the 1114 cm⁻¹ vibration. The C-O, C=O and ester benzoate vibrations (Fig 4.28 Graph 3) did not show a very large order parameter in the crystal phase. The C=O vibration at 1296 cm⁻¹ only had an order parameter of 0.2, while the C=O vibration at 1724 cm⁻¹ had an order

parameter of 0.4. This would seem to suggest that these two vibration modes are orthogonal. As mentioned previously, due to steric hindrance effects between the methyl group and the triphenylene core, the ester benzoate linkage may be in two possible conformations. This in turn leads to the C=O taking two possible conformations relative to the plane of the triphenylene core. When the cores are aligned with their directors parallel to the plane of the KBr cell, then the two following modes of vibration for the C=O will be detected (Fig 4.31).

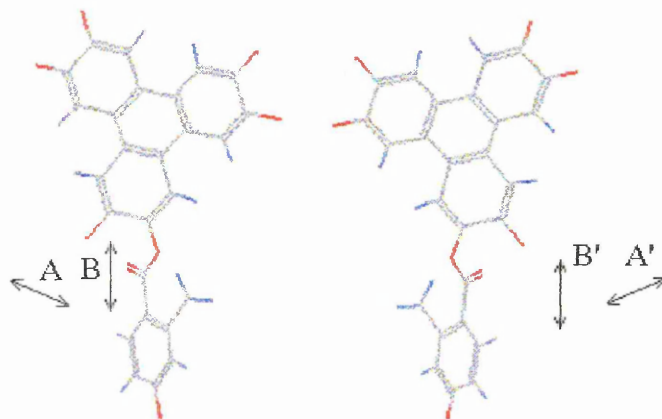


Figure 4.31 Two possible vibration modes for C=O

Due to the different orientations of the C=O relative to each other, the vibrations A and A' combine to give a resultant vibration where the magnitude will be less than each component, whereas the B and B' vibrations will result in a larger order parameter. The A and A' vibrations correspond to the C=O 1296 cm^{-1} vibration, while the B and B' vibrations correspond to the 1724 cm^{-1} vibration.

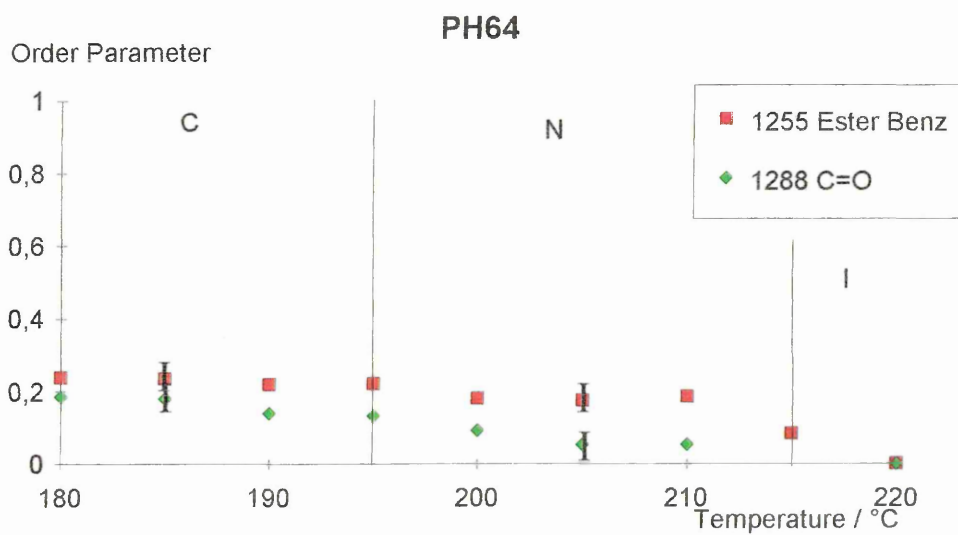
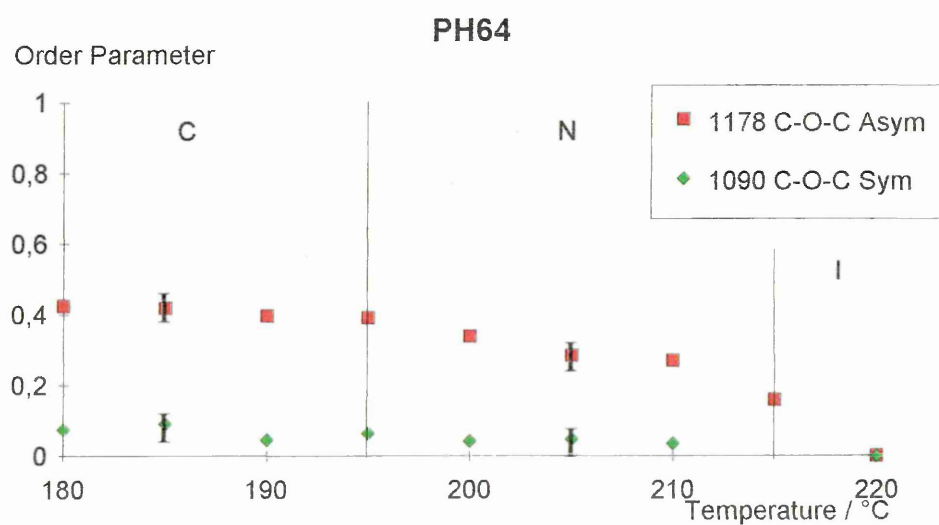
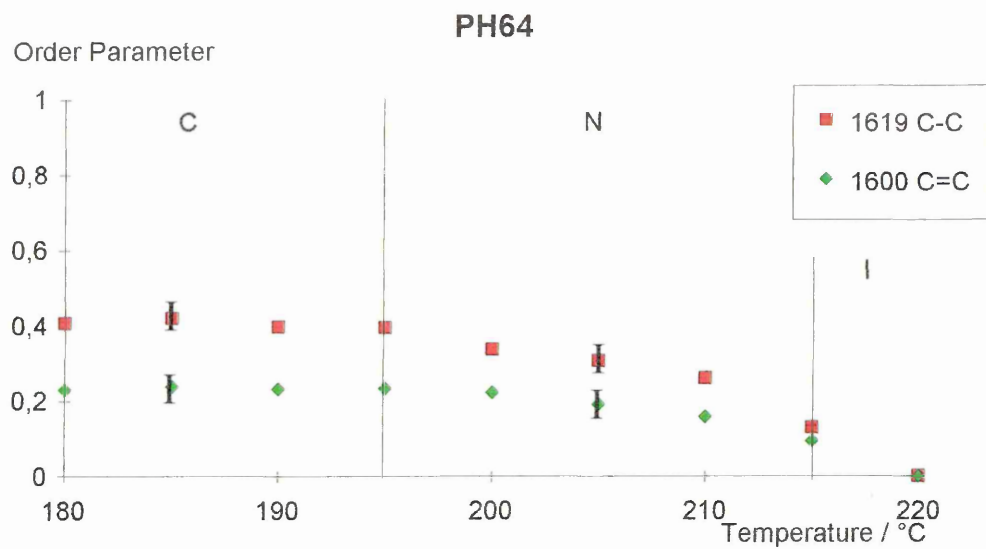


Figure 4.32 Order parameters for PH64

PH64 showed order parameters lower than DB118 or DB125 (Fig 4.32). Fig 4.32 Graph 1 shows the order parameter for C=C and C-C bonds. There is no obvious increase of the order parameter at the nematic to crystal transition. From the isotropic phase there is a gradual increase of the order parameter to 0.4 on cooling through the nematic phase for the C-C 1619 cm^{-1} vibration. The C-O-C asymmetric vibration at 1178 cm^{-1} (Fig 4.32 Graph 2) also gives a maximum of ≈ 0.4 for the order parameter in the crystal phase.

The ester benzoate vibration at 1255 cm^{-1} and the C=O vibration at 1288 cm^{-1} (Fig 4.32 Graph 3) only give order parameters a little larger than 0.2, indicating that the PH64 sample was only poorly aligned by the SiO surface treatment of the KBr plates.

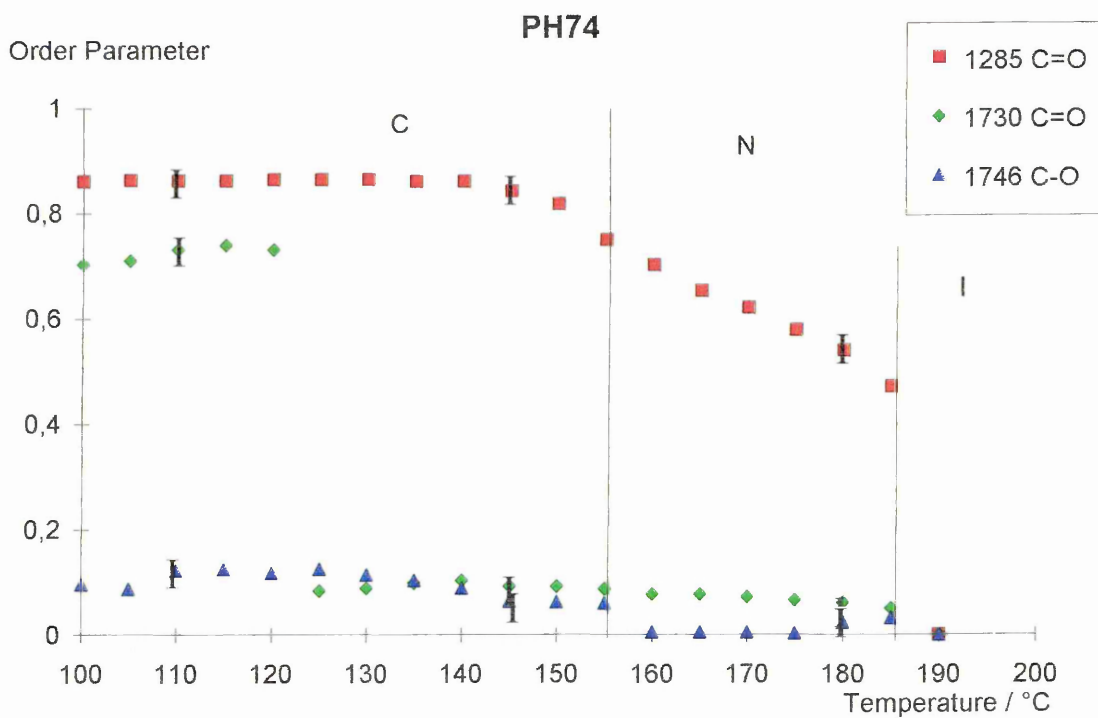
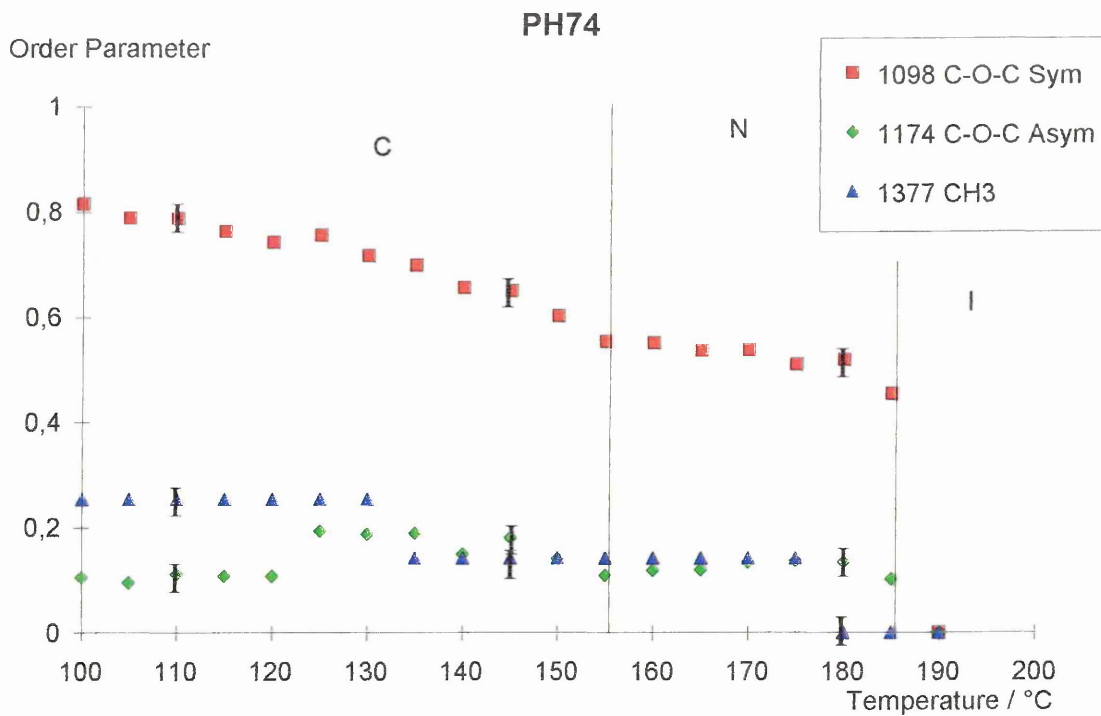


Figure 4.33 PH74 Order Parameters

PH74 showed a very small order parameter, 0.1, for the C-O 1746 cm^{-1} vibration, while the C=O vibration at 1730 cm^{-1} resulted in a maximum order parameter of 0.7 in the crystal phase. It should be noted that there was a large jump in this order parameter

from 0.1 to 0.6 between 125°C and 120°C, this increase was well below the nematic to crystal transition temperature, indicating a possible crystal to crystal transition.

For PH74 it was also possible to determine the order parameter for the CH₃ vibration at 1377 cm⁻¹. PH74 is similar in structure to PH64, with two methyl groups attached to the benzene ring of the ester benzoate linkage pointing away from the triphenylene core. There is also an additional methyl (CH₃) group attached to the first carbon atom of each alkyl arm (Fig 4.34)

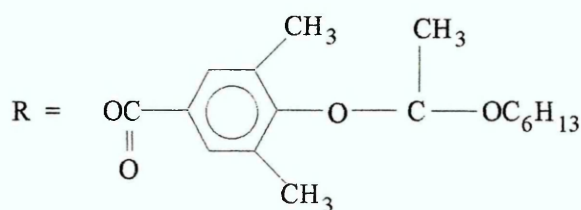


Figure 4.34 PH74

The order parameter that was obtained for the CH₃ group is probably directly related to the ordering of the CH₃ unit on the alkyl arm. With PH64 the CH₃ vibration was very weak, but for PH74 the vibration was clear and easy to fit. When the triphenylene cores are aligned edge-on this CH₃ group will be perpendicular to the IR beam and the intensity of IR absorbance will be stronger than from the other CH₃ vibrations.

There is also an increase in the CH₃ order parameter between 135°C and 130°C on cooling, which occurs before the change in the C-O-C antisymmetric 1174 cm⁻¹ and C=O 1730 cm⁻¹ vibrations which were observed between 125°C and 120°C. It appears that within the crystal phase further ordering of the structure occurs as the sample cools, initiated by an increased ordering of CH₃ between 135°C and 130°C which in turn results in a slight decrease of the C-O-C order parameter and a large increase of the C=O order parameter between 125°C and 120°C.

4.8.4. Order parameter conclusion

The order parameters for the ester benzoate linkage of DB118, DB126, PH64 and PH74 were presented in the previous section (See figures 4.27, 4.28, 4.32 and 4.33). From these results it was possible to observe the behaviour of the ester benzoate linkage using the ester benzoate, C-O-C symmetric and antisymmetric and C=O vibrations. Observing how the order parameters of these separate vibrations changed with decreasing temperature it was possible to speculate how the order parameter of the ester benzoate group must follow the same basic pattern as displayed by the individual components.

At the nematic to crystal transition temperature, small increases in the order parameter of the ester benzoate group were observed. Order parameters of between 0.6 to 0.9 were observed for ester benzoate components from approximately half way through the liquid crystalline phase, indicating quite a high degree of ordering of the ester benzoate group.

Although the samples as a whole were aligned within the liquid crystalline phase, determined using polarising optical microscopy, it was observed through the order parameter results from the I.R. analysis that parts of the molecule were not at all aligned or only aligned slightly, indicated by order parameter values less than 0.2.

It was observed how the order parameters of the various vibrations associated with the ester benzoate linkage increased as the samples were cooled through the liquid crystalline phase. This would appear to indicate that the alignment by the SiO layer was only responsible for alignment of the triphenylene cores, the molecular arms still retaining a high degree of freedom and flexibility. As the samples were cooled through the nematic phase there was a sudden increase in the order parameter of the C-O-C symmetric and antisymmetric vibrations of DB118 and DB125 approximately half way through the nematic phase, indicating that the ester benzoate linkages are now aligned as well, although the alkyl arms still retain their flexibility allowing a degree of fluidity within the sample. When the sample enters the crystal phase the alkyl arms finally lose all freedom

of movement. A further slight increase in the order parameter of the ester benzoate group is also observed to occur, probably induced by the loss of flexibility of the alkyl arms.

Chapter 5. Computer Modelling.

5.1. Introduction.

For years chemists have been creating ball and stick models of the molecules they have synthesized using various molecular building systems in order to help visualise the three dimensional shape. Working with these systems was often very time consuming and the final model was generally rather fragile. These systems allowed a fairly accurate representation of the molecules to be produced but it was often difficult to rotate the molecule in three dimensions. Small molecules could be easily held in the correct conformational position and rotated with care. As the size of the molecule increased so did the number of hands required to rotate it without disrupting the conformation, due to the high degree of flexibility and large number of links of the structure. By rigidly fixing the links either by gluing or welding in the case of metal kits the molecular representation could be made rigid and easy to handle, but this greatly increased the difficulty of making minor changes to the molecular structure.

The traditional ball and stick molecular building systems offer a simple method of producing a representation of a molecule, but have certain limitations. The number of components limits the size of the molecule that can be built, so that it is not practical to construct long chain polymers using this method, although short sections of a polymer chain are relatively easy to build.

Computers, traditionally a powerful tool for large complex calculations, may also be utilised as a powerful graphics tool by the use of various software packages especially in the area of computer aided design (CAD). A number of chemistry-orientated CAD style packages are available that turn the computer into a molecular building system. The essential building elements consist of bonds, atoms and parts of molecules referred to as

molecular fragments. The programs allow the user to construct any molecular representation by combining the correct sequence of atoms and bonds.

A large number of the more frequently used fragments may already be pre-defined e.g. phenyl rings, alkyl arms or methyl groups, using optimised parameters for bond lengths and angles. Users are also able to build their own library of fragments, which can be recalled at a latter date and used in the building of new molecules.

The use of molecular fragments increases the speed with which molecules may be built, repeated units needing only to be defined once and then copied as often as required. The computer packages also contain all the chemical information about a molecule, allowing users with a limited chemical background to build molecules with the correct chemistry. While building the molecules all the available valences are unoccupied by default - when the final model is ready, any unfilled vacancies are automatically 'hydrogen filled', saving the user the effort of manually completing the task and guaranteeing that all the vacancies are filled.

When the molecule has been built various molecular conformations can be obtained by adjusting the bond angles. Once a suitable molecular conformation has been achieved the computer model can be saved. The computer model may be easily shrunk, expanded and rotated by use of menu dials or the mouse, allowing for easy visualisation of the structure. The molecule created by the computer is a 2 dimensional representation of a 3 dimensional object.

A number of different techniques are employed by the various chemistry software packages to give the molecule a 3 dimensional quality.

1. When the molecule is rotated the effects of perspective on the view are taken into account and closer parts of the molecule are subsequently larger than parts further away.
2. The 3 dimensional nature of the computer model can be enhanced by suitable shading, lighting and ray tracing of the object to give an illusion of depth.
3. Stereo-pairs of a molecule, two separate images that correspond to left eye and right eye views of the structure are calculated and displayed.

Three methods of stereo-graphic visualisation systems exist:

1. Use of special filters (red and green) along with red and green coloured superimposed images.
2. Polaroid spectacles, where the planes of polarisation of the two lenses are mutually perpendicular and a liquid crystal display attached to the monitor rapidly alters the plane of polarisation of light from the monitor as the left and right eye images are rapidly displayed in synchronisation with the display matrix.
3. Special spectacles, which consist of twisted nematic liquid crystal lenses that rapidly switch from opaque to clear in synchronisation as the left and right eye images are flashed on the computer screen.

The simple two colour filter idea is the easiest to use, but gives a distorted view of the colours. The other two systems, although more complex, retain the true colours of the image and also give clearer image quality.

All the systems work on the same principle of only allowing the left eye to see the left stereo-graphic image and the right eye to see the right stereo-graphic image. Allowing the two eyes to view separate independent views of the molecule coupled with perspective and suitable shading fools the brain into recombining the two separate images as though they came from the same object, giving the illusion of a solid 3 dimensional object.

When the model has been created and a suitable conformation chosen, a high quality hard copy of the image can be easily output for inclusion in documents and reports.

A chemistry molecular modelling computer package offers an easy-to-use method of producing molecular representations with only a limited knowledge of chemistry. The molecules can be as large or as small as the user desires: they are not constrained by the number of parts available as with traditional ball and stick building systems. High quality images of the molecule can be produced.

A number of chemistry modelling packages offer many advanced features in addition to the visualisation interface. In particular energy minimisation routines allow the minimum energy of a molecule to be calculated and the resulting minimised structure to be displayed. A few of the more recent modelling packages even allow complete crystal structures to be built and viewed.

Two chemistry molecular modelling computer packages were used to simulate the discotic molecules. The first package, Alchemy was P.C. based and, although limited in its functions, offered an insight into what was possible with computer modelling. The second more powerful modelling software was Cerius 3.2 running on a Silicon Graphics workstation.

5.2. Alchemy.

Alchemy is a piece of chemistry software designed to run on an IBM P.C. which allows the user to build a molecular structure to help visualise its shape in three dimensions. The program offers an easy to use front end allowing easy construction of a molecule, and a range of different atom types may be chosen. The mouse is used to build the structure, with the bonds between the various atoms adjustable to single, double or triple bonds depending upon the required chemistry of the molecule. Both organic and inorganic molecules can be constructed within the computer. When a molecule has been created a wire-frame, ball and stick or a space filled version of the molecule can be displayed and rotated.

The different compounds from Hull University were entered into the program and 3-dimensional computer models produced. Initially the program was used to visualise the structure of these compounds, the bond angles being adjusted manually to obtain the alkyl chains in a fully extended configuration. Measurements of the diameter of this fully extended molecule and the diameter of the core were obtained. Due to the large size of the molecules, (approximately 250 atoms per molecule), and the number of calculations involved, the computer software was very slow when rotating the compound. Using a 486 computer equipped with a math co-processor speeded up this process, but it still required about a second of calculations in order to generate a new image rotated by a few degrees, resulting in a lot of time being required to rotate the molecule. Generating a space filled image required about five minutes of calculations (Fig 5.1.). The molecule was rotated using a low resolution wire frame model and then the space filled image was generated.

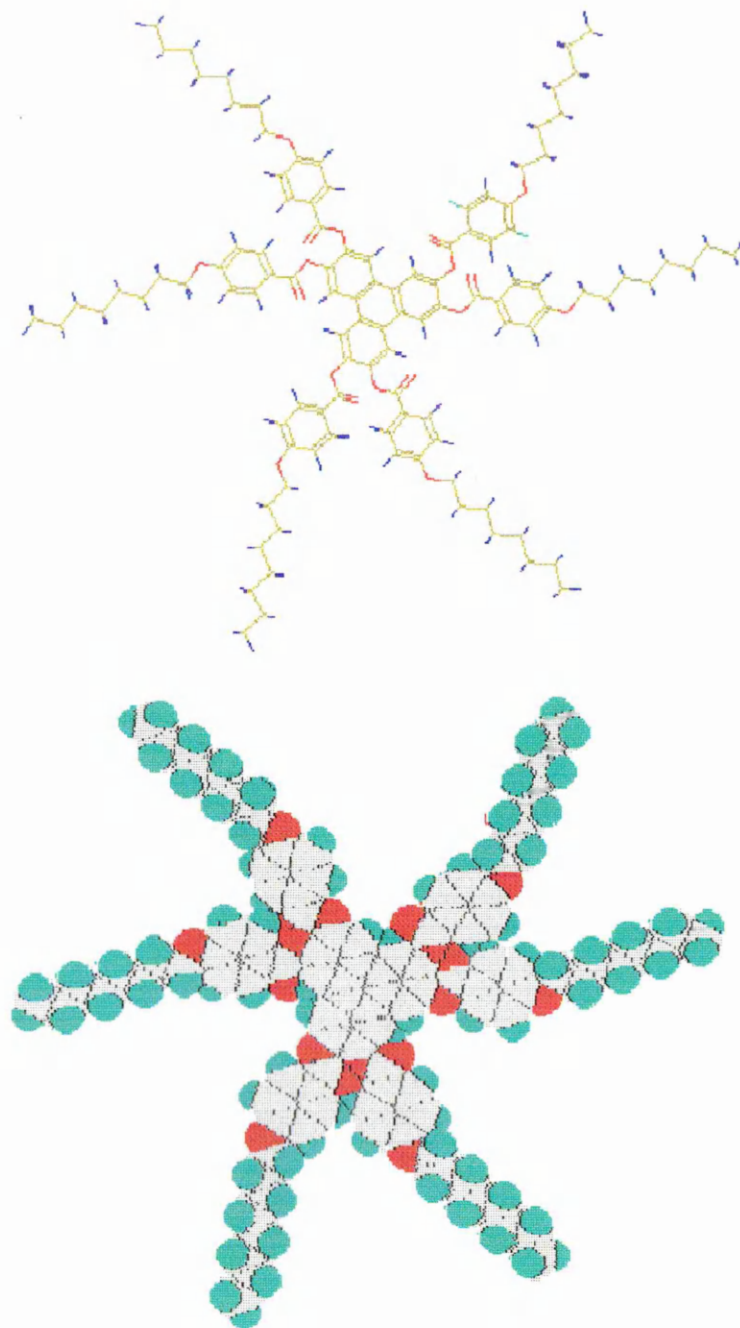


Figure 5.1. Alchemy wire-frame and space filled models DB26.

The energy minimisation routine within the package could also be used to adjust the various bond angles and distances until a minimum energy conformation for the structure was achieved. This used a molecular mechanical routine and, although it would generate a structure with a lower energy, there were a number of important limitations that the user needed to be aware of :

1. The energy minimisation routine only minimised the energy of the molecule: it did not take into account any temperature dependence or interactions between nearest neighbours, e.g. hydrogen bonding or steric hindrance caused by adjacent molecules.
2. The energy minimisation was also greatly influenced by the initial starting configuration: atoms were only adjusted slightly from their initial positions so there was the possibility that the routine would find a local energy minimum, where small adjustments to the bond angle would result in increasing energy from which it was unable to obtain the absolute minimum for example see (Fig 5.2.).

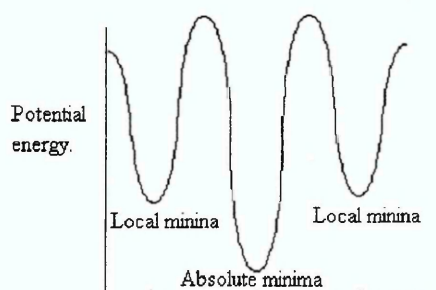


Figure 5.2. Local minimum.

The possibility of confinement to a local minimum can be reduced by minimisation of a number of different initial starting configurations in order to be sure that the conformation with the true lowest energy has been obtained.

3. Due to the number of atoms in the molecule, the energy minimisation took a long time - up to 30 hours for one starting configuration on a powerful P.C. The minimisation time was directly related to the number of calculations required, which is related to the square of the number of atoms in the molecule. By minimising smaller parts of the molecule separately, e.g. the triphenylene core, the ester benzoate linkage group and the alkyl arms, and then combining these minimised parts to form a whole molecule, the minimisation time could be greatly reduced. This two stage minimisation process reduced the total minimisation time to approximately 12 hours.

The Alchemy program was limited in the results that could be obtained, the main result being a model of a molecule from which the maximum diameter of the whole molecule and the core could be obtained. The thickness of the molecule with alkyl chains in their planar configuration was also able to be measured.

Simulated results for DB26 using Alchemy (Fig. 5.3.):

| | | | |
|----------------|---------|---------------------|---------|
| Core diameter | = 6.7Å | Molecular thickness | = 2.5Å |
| Arm length | = 11.1Å | Molecular diameter | = 39.9Å |
| Ester Benzoate | = 5.5 Å | | |

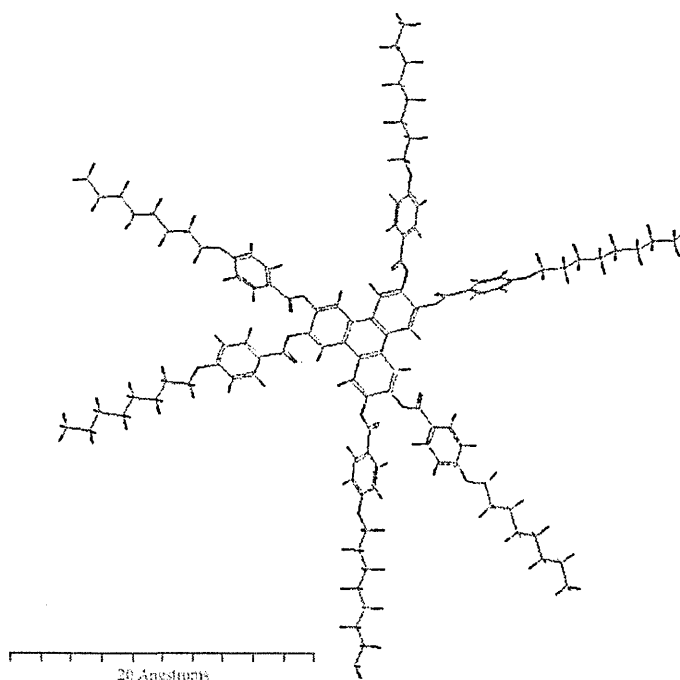


Figure 5.3. Molecular dimensions.

Taking these calculated measurements and relating them to results obtained from the X-ray diffraction data, assuming a perfect hexagonal crystal lattice, it was possible to see that even with fully extended alkyl arms the arms of adjacent molecules could interdigitate fully without interacting with the triphenylene core of the adjacent molecule (Fig 5.4.). Use of space filled models highlighted possible areas of steric hindrance, particularly between the ester benzoate linkage of one arm and the end of an arm from an adjacent molecule.

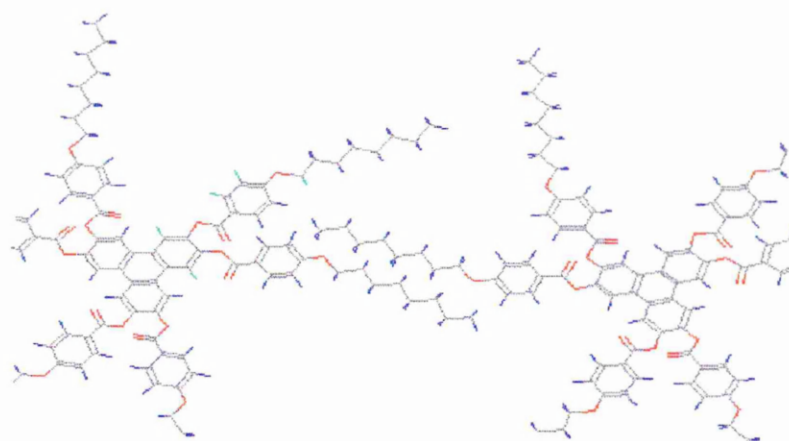


Figure 5.4. Two interdigitated molecules.

Addition of methyl groups to the ester benzoate linkage at the 2,3,5,6 positions (Fig 1.16.) would greatly increase the potential for steric hindrance and cause either the plane of the arm to twist out of the plane of the central triphenylene core or a disruption of the interdigitated arms of adjacent molecules. Unfortunately this software was limited in its calculation abilities and these possibilities were not able to be simulated.

Alchemy was initially used only to help with the visualisation of the shape of these discotic liquid crystals, but it also offered an insight into some of the possibilities that could be obtained through simulation, in particular molecular structure calculations.

In order for a more realistic model of a molecule's structure to be obtained, a more powerful energy minimisation routine was required that would overcome some of the limitations of the Alchemy routine by allowing interactions between adjacent molecules to be considered. In order that these calculations could be obtained in a relatively short period of time a more powerful computer would also be necessary. A P.C. does not have the necessary processing power, so a workstation was required.

5.3. Cerius 3.2 running on a Silicon Graphics workstation.

A number of Silicon Graphics workstations were available in the department, one of which was equipped with Cerius 3.2 molecular simulation software developed by Molecular Simulations Inc. This software was a lot more powerful and versatile than the Alchemy software, and running on a workstation allowed for more rapid calculations.

Cerius 3.2 employed a graphical user interface enabling the entire program to be operated using the mouse. Molecules could be built up from their component atoms and the various bonds adjusted as necessary. The molecule could be rotated in 3 dimensions simply by moving the mouse. The basic layout and operation of the program was similar to Alchemy, although the increased processing power allowed very fast rotation of wire-frame and ball and stick models and a reasonable rate of rotation of the space filled models. The increased processing power not only enhanced the graphic capabilities and quality of output but also allowed a more complex energy minimisation routine to be employed.

5.3.1. Energy minimisation.

The energy minimisation incorporated both molecular mechanical and molecular dynamical calculation routines. The molecular mechanical routines allowed the energy of the molecular conformations to be calculated, while the molecular dynamical routines enabled the energy of the interactions between two adjacent molecules also to be calculated. Employing both these particular calculation techniques, both conformational and some limited dynamical information about the molecule could be obtained. During the energy minimisation all the bond angles, bond lengths and unit cell parameters were

available to be adjusted, this requires a very large number of calculations, only possible on a workstation.

Cerius came equipped with a number of different energy minimisation routines based on various force field programs, DREIDING I and II [2], MM2 [3] and MMP2 [4], AMBER [5] and Universal FF [6]. These force fields are used automatically by certain modules within Cerius and allow the potential energy of specific model types to be minimised using the correct type of force field.

5.3.2. Cerius force fields.

The force fields used in Cerius are based on the energy of a structure which is defined by superposition of various two-body, three-body and four-body interactions. Analysis of these interactions allows the forces on each particular atom to be calculated and in turn optimum geometries and dynamics of motion can be calculated. Cerius has 6 main force fields designed for specific applications and a number of minor force field routines for more specialised calculations. The six main force fields are :

- 1,2 The DREIDING I and II force fields developed by Mayo *et al* [2] which may be used for structure prediction and dynamic calculations of large organic, biological and main group inorganic molecules.

- 3,4 MM2 [3,4] and MMP2 [5] force fields developed by Allinger *et al* which are particularly suitable for accurately predicting the conformations of small organic molecules up to about 20-25 atoms. They may be used to minimise much larger molecules, but as the number of atoms doubles the calculation time of the energy minimisation is squared, thus resulting in very time consuming minimisation for the larger molecules.

- 5 The AMBER force field developed by Wiener *et al* [6,7] specifically for the simulation of biological compounds, particularly proteins and nucleic acids. The only available atom types with which this force field can be used are those atoms necessary in the description of nucleic acids e.g. H, C, O, S, N and P.
- 6 The Universal FF developed by Rapeé *et al* [8], another specialised force field for specific use in the field of materials science. 130 atom types are defined and a number of functional forms have been developed with primarily inorganic crystal structures in mind.

5.3.3. DREIDING I and II force fields.

The DREIDING II [2] force field was chosen to minimise the discotic liquid crystal molecular structure. It is an extension of the DREIDING I force field available with earlier versions of the Cerius software. The DREIDING force field is an all purpose force field that can be used for the structure prediction and dynamic calculations of large organic, small biological and inorganic molecules. The DREIDING force field has the advantage over other more specialised force fields of being fairly robust, using general force constants and geometry parameters based on simple hybridizations rather than the more computationally complex routines based on specific combinations of atoms.

The DREIDING II force field allows reasonable predictions for a large number of structures, including those with novel combinations of atoms or novel chemical structures for which there is little or no experimental data to generate a valid specific combination model.

The minimisation routine minimises the potential energy of the molecule. The potential energy may be described as the sum of energies of each atom where the energy of one atom is defined as :

$$E = E_{bond} + E_{angle} + E_{torsion} + E_{inversion} + E_{vdw} + E_{hb} + \dots$$

- E_{bond} - bond stretching energy term. This is a short range energy term and only affects atoms that are connected directly.
- E_{angle} - energy associated with the bond angle. This is also a short range energy term only affecting directly connected atoms.
- $E_{torsion}$ - energy of bond torsion. This is a short range energy term which only affects atoms that are jointly connected to a third atom.
- $E_{inversion}$ - energy associated with two different structural forms of the same molecule.
- E_{vdw} - Van der Waal's energy term, a long range interaction between two parts of a molecule or between two different molecules not closely connected.
- E_{hb} - An energy term related to hydrogen bonded components, a long range term that acts between neighbouring molecules or parts of the same molecule that are bent back on themselves.

In the DREIDING II force field the bond stretching energy, for example, is defined as :

$$E_{bond} = \frac{1}{2}K_b(R-R_0)^2$$

K_b is a force constant which is dependent on the nature of the bonded atoms.

R_0 is the equilibrium bond length and is also dependent upon the bonded atom types.

R is the actual bond length.

The energy terms are dependent upon the nature of the bond, which atoms are bonded together and how they are bonded (i.e. either single or multiply bonded). The force field contains the necessary force field parameters for any combination of atoms or functional forms.

5.3.4. Crystal builder.

The Cerius force field modules are able to handle periodic boundary conditions, so it is possible for the molecule not only to be minimised on its own but as part of a crystal lattice. The minimisation of a crystal lattice is computationally more expensive but the interactions between the nearest neighbours are considered, giving a more realistic representation of a possible crystal structure. The software uses a builder module [9] that incorporates a number of crystal building and visualisation tools. Cerius is able to simulate any type of crystal structure from small molecules occupying a single unit cell to continuous polymer chains extending to infinity in any one direction. Once a molecule has been built it is a simple process to build a crystal.

- The first step in building a crystal is specifying the asymmetric unit, the repeating unit. An atom or molecule within the current store may be selected.
- The unit cell parameters are entered, unit cell lengths (a , b , c), cell angles (α , β , γ) as well as the crystal system.
- Symmetry operators which replicate the asymmetric unit in several positions throughout the crystal can also be defined.

Once these have been selected the crystal is built by pressing the build button. The unit cell is displayed with the atom or molecule at a position within the unit cell. The molecule can be moved within the unit cell. For consistency all molecular centres were placed at a cell corner.

After building the unit cell it is possible to display a larger area of the crystal by altering the visualization parameters, which allow the number of unit cells shown along the 3 axes x , y , z to be altered. The crystal structure was normally displayed using a 3x3x3 matrix. The entire crystal structure can be viewed as either wire-frame, ball and stick or as space filled. The crystal can be easily rotated within three dimensions by use of the mouse,

allowing easy visualisation of the crystal structure from any angle. The crystal structure of DB26 generated using Cerius 3.2. by this method is shown in (Fig 5.5.). The model does not give an actual accurate visual representation of a crystal structure, only an average representation, but this is sufficient for visualisation purposes and measurements of molecular parameters and parameters related to packing within the crystal structure.

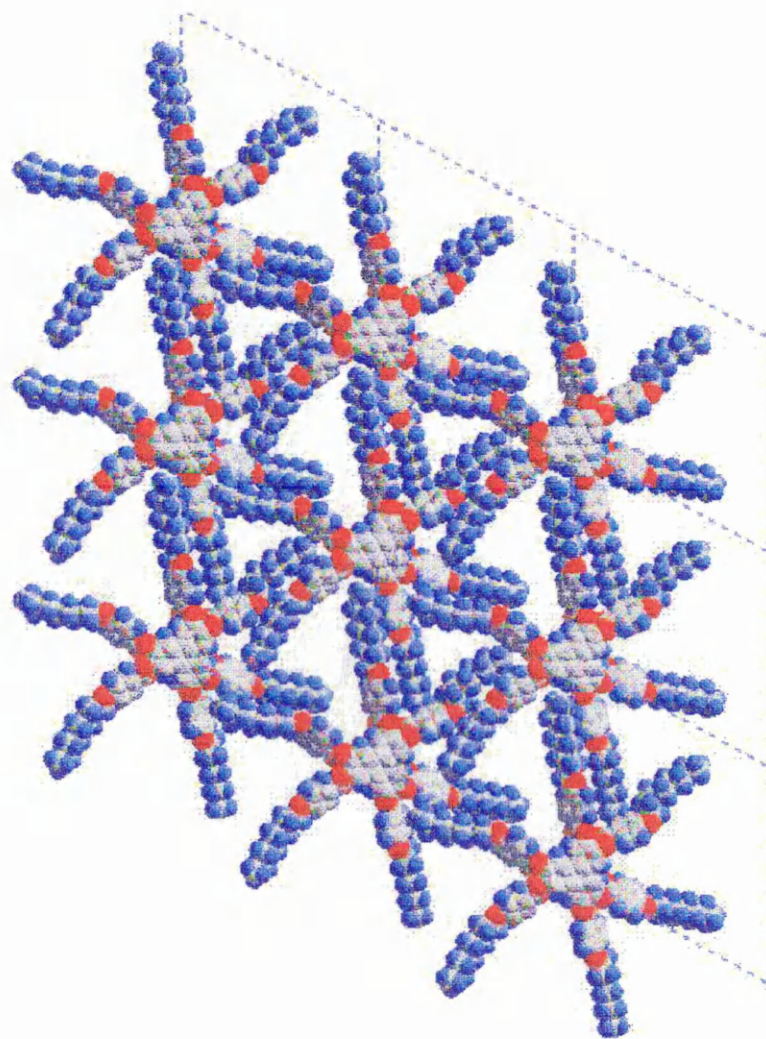


Figure 5.5. DB26 crystal structure.

When the crystal has been built the entire structure can be minimised, both molecular conformations and adjustable cell parameters are altered at each minimisation step. It is possible to fix some or all of the cell parameters if necessary. The interactions between the nearest neighbours are considered, but this model cannot be assumed to accurately

represent the molecular conformations. The use of periodic boundary conditions is apparent in (Fig 5.5.), the unit cell being used as the repeating unit for the periodic boundary conditions. All the molecules in the crystal structure are therefore similarly distorted to that in the unit cell.

To determine if the calculated crystal structure is a valid representation of an actual crystal of the material, an additional piece of software can be used which takes the calculated crystal structure of the crystal and generates a diffraction pattern which can be compared with experimentally obtained diffraction patterns from either X-ray diffraction or electron diffraction. Voigt-Martin *et al* [10, 11] have carried out this operation and achieved very good agreement between the calculated diffraction pattern and an experimentally obtained electron diffraction pattern obtained from a triphenylene ester.

Chapter 6. Results and Discussion.

6.1. Reduction of Transition Temperature.

From the optical microscopy results (Chapter 2), it was found that the I - N transition temperature of the compounds was reduced by methyl additions to the ester benzoate linkage of the symmetrical substituted compounds from the DB and PH series. Considering the results from chapter 2 (Table 2.1 page 53) and reorganising them with respect to decreasing nematic to isotropic transition temperature the following table can be drawn up (Table 6.1.). The methyl substitution positions are shown in Fig 6.1.

| | I-N/°C | N-C/°C | Nematic range/°C | Methyl substitution position. |
|-------|--------|--------|------------------|---|
| DB26 | 241 | 171 | 70 | No methyl additions. |
| DB118 | 230 | 150 | 80 | 1 methyl pointing away from the core, [3']. |
| PH64 | 217 | 197.5 | 20 | 2 methyls pointing away from the core, [3',5'] |
| DB125 | 199.5 | 126.5 | 73 | 1 methyl pointing towards the core, [2']. |
| PH74 | 187 | 159 | 28 | 2 methyls pointing away from the core, [3',5'], and one on the alkyl arm 1 st carbon unit. |
| PH76 | 171 | 74 | 97 | 2 methyls pointing towards the core, [2',6'] |

Table 6.1. Decreasing transition temperature with increasing methyl addition.

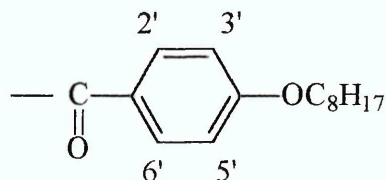


Fig 6.1 Methyl substitution positions.

6.1.1 Methyl Additions to the Benzene of the Ester Benzoate Linkage.

The effects of methyl additions to the 2',3',5',6' positions on the ester benzoate linkage are considered here.

DB26 has no methyl additions to the ester benzoate linkage and is seen to have the highest N-I transition temperature. By introducing a methyl addition to the 3' position on the ester benzoate linkage pointing away from the core (DB118) both the C-N and N-I transition temperatures are reduced slightly and the nematic range is increased.

Further reduction of the N-I transition temperature was observed by two methyl substitutions at the 3',5' positions on the ester benzoate (PH64).

A larger drop in the N-I transition temperature was observed when a methyl group was substituted at the 2' position, pointing towards the triphenylene core (DB125), the nematic range is comparable with that of the unsubstituted compound (DB26).

Further additional methyl substitution at the 6' position resulting in a 2',6' substituted ester benzoate with both the methyls pointing towards the core (PH76), showed the lowest C-N and N-I transition temperatures and also displayed the largest nematic range, almost 100°C, 20°C more than the unsubstituted DB26 compound. The N-I transition temperature of the PH76 compound is 100°C lower than the C-N transition temperature of the unsubstituted DB26 compound.

The addition of a methyl group to the ester benzoate linkage increases steric hindrance effects in this region with the core and causes the benzene group of the ester benzoate to rotate. Rotation of the ester benzoate prevents columnar packing of the molecules. No discotic columnar phases were observed in the substituted compounds using optical microscopy or XRD. Due to the rotated ester benzoate linkage, the molecules are more

disordered and enter the isotropic phase at a lower temperature. It was observed that methyl additions pointing away from the core (DB118 and PH64) have a much smaller effect on the N-I transition temperature than methyl groups pointing towards the core (DB125 and PH76).

The methyl substitution of DB118 pointing away from the core is in a region where steric hindrance arises from interactions between the methyl addition and interdigitated arms of adjacent molecules. Through a combination of a small rotation of the ester benzoate linkage and increased disruption of the interdigitated arm, in particular end gauche deformations, the minimum energy configuration can be obtained. The molecule remains roughly planar in form, the rotation of the ester benzoate group is much smaller compared with the molecules where the methyl additions pointed towards the core.

PH64 with two methyls pointing away from the core, experiences similar conditions as the DB118 molecule above, but in addition the methyl substitution at the 2' position interacts with the 5' methyl substitution of the adjacent arm on the same molecule. In this case the benzene of the ester benzoate linkage rotates further out of the plane of the triphenylene core, further disrupting columnar packing above and below the plane of the triphenylene core resulting in the reduced N-I transition temperature. The PH64 compound, although it displays a lower N-I transition temperature than DB118, does not have a lower C-N transition temperature than DB118 or DB26. The C-N transition temperature was observed to be much higher than the DB118 C-N transition temperature. The reason that PH64 has a much higher C-N transition temperature may be explained by the fact that the ester benzoate linkage is rotated to a particular angle that can be easily accommodated in the crystal structure, resulting in a more stable crystal phase with a correspondingly higher C-N transition temperature and reduced nematic range. Similar transition temperature behaviour is observed with PH74, a more detailed comparison of PH64 and PH74 may be found later in this chapter 6.1.2.

Methyl additions to the ester benzoate at the 2' (DB125) and 2',6' (PH76) positions showed the largest reduction in the transition temperature. The methyl additions of DB125 and PH76 both point towards the triphenylene core and experience a completely different environment than their DB118 and PH64 counterparts.

A methyl addition at the 2' position (DB125) experiences steric hindrance from the C=O of the ester benzoate linkage. This will cause the benzene ring to rotate further out of plane than the methyl substitutions at the 3',5' position due to the fact that both the C=O and methyl substitutions are in very close proximity and the steric hindrance can only be reduced by benzene ring rotation, unlike the 3',5' substitution case where a combination of benzene ring rotation and interdigitated arm deformation were possible to reduce the steric hindrance. A larger rotation of the benzene group increases disorder and both the C-N and N-I transition temperatures are reduced. The nematic range for DB125 is observed to be 73°C, comparable to the 70°C nematic range measured for the unsubstituted DB26 compound, but both the transition temperatures (C-N and N-I) for DB125 were observed to be approximately 40°C lower than DB26.

The PH76 compound with methyl group substitution at both the 2',6' positions showed the lowest transition temperatures of this series of compounds investigated. In the case of PH76, with two methyls pointing towards the core, there is a very large steric hindrance effect with interactions between the methyl substituents and the C=O component of the ester benzoate linkage. In this region the benzene rings of neighbouring arms are very close together and addition of bulky methyl substituents causes very large steric hindrance effects. In particular substituents at the 2' position on one arm and the 6' position of a neighbouring arm as well as the C=O which was originally present in this region results in all three elements effectively trying to occupy the same space and will induce very large steric hindrance effects which can only be compensated by a very large out of plane rotation of the benzene of the ester benzoate linkage, accounting for the much lower transition temperatures. The nematic range is

also observed to increase to 100°C compared with the 70°C range of the unsubstituted DB26. This may be accounted for by the fact that the particular conformation of the ester benzoate is not favoured in the crystal structure, resulting in a higher internal energy within the crystal, allowing a much lower C-N transition temperature. Also, as the benzene linkage is rotated out of the plane of the triphenylene core, certain deformations of the alkyl arm become more favourable, in particular the end gauche and kink conformations, which are essentially planar conformations of the alkyl arms. Due to the interdigitation of alkyl arms from adjacent molecules, planar conformations would have proved difficult to adopt, but as the ester benzoate linkage is rotated further out of plane these conformations, although still planar with respect to the plane of the alkyl arms, occur at an angle with respect to the plane of the triphenylene core. Interactions between the interdigitated arms is reduced and the possibility of one of these conformations occurring increases. The fact that the possibility of such a conformation occurring increases, aids in explaining the reduction in the N-I transition temperature arising from rotation of the ester benzoate linkage. The alkyl arms can adopt a number of different conformations and as the disorder with the arms increases, so the N-I transition temperature drops.

6.1.2. Additional Methyl Addition to the Alkyl Arm.

PH74, although this compound contained two methyl substitutions at the 3',5' positions pointing away from the core, it also contained an additional methyl substitution on the first carbon unit on the alkyl arm away from the core. Thus the methyl substitutions cannot be solely considered, as alterations to the ester benzoate linkage, and thus the transition temperatures cannot be easily compared against the transition temperatures of the other compounds. However, it is possible to directly compare and contrast the transition temperatures of this compound PH74 with PH64, which also has the 2 methyl substitutions pointing away from the core. The only difference between the two

compounds is the additional methyl substitution to the first carbon unit on the alkyl arms of PH74.

| | C-N/°C | N-I/°C | Nematic range/°C | Methyl substitution position. |
|------|--------|--------|------------------|---|
| PH64 | 197.5 | 217 | 20 | 2 methyls pointing away from the core, [3',5'] |
| PH74 | 159 | 187 | 28 | 2 methyls pointing away from the core, [3',5'], and one on the alkyl arm 1 st carbon unit. |

Table 6.2. Extract from Table 6.1, showing transition temperature for PH64 and PH74.

Earlier (Section 6.1.1) it was observed that the two methyl additions at the 3',5' positions interact with the methyl substitutions of neighbouring arms and also the ends of interdigitated arms, resulting in an out of plane rotation of the ester benzoate linkage. This allowed the larger possibility of planar alkyl conformations and prevented columnar packing, thus reducing the N-I transition temperature. It was also suggested that the particular conformation of the ester benzoate linkage could be favourably accommodated in the crystal structure thus resulting in a much higher C-N transition temperature and a reduced nematic range. The PH74 molecule follows the transition temperature behaviour exhibited by PH64, a lower N-I transition temperature, a relatively high C-N transition temperature and a small stable nematic temperature range, these effects being primarily determined by the methyl substitution at the 3',5' positions. The additional methyl substitution on the alkyl arm introduces a further interaction between this methyl substitution and the methyl substitution at the 3' position on the ester benzoate linkage. Steric hindrance effects between the methyl on the alkyl arm and the substitution at the 3' position causes the plane of the arm of PH74 to be rotated a little more relative to the arms of the PH64 compound while the benzene rings of both compounds adopt approximately the same conformation relative to the triphenylene core in both compounds. As described earlier, the rotation of the alkyl arm will increase the

possibility of planar alkyl conformations. Increased disorder in the alkyl arms of PH74 will result in the observed lower transition temperatures when compared against PH64. The lower C-N transition temperature and larger nematic range of PH74 may be explained by the increased possibility of alkyl deformations occurring along the arms, resulting in an earlier C-N transition temperature and a slightly larger nematic temperature range.

6.1.3. Conclusion on Methyl Substitutions.

Methyl addition to the ester benzoate linkage causes the N-I transition temperature to reduce, with methyl substitutions pointing towards the triphenylene core having the greatest effect.

Two methyl substitutions pointing away from or towards the triphenylene core cause a further reduction of the N-I transition temperature compared with the corresponding single methyl substitution.

Addition of 2 methyl groups pointing away from the core results in a conformation of the ester benzoate linkage which is favoured and easily accommodated in the crystal structure, resulting in a higher C-N transition temperature and smaller nematic temperature range, observed in both PH64 and PH74. The methyl groups from molecules above and below a particular molecule may become anchored to the molecule by the methyl units. More energy is then required to break this anchoring and this leads to the higher C-N transition temperatures observed in PH64 and PH74.

An increased possibility of planar conformations of the alkyl arms occurring, arises from rotation of the ester benzoate linkage with respect to the plane of the core. This results in the plane of the alkyl arms being rotated with respect to the triphenylene core.

Without the rotation of the ester benzoate linkage, these conformations are hindered by the interdigitated arms of adjacent molecules.

Methyl addition to the first carbon unit on the alkyl arm further increases the out of plane rotation of the alkyl arm relative to the triphenylene core, enhancing the possibility of planar alkyl deformations occurring.

6.2 X-ray Diffraction.

X-ray diffraction coupled with microdensitometer measurements allowed molecular spacings to be measured accurately. With the majority of the X-ray diffraction patterns from the various samples, only one diffuse ring was visible in the liquid crystal phase indicating that the samples were not very highly ordered in the discotic phase. Plane spacings of the order 22 - 30 Å were measured, these plane spacings relating to the core - core separation. The diffraction rings from the nematic phase samples were sharper than those of the isotropic phase, indicating that there was a higher degree of order within this phase. The rings were not as sharp as those from the crystal phase indicating that the ordering was only short range.

The lack of other rings indicates that the molecules do not assume a columnar structure. If a columnar structure had formed then molecular spacings of the order 4 Å would be expected to be observed, relating to the molecular separation within the columns. The only sample where a diffraction ring of 4.1 Å was observed was the DB26 sample. This planar spacing corresponds to the spacing between molecules stacking on top of one another to form molecular columns. This ring was faint and very diffuse, indicating the although the DB26 molecules stack in a columnar arrangement the columns are very short and easily disrupted. The diffraction ring was not evident on all DB26 diffraction

photographs indicating that the formation of molecular columns may be helped by alignment within the capillary tube.

The columnar separation was not observed with any of the other compounds. DB26 was the only symmetrical substituted compound that displayed evidence of the formation of molecular columns. The compounds with additional methyl units substituted to the ester benzoate linkages did not display columns - it appears that these methyl additions disrupted the formation of columns, in turn lowering the transition temperatures. With no molecular columns 2-D ordering is lost, the liquid crystal phase is more disordered and the associated transition temperature for the nematic to isotropic phase does not need to be as large.

6.2.1 Symmetrical Compounds.

Considering the X-ray diffraction data (Chapter 3), with DB26 the planar spacing is observed to reduce as the temperature is decreased. In the isotropic phase the alkyl arms are highly disordered and there is therefore no interdigitation of the alkyl arms. The X-ray diffraction ring of the isotropic phase was very broad and very diffuse indicating a lack of structure. The ester benzoate linkage of DB26 contains no methyl substituents and is therefore relatively free to rotate, allowing the alkyl arms to adopt any number of possible configurations. As the molecule is cooled and enters the liquid crystal phase, rotation of the ester benzoate linkage is reduced and the number of possible configurations of the alkyl arms is reduced, and the X-ray diffraction peak becomes sharper. A single diffraction ring is still observed, indicating that there is no long range ordering within the liquid crystal phase. From optical observations the liquid crystal phase displayed the classical schlieren texture of a nematic liquid crystal. At the beginning of the liquid crystal phase, on cooling from the isotropic, the alkyl arms are still relatively disordered and there is very little interdigitation. As the sample was cooled the planar spacing was observed to decrease, indicating that as the arms become more

ordered there was a greater degree of interdigitation and the molecular cores can pack closer together. The planar spacing was observed to reduce further as the sample entered the crystal phase as well as sharpening of the diffraction ring.

In the case of DB118 the ester benzoate linkage is not as free to rotate as that of DB26, due to steric hindrance effects of the CH₃ methyl substituent. In the liquid crystal phase the planar spacing of DB118 was observed to be smaller than that of DB26. This arises from the fact that the ester benzoate linkage is rotated slightly out of plane and that the last carbon unit of the interdigitated alkyl arms is more likely to adopt an end gauche configuration, due to steric hindrance effects caused by the methyl substitution at the 3' position. As DB118 entered the crystal phase the planar spacing was observed to increase. In the crystal phase, rotation of the ester benzoate linkage may be reduced and may actually be locked in a particular conformation, while the alkyl arms still retain a degree of flexibility. The CH₃ unit on the benzene ring is now in a position where it further disrupts interdigitation of the alkyl arms, causing the molecular cores to move further apart, thus increasing the observed planar spacing. As the molecule was cooled further into the crystal phase the planar spacing increased still further, indicating that the alkyl arms became more ordered, causing the triphenylene cores to move further apart. The bulky methyl group on the benzene ring prevents plate like stacking of the discotics. No planar spacing of approximately 5Å indicative of this type of molecular spacing was observed in the crystal phase of DB118.

The planar spacings for DB125 do not alter significantly at the transition from isotropic to nematic. In the case of DB125 the methyl substituent on the benzene ring points towards the molecular core and interacts with the C=O of the ester benzoate linkage, causing the benzene group to be rotated and unable to freely rotate. Therefore the environment around the benzene group remains relatively unchanged during the cooling process. As the alkyl arms become more ordered they are free to interdigitate fully until they encounter the core region of the adjacent molecule. The alkyl arms can fully

interdigitate without encountering any obstacle and the planar spacings remain relatively unchanged.

In the crystal phase of PH64, interactions between the methyl groups at the 3',5' positions on adjacent arms cause the ester benzoate to be rotated with respect to the plane of the core and alkyl arms can interdigitate. As the sample enters the liquid crystal phase and disorder of the alkyl arms increases there will be an increase of interactions with the methyl groups on the benzene ring. This initially causes the planar spacing to increase as the ester benzoate linkage is still initially fairly immobile and the only way to reduce the steric hindrance is for the molecules to move slightly apart. As the temperature within the liquid crystal phase increases further, the ester benzoate linkage becomes slightly more mobile and can rotate to accommodate alkyl arm interdigitation and also reduce steric hindrance associated with the interdigitation. Thus the planar spacing is observed to reduce as the sample is heated through the nematic liquid crystal region. In the isotropic phase the planar spacing is observed to increase and the diffraction ring of the isotropic phase is broader and more diffuse than those of the liquid crystal phase. The planar spacing increase may be related to increased freedom of the ester benzoate to rotate causing more interactions between the disordered alkyl arms of adjacent molecules, increasing the planar spacing.

The PH74 molecule, structurally similar to PH64 but with an additional methyl substitution at the first carbon unit on the alkyl arms, exhibits similar behaviour to PH64. At room temperature the ester benzoate is rotated with respect to the plane of the triphenylene core arising from steric hindrance from the substituted methyls. The additional methyl substituted group of the alkyl arm is also rotated out of plane, allowing the alkyl arms from adjacent molecules to interdigitate fully. The PH74 has a shorter alkyl arm than other molecules and thus exhibits a smaller planar spacing in the crystal phase when compared with the other compounds from the DB and PH series. As the temperature of the sample increases and the sample enters the nematic liquid crystal

phase, increased flexibility of the alkyl arms results in an increase in steric hindrance in the region of the ester benzoate linkage. This forces the molecular cores of adjacent molecules further apart resulting in a larger planar spacing as determined by X-ray diffraction. As the temperature is increased further through the liquid crystal phase, the ester benzoate linkage becomes more mobile and the alkyl arms become more disordered. The central molecular cores can then pack closer together and the planar spacing was observed to decrease. In the isotropic phase the ester benzoate is free to rotate and the alkyl arms are completely disordered. Interactions between adjacent alkyl arms increase and force the molecules further apart, resulting in an increase in measured planar spacing.

PH12IME, a molecule from the PH series of compounds, with long, C₁₂, alkyl arms and two methyl substitutions pointing towards the triphenylene core, was investigated using XRD. As the sample was heated into the liquid crystal phase, increased disorder within the alkyl arms resulted in decreased arm interdigitation and thus an increase in planar spacing. This increase in planar spacing was observed until close to the N-I transition temperature. In the liquid crystal phase the ester benzoate linkages are not free to rotate freely due to large steric hindrance encountered between neighbouring methyl units and the C=O of the ester benzoate linkage. In the isotropic phase the alkyl arms assume a completely disordered configuration. Due to the length of the alkyl arms it is possible for the arms to disorder in such a way that they loop round upon themselves, giving the molecule a compact 'spherical' configuration allowing the isotropic phase planar spacing to be reduced by 3Å when compared to the crystal planar spacing.

PH12OME showed a larger planar spacing than PH12IME at room temperature. This can be explained by the fact that the methyl substituents of PH12OME point away from the core of the molecule and are located in the region where the alkyl arms of adjacent molecules interdigitate, preventing the alkyl arms from fully interdigitating due to steric hindrance. As the sample was heated into the liquid crystal phase, increased disorder in

the alkyl arms reduces the interdigitation and the planar spacing was observed to increase. As the temperature increases and the internal molecular energy increases, the ester benzoate was able to deform and rotate. The two methyl substitutions on the ester benzoate can rotate further out of the plane of the core. Steric hindrance effects with the interdigitated arms are reduced, allowing the disordered alkyl arms to interdigitate past the methyl positions, resulting in a decrease in the planar spacing. In the isotropic phase the alkyl arms are completely disordered and conformations that effectively loop back on themselves are possible, allowing the molecules to pack closer together, observed by a decrease in planar spacing.

6.2.2. Unsymmetrical Compounds.

TW73 is an unsymmetrical substituted compound with 4 C₈ and 2 shorter C₆ alkyl arms. The TW series of compounds do not contain ester benzoate linkages. As the sample was heated from the crystal phase, through the liquid crystal phase and into the isotropic phase the planar spacings did not alter very much, only 0.5Å from the initial room temperature value, indicating that the alkyl arms are probably disordered in the crystal phase. As the temperature increases the alkyl arm flexibility increases, but this does not affect the measured planar spacing.

TW75 consisted of 4 C₈ alkyl arms and 2 longer C₁₀ alkyl arms. As the sample was heated into the liquid crystal the planar spacings were seen to reduce. Having two longer alkyl arms allows more sites for CH₂ deformations to occur and increases the possibility of out of plane deformations occurring, allowing adjacent molecules to interdigitate and so reduce the measured planar spacing.

TW77 consisted of 4 C₈ alkyl arms and 2 C₁₂. Through XRD, the observed planar spacing of this sample did not alter very much (0.3Å). The minimum energy configuration is a compromise between the minimum energy conformation of a single

isolated molecule and the minimum energy configuration of the unit cell. For the TW77 sample with 2 longer C₁₂ arms, to display a smaller planar spacing than TW73 requires that the alkyl arms cannot be in a fully extended conformation and must therefore be highly disordered in the crystal phase. Heating the sample increases the alkyl chain flexibility but the degree of disorder remains constant, leaving the measured planar spacing virtually unaltered.

Comparison of the transition temperatures of TW75 and TW77, both with 2 sets of longer alkyl arms, shows that the molecule with the longest arms has the lower nematic to isotropic transition, but also a smaller nematic region. A similar effect is observed with calamitics (rod like molecules), increasing the alkyl arm length reduces transition temperatures at the expense of the liquid crystal range and number of liquid crystal transitions. Calamitics exhibit the so called 'odd-even' effect of temperature reduction through carbon addition to the alkyl chains, where an even number of carbon units in the chain results in the largest reduction in transition temperature, while with an odd number of carbon units the transition temperature is actually observed to increase.

From the transition temperature results it appears as though TW75 and TW77 follow this pattern of behaviour. It is not known if odd carbon addition for these unsymmetrical compounds would also fit with this pattern.

6.3. Alignment

6.3.1 Accidental Alignment

Accidental alignment of DB118 and PH76 was observed, Chapter 2.3. On cooling from the isotropic phase to the nematic phase the sample briefly exhibited a schlieren nematic texture and then the sample aligned homeotropically with the molecular director perpendicular to the glass surface, Fig. 6.2.

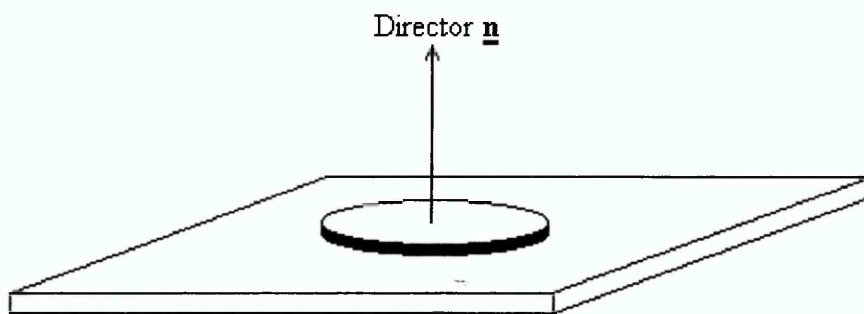


Figure 6.2. Homeotropic alignment of a discotic molecule.

Appendix A pages A-II and A-VII show this alignment process occurring for the DB118 sample and the PH76 sample respectively. As the sample was rotated between crossed polars the central region remained uniformly dark, indicating the alignment was homeotropic. The sample temperature was maintained at the nematic to isotropic transition temperature and when the sample slide was moved from left to right or backwards and forwards under the microscope it was noted that the nematic schlieren texture appeared briefly before disappearing - due to the short life span of this phenomenon, approximately 1 s, it was difficult to be recorded on film. It is believed that this effect of loss of realignment and re-establishment can be accounted for by a very small temperature gradient across the window of the heated cell. A gradient of 0.2°C across the heated cell field of view is sufficient to explain this effect. The sample area outside the field of view being at a slightly higher temperature than the hot stage

window. The hot stage consists of a silver heating block with a small sapphire window. The sapphire window is heated by conduction from the silver block, Fig. 6.3.

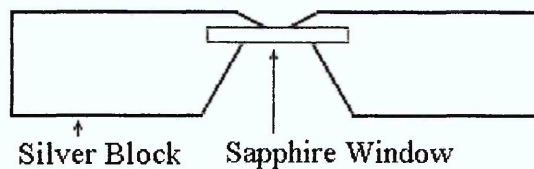


Figure 6.3. Microscope Hot Stage

The centre of the sapphire window is at a slightly lower temperature than the surrounding silver block. This was confirmed during the calibration of the heated block using benzoic acid, Chapter 2.1.3.

6.3.2 Alignment by Magnetic Fields.

It was found that with a magnetic flux density of 1 Tesla using BreMag rare earth magnets, alignment of the various discotic samples, during X-ray diffraction experiments, could not be achieved. Due to the rotational symmetrical nature of the hexa-alkoxy benzoates of triphenylene investigated, the magnetic anisotropy is very small. It should be possible for these samples to be aligned using much larger magnetic fields. This would mean moving away from relatively small permanent magnets to much more powerful, but also physically larger, electro magnets. This in turn poses a number of technical problems concerning the X-ray diffraction set-up, a feasible solution would not be possible to implement with the current X-ray diffraction configuration.

6.3.3 Alignment by Surface Treatments.

A number of successful methods of aligning the discotic materials using surface treatment methods were presented in Chapter 2.4.3. Hexadecyl trimethyl ammonium bromide (HTAB) and poly-vinyl alcohol (PVA) layers were coated from 5% and 3% solutions dissolved in water. Both methods successfully aligned the discotic materials, confirmed using optical microscopy. The rubbed PVA layers were observed to produce better more uniform alignment of the sample than that produced using the HTAB layer.

When both samples, in the nematic phase, were rotated under the microscope between crossed polarisers, the samples remained uniformly dark, indicating that the samples were homeotropically aligned, with the directors perpendicular to the glass cell surface. This is the opposite of that observed for the calamitic rod-like liquid crystal molecules, where the molecules align homogeneously with the directors aligned parallel to the rubbing direction of the PVA layer. Rotation of homogeneously aligned calamitic liquid crystals under the microscope results in the sample appearing alternatively light then dark.

The fact that a homogenous alignment method for calamitic materials resulted in a homeotropic alignment for discotics lead to the assumption that the reverse process may also occur, namely a method for producing homeotropically aligned calamitic materials might produce homogeneously aligned discotic materials. The standard method of producing homeotropically aligned calamitics, SiO evaporation was used. Using an evaporation angle of 5° it was found that the discotic materials did not align.

Vaucher *et al*_[1] and Raghunathan *et al*_[2] used SiO deposition at an oblique angle of 20° combined with an additional treatment of the coated plates with octadecyl triethoxy silane to produce an aliphatic surface and an homeotropically aligned hexa-*n*-dodecanoyloxy turene dicotic liquid crystal.

Variation of the deposition angle from 5° to 55° and investigation of the effect of alignment with deposition angle resulted in the following observation. Deposition angles between 5° and 35° resulted in a homeotropic alignment of the discotic materials. Deposition angles in the range 40° to 55° showed large areas where homogeneous (parallel) alignment was observed to be occurring. A deposition angle of 45° resulted in very good homogeneous alignment, as observed using optical microscopy.

During the SiO deposition it was determined that a point source produced a non uniform deposition, layers were deposited too quickly and unevenly. Layers were noted to peel off, indicating stresses within the deposited layer. A method was devised where the evaporating source no longer consisted of a single point source, but instead effectively multiple point sources. Due to the modifications this produced a much slower rate of evaporation and produced a much more uniform coating over the target area, indicated by a uniform interference colour as opposed to the rainbow like pattern of colours produced by the point source. The deposited layers were more stable and did not flake off even when the samples were rubbed or scraped.

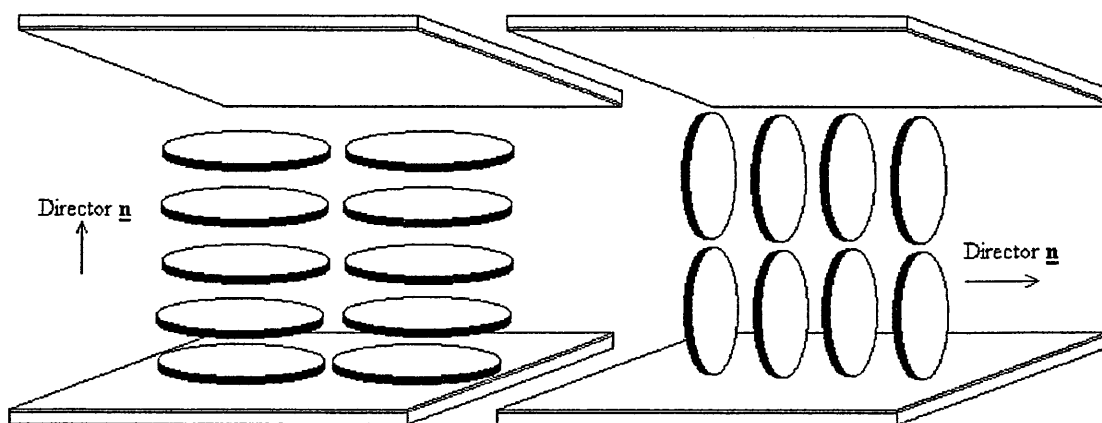
The symmetrical compounds from the DB and PH series all aligned to a very high degree, while the unsymmetrical compounds from the TW series only aligned poorly if at all. The DB and PH compounds are symmetrical and contain ester benzoate linkages. The molecular symmetry may aid the alignment process, the ester benzoate linkage of the DB and PH compounds also playing a role in the alignment process on SiO or HTAB treated surfaces.

6.3.4 Alignment conclusion

As already stated in chapter 4.8.4 the alignment of the discotic materials on SiO treated surfaces occurs in a number of stages as the sample was cooled.

The first stage involves the alignment of the triphenylene cores on the SiO treated surface as the sample cools from the isotropic phase to the nematic phase. The sample is still in a liquid phase although observation using polarising optical microscopy indicates that the sample is aligned.

Rotation of the sample in the isotropic phase between crossed polars results in the sample appearing uniformly dark, while rotation of the aligned sample in the nematic liquid crystalline phase results in the sample appearing first uniformly dark and then uniformly bright, indicating that the planes of the molecules are aligned perpendicular to the plane of the coated glass slides. The molecule can be visualised as standing edge-on on the surface, homogenous alignment, Fig 6.4.



Homeotropic Alignment

Homegenous Alignment

Figure 6.4 Two possible alignments of discotic molecules.

As the sample cools from the isotropic phase to the nematic phase, perfect alignment is not obtained. The molecular arms still retain a high degree of flexibility and freedom, with the ester benzoate groups still able to rotate freely.

The second stage of the alignment process involves the alignment of the ester benzoate groups. From the I.R. analysis of this region, chapter 4.8.3, the order parameter of various components of the ester benzoate linkage were seen to increase as the temperature was reduced through the liquid crystalline phase. The ester benzoate linkage was observed to align approximately half way through the liquid crystalline phase. The samples still remained fluid, the cover slips of the microscope cell could still be easily sheared. During shearing, the alignment within the cell was temporarily lost and the schlieren nematic texture was observable. After shearing the sample returned to the aligned state and the sample appeared uniformly dark or light, depending on the original rotation of the sample.

The final stage was the loss of the rotational freedom of the alkyl arms as the sample was cooled from the nematic phase to the solid phase. This also caused a further small increase in the order parameter of the ester benzoate linkage.

6.4 Infra Red Analysis

The major infra red peaks from the various discotic compounds were identified by consulting I.R. correlation charts [Chapter 4.5.1, Table 4.1].

6.4.1 Alkyl arm conformations

It was initially intended to utilise the I.R. spectroscopy to observe the CH₂ wagging vibrations in the region 1400-1300 cm⁻¹ and then use this information to determine the conformation of the alkyl arms, but due to the large intensity of bands adjacent to this region it was not possible to clearly identify the various CH₂ conformations for all the discotic compounds and to monitor their behaviour as the samples were heated and cooled through the liquid crystalline phases. In order to extract the CH₂ wagging information from some of the data it was necessary to perform a number of mathematical transformations in order to determine peak positions before fitting curves to the data. Deconvolution and 2nd derivative were both used on the sample data using the advanced FIRST software to determine the peak positions. For much of the data the deconvolution and 2nd derivative were unable to resolve the CH₂ information, although for DB26 and TW75 it was possible to determine the peak positions and to analyse this region further by fitting curves to the spectra within this region.

6.4.2 Curve fitting to the I.R. data

Using both the 2nd derivative and deconvolution options in the advanced FIRST software on the spectra, peak positions were able to be determined.

Use of the deconvolution routine identified no extra peaks that had not already been detected by the 2nd derivative routine. Noise was present in the original spectrum, but

use of two different methods ensured that the spectra were not over-manipulated by the software, which could accentuate the noise, inducing peaks that could be mistaken for vibrational peaks.

It was possible for a number of slightly different initial fits to be optimised equally well, giving a number of different curve fit possibilities with similar "good fit criterion" values. In order to determine which curve fit possibilities closely matched the possible answer, use of the good fit criterion was not enough. Fits with unrealistic peak shapes and fits where the area of one peak in relation to the others did not agree with the results of Maroncelli [3] and Senak [4] were rejected. Another rejection method involved taking a fit optimised at one temperature and re-optimising it for data at a slightly lower temperature. If the initial fit optimised quickly then it indicated only a few parameters from one fit to the next fit required altering, thus indicating that the initial guess was fairly close to the actual answer. During this second optimisation stage any possible fits that caused the optimisation routine to crash through numerical instability were rejected. Fits that required many optimisations were also rejected and new possible fits were attempted. Rejection of some initial possible fits reduced the possible number of candidates for the correct fit. All the remaining fits had similar good fit criterion values and optimised quickly from one temperature to a lower temperature. It could be argued that any of these possible fits was equally valid. By taking an average of all the results from the selected fits, an average area for each fitted curve could be calculated with error bars showing the possible range of results.

6.4.3 CH₂ wagging results

From the I.R. analysis and curve fitting to the CH₂ wagging region of DB126 and TW75 (Chapter 4.6.3), it was determined:

The ratioed areas for kink conformation of DB26 agreed with calculated values using the rotational isometric state (RIS) model for alkanes, although the number of double gauche conformations was observed to be slightly larger Fig 6.5. (Copy of Fig 4.20)

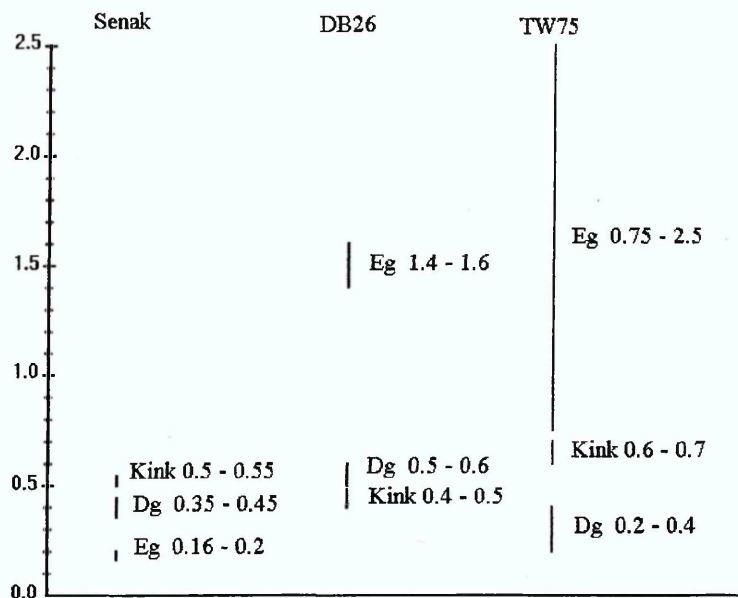


Figure 6.5. Numbers of various conformers per molecule.

For the TW75 compound the number of double gauche conformations agreed with calculated values although more kink conformations were observed.

In both cases the number of measured end gauche conformations was much larger than predicted using the RIS model, after taking into account that the RIS model calculates the number of end gauche conformations. For alkyl chains where there are two possible positions for end gauche conformations to occur, with the molecules investigated the alkyl chains have only one end where the CH₃ unit may assume an end gauche conformation, the other end of the chain being attached to the central triphenylene core.

The number of end gauche conformations measured was significantly larger, approximately a magnitude of 10 times larger, than calculated from the RIS model. The end gauche conformation appears to be highly favoured by the alkyl arms of the discotic molecules. When the alkyl arms of adjacent molecules interdigitate the ends of the arms

may be forced to assume an end gauche conformation arising through steric hindrance experienced from the core region.

As the unsymmetrical compound TW75 was cooled there was a marked decrease in the intensity of the end gauche conformations. In TW75 the kink conformation was favoured over the double gauche conformation. The alkyl arms of TW75 are planar with respect to the plane of the triphenylene core. A double gauche conformation results in an approximate 90° bend in the arm perpendicular to the plane of the core. This would interfere with adjacent molecules. The kink conformation maintains the planarity of the alkyl arm and is therefore easier to accommodate, producing less interference with adjacent molecules.

For DB26 the alkyl arms are not connected directly to the triphenylene core, but are attached to the ester benzoate group. The plane of the ester benzoate group is rotated by approximately 56° relative to the plane of the triphenylene core, determined from computer modelling simulations using Cerius, Chapter 5.3.

A double gauche conformation still produces a 90° bend in the alkyl arm, but the plane of the arm is no longer parallel to the plane of the core and this conformation is therefore easier to accommodate without causing major disruptions to adjacent molecules. The kink conformation is still in the plane of the alkyl arm but as this plane is rotated relative to the plane of the core, kink conformations in the arms of DB126 will interfere more with adjacent molecules than when compared with kink conformations occurring in TW75.

6.4.4 FTIR studies of aligned samples

Results from polarising optical microscope observations (Chapter 2) indicated that it was possible to successfully align the discotic materials using various surface treatment methods, homeotropically using hexadecyl trimethyl ammonium bromide (HTAB) and poly-vinyl alcohol (PVA) and both hometropically and homogeneously using evaporated SiO, the particular ordering depending on the evaporation angle used.

Both HTAB and PVA were dissolved in water, thus the standard KBr plates normally used in IR investigations could not be used with these solutions as they are themselves soluble in water. CaF₂ plates provided a suitable alternative to KBr, the CaF₂ plates after being coated successfully aligned the discotic samples, verified using the polarising optical microscope. Unfortunately due to the high water content of the deposited HTAB and PVA films as well as the relative thickness of the films, which absorbed a large proportion of the incident IR energy, a complex background spectrum was obtained which proved unsuitable for further FTIR investigation of the aligned samples.

With the SiO coated plates better results were obtained. SiO is relatively transparent to Infrared radiation from 10 000 - 1500 cm⁻¹, although around 1500 cm⁻¹ SiO absorbs strongly. When KBr plates coated with SiO were analysed in the spectrometer, the absorption below 1500 cm⁻¹, especially between 1300 cm⁻¹ and 800 cm⁻¹, was clearly evident, but due to the relatively thin deposited layer this absorbance had a fairly low intensity and a simple stable structure (Fig 4.23) that posed no problems when subtracted from the sample spectrum.

With successfully aligned samples, vibrations within the plane of the radiation will increase in intensity, while out of plane vibrations will decrease in intensity. Comparison between spectra from aligned and unaligned samples highlighted these vibrations and allowed structural information from the liquid crystal phase of the aligned sample to be determined.

6.4.5. Order Parameter determination

With the aligned discotic samples it was possible to determine the order parameters of certain molecular groups using Neff's methods of analysis (Chapter 4.8.2). It was possible to observe the behaviour of the ester benzoate linkage using the ester benzoate, C-O-C symmetric and asymmetric and C=O vibrations, observing how the order parameters of these separate vibrations changed as the temperature of the sample decreased, enabling the order parameter of the ester benzoate group as a whole to be determined based on the order components of the individual components.

Although the samples as a whole were aligned within the liquid crystalline phase, determined by polarising optical microscopy observations, it was observed through the order parameter results from the IR analysis that parts of the molecule were not at all aligned or only poorly aligned, indicated by order parameter values of less than 0.2.

The SiO layer would appear to be responsible only for the alignment of the triphenylene cores, the molecular arms still retaining a high degree of freedom and flexibility. As the samples cooled through the nematic phase, about halfway, there was a sudden increase in the order parameter of the C-O-C symmetric and unsymmetric vibrations. Order parameter values of between 0.6 and 0.9 were observed for the ester benzoate about halfway through the liquid crystalline phase, indicating quite a high degree of ordering of this ester benzoate group.

6.5 Computer Modelling Simulations.

Molecular modelling of the liquid crystals using Cerius indicated that addition of methyl units to the ester benzoate linkages caused the plane of the benzene ring to rotate relative to the plane of the triphenylene core due to steric hindrance between the methyl additions and the molecular core. The rotation of the benzene ring in turn brings the additional methyl group(s) into a position where interactions with the molecular layer above occur. These interactions disrupt the planar nature of the molecule, in turn hindering the formation of molecular columns, observed by the lack of X-ray diffraction evidence for planar spacings corresponding to the molecular separation of approximately 4Å.

The molecular modelling software, Cerius 3.2, allowed a molecular structure to be entered and an energy minimisation calculation on the molecular structure to be carried out. Molecular dimensions could be easily measured and molecular conformations could be viewed and rotated in 3 dimensions. Advanced software features included a crystal building package. Use of information obtained from the X-ray diffraction data and the generated molecular model allowed possible crystal structures to be observed and energy minimisations for complete crystals to be carried out. The software was limited in that it could only display crystal structures. It was not possible for liquid crystal structures to be simulated. The crystal building software allowed the crystal structure to be energy minimised and the results obtained were useful in mentally visualising how a nematic structure would appear and how the arms of adjacent molecules could interdigitate and assume different molecular configurations, namely the kink, bend, double gauche and end gauche conformations of the alkyl arms.

From the simulations it could be seen that the planes of the ester benzoates in the arms were rotated relative to the plane of the molecular core by the methyl additions. This brought the methyl groups directly into the region between molecular planes, disrupting

the stacking of the molecules in columns arising from steric hindrance effects of the methyl units.

The computer modelling of the crystal structure used periodic boundary conditions, i.e. a small simulation region was copied and transposed to give a larger view and to also eliminate the need to take into account surface effects, only the bulk sample was considered. In this case the simulation region was taken as the basic crystal unit cell, and the transposition directions used were the unit cell axes. The model therefore does not give an actual accurate visual representation of a crystal structure, only an average representation, but this is sufficient for visualisation purposes and measurements of molecular parameters and parameters related to packing within the crystal structure.

6.6 Further Work

6.6.1 Reduction of Transition Temperatures through Mixtures and Dopants.

Changes in the alkyl arm length and additional methyl additions to the ester benzoate linkage have reduced the transition temperatures of hexa alkoxy benzoates of triphenylene. Phillips *et al*^[5] have already shown that transition temperatures for similar compounds to those investigated, can be reduced by the mixing of two compounds DB126 and PH8. With a 75% PH8 and 25% DB126 mixture, transition temperatures were reduced by 10°C compared with the pure compounds. Calucci *et al*^[6] showed that addition of dopants, Lewis acid or trifluoroacetic acid can broaden the thermal stability and increase the degree of order for alkoxy discotic compounds. Addition of dopants could also improve the mesomorphic properties of hexa alkoxybenzoates of triphenylene. A combination of mixtures and dopant addition could lower the transition temperatures.

6.6.2 Alignment

Accidental alignment of DB118 and PH76 has been observed through optical microscopy. Sikharulidze *et al*^[7] have reported an optical effect where an electrically aligned pentakis [(4-pentylphenyl)ethynyl]phenyl-10-carbethoxy decyl ether realigned upon illuminating the sample with the white light source of the microscope - the process was reversible upon removal of the illumination. The question arises, could the accidental alignment observed for DB118 and PH76 also be a manifestation of a similar opto effect. The DB118 and PH76 compounds are chemically unrelated to those used by Sikharulidze but the possibility does exist that the observed effect is an optical effect and not a thermal effect as first proposed. It would be necessary to investigate this alignment effect further bearing in mind the two possible explanations to determine if the observed

effect is indeed thermal or possibly the first evidence of an optical effect for the hexa alkoxybenzoate triphenylene series of compounds.

6.6.3 Computer Modelling.

The Cerius molecular modelling package has successfully been used by various groups in conjunction with electron diffraction to display the crystal structures of various discotic compounds. Electron diffraction results or even atomic force microscopy results could be combined with the computational power of the Cerius package to allow accurate visualisation of the crystal structures of the discotic compounds.

6.6.4 Viscosity Measurements.

In chapter 4.8.4. it was observed that the alignment of the DB and PH molecules on SiO treated surfaces occurred in stages. Cooling from the isotropic phase to the nematic phase caused alignment of the triphenylene cores, observed by optical microscopy, on further cooling through the nematic phase resulted in alignment of the ester benzoate linkages. It would be interesting and informative to perform viscosity measurements on aligned samples in order to determine if the alignment of the ester benzoate group determined using I.R. analysis also results in an increase in viscosity at the same temperature as the increase of the order parameter of the ester benzoate group.

References.

References. Chapter 1.

1. Virchow R., *Virchows Archive*, **6**, 571 (1854)
2. Lehmann O., *Z.Kristallogr Mineral*, **18**, 464 (1890)
3. Kelker H., *Molecular Crystals and Liquid Crystals*, **21**, 1 (1973)
4. Colling P.J., *Liquid Crystals*, Iop Publishing, Adam Hilger, Ch 8, (1990)
5. Chandrasekhar S., *Liquid Crystals*, Cambridge, 2nd Edition, Ch 6, (1992)
6. Leadbetter A.J., *Thermotropic Liquid Crystals*, Wiley, (1987)
7. Persham P.S., *Structure of Liquid Crystal Phases*, World Scientific Singapore, (1988)
8. Chandrasekhar S., Sadashiva B.K., Suresh K.A., *Pramana*, **9**, 471, (1977)
9. Billard J., Dubois J.C., Tinh N.H., Zann A., *Nouv. J. Chim*, **2**, 535, (1978)
10. Destrade C., Mondon M.C., Malthete J., *J. Phys. Paris*, **40**, 3, (1979)
11. Tinh N.H., Destrade C., and Gasparoux H., *Physics Letters A*, **72**, 251, (1979)
12. Destrade C., Bernaud M.C., Gasparoux H., Levelut A.M., Tinh N.H., *Proc. Intern. Liq. Cryst. Conf.*, Bangalore, (1979)
13. Destrade C., Tinh N.H., *Physics Letters*, **79A**, 189 (1980)
14. Malthete J., Destrade C., Tinh N.H., Jaques J., *Molecular Crystals and Liquid Crystals*, **64**, 233, (1981)
15. Destrade C., Tinh N.H., Gasparoux H., *Molecular Crystals and Liquid Crystals*, **71**, 111, (1981)
16. Levelut A.M., Hardouin F., Gasparoux H., Destrade C., Tinh N.H., *J. Phys. Paris*, **42**, 147, (1981)
17. Vauchier C., Zann A., Le Barny P., Dubois J.C., Billard J., *Molecular Crystals and Liquid Crystals*, **66**, 103, (1981)
18. Tinh N.H., Gasparoux H., Destrade C., *Molecular Crystals and Liquid Crystals*, **68**, 101, (1981)
19. Destrade C., Foucher P., Malthete J., Tinh N.H., *Physics Letters A*, **88**, 187, (1982)

20. Backer H.J., Van Der Baan S., *Red. Trav. Chim. Pays. Bas. Belg.*, **56**, 1161 (1937)
21. De Jeu W.H., *Phil. Trans. R. Soc. A*, **309**, 102, (1983)
22. Giannesi C., *Physical Review A*, **28**, 350, (1983)
23. Chandrasekhar S., *Phil. Trans. R. Soc. Lond. A*, **309**, 93, (1983)
24. Dowell F., *Physical Review A*, **28**, 3520, (1983)
25. Dowell F., *Physical Review A*, **28**, 3526, (1983)
26. Levelut A.M., *J. Chim. Phys.*, **80**, 149, (1983)
27. Destrade C., Foucher P., Gasparoux H., Tinh N.H., Levelut A.M., Malthete J., *Molecular Crystals and Liquid Crystals*, **106**, 121, (1984)
28. Tinh N.H., Foucher P., Destrade C., Levelut A.M., Malthete J., *Molecular Crystals and Liquid Crystals*, **111**, 277, (1984)
29. Safinya C.R., Liang K.S., Varady W.A., Clark N.A., Anderssen G., *Phys. Rev. Lett.*, **53**, 1172, (1984)
30. Chiang L.Y., Safinya C.R., Clark N.A., Liang K.S., Bloch A.N., *Journal of the Chemical Society-Chemical Communications*, **11**, 695, (1985)
31. Gramsbergen E.F., Hoving H.J., Dejeu W.H., Praefcke K., Kohne B., *Liquid Crystals*, **1**, 397, (1986)
32. Kardan M., Reinhold B.B., Hsu S.L., Thakur R., Lillya C.P., *Macromolecules*, **19**, 616, (1986)
33. Giannesi C., *Physical Review A*, **34**, 705, (1986)
34. Raghunathan V.A., Madhusudana N.V., Chandrasekhar S., Destrade C., *Molecular Crystals and Liquid Crystals*, **148**, 77, (1987)
35. Kardan M., Kaito A., Hsu S.L., Takur R., Lillya C.P., *Journal of Physical Chemistry*, **91**, 1809, (1987)
36. Yang X., Kardan M., Hsu S.L., Collard D., Heath R.B., Lillya C.P., *Journal of Physical Chemistry*, **92**, 196, (1988)
37. Snyder R.G., Maroncelli M., Strauss H.L., *J. Am. Chem. Soc.*, **105**, 133, (1983)
38. Maroncelli M., Strauss H.L., Snyder R.G., *J. Chem. Phys.*, **82**, 2811, (1985)
39. Maroncelli M., Strauss H.L., Snyder R.G., *J. Chem. Phys.*, **89**, 4390, (1985)

40. Boden N., Bushby R.J., Jesudason M.V., Sheldrick B., *Journal Of The Chemical Society-Chemical Communications*, **19**, 1342, (1988)
41. Fontes E., Heiney P.A., *Physical Review Letters*, **37**, 1329, (1988)
42. Fontes E., Heiney P.A., Dejeu W.H., *Physical Review Letters*, **61**, 1202, (1988)
43. Warmerdam T., Frenkel D., Zijlstra R.J.J., *Liquid Crystals*, **3**, 149, (1988)
44. Warmerdam T., Frenkel D., Zijlstra R.J.J., *Liquid Crystals*, **3**, 1087, (1988)
45. Warmerdam T., Frenkel D., Zijlstra R.J.J., *Liquid Crystals*, **3**, 369, (1988)
46. Warmerdam T., Frenkel D., Zijlstra R.J.J., *Liquid Crystals*, **3**, 1105, (1988)
47. Lee W.K., Winter B.A., Fontes E., Heiney P.A., *Liquid Crystals*, **4**, 87, (1989)
48. Yang X., Nitzsche S.A., Hsu S.L., Collard D., Thakur R., Lillya C.P., Stidham H.D., *Macromolecules*, **22**, 2611, (1989)
49. Ebert M., Jungbauer D.A., Kleppinger R., Wendorff J.H., Kohne B., Praefcke K., *Liquid Crystals*, **4**, 53, (1989)
50. Praefcke K., Kohne B., Singer D., *Angewandte Chemie-International Edition in English*, **29**, 177, (1990)
51. Praefcke K., Kohne B., Singer D., Demus D., Pelzl G., Diele S., *Liquid Crystals*, **7**, 589, (1990)
52. Lillya C.P., Murthy Y.L.N., *Molecular Crystals and Liquid Crystals Letters*, **2**, 121, (1985)
53. Kohne B., Marquardt P., Praefcke K., Psaras P., Stephan W., Turgay K., *Chimia*, **40**, 360, (1986)
54. Kreuder W., Ringsdorf H., Herrmann-Schönherr O., Wendorff H., *Angew. Chem. Int. Ed. Engl.*, **26**, 1249, (1987)
55. Chandrasekhar S. Ranganath G.S., *Rep. Prog. Phys.*, **53**, 57, (1990)
56. Belarbi Z., *Journal Of Physical Chemistry*, **94**, 7334, (1990)
57. Carton J.P., Duboisviolette E., Prost J., *Liquid Crystals*, **7**, 305, (1990)
58. Baehr C., Ebert M., Frick G., Wendorff J.H., *Liquid Crystals*, **7**, 601, (1990)
59. Kranig W., Boeffel C., Spiess H.W., *Macromolecules*, **23**, 4061, (1990)

60. Lee W.K., Heiney P.A., Ohba M., Haseltine J.N., Smith A.B., *Liquid Crystals*, **8**, 839, (1990)
61. Rey-Lafon M., Hemida A.T., *Molecular Crystals and Liquid Crystals*, **178**, 33, (1990)
62. Lee W.K., Heiney P.A., Mc Cauley J.P., Smith A.B., *Molecular Crystals and Liquid Crystals*, **198**, 273, (1991)
63. Lawler K.A., Vanhecke G.R., *Liquid Crystals*, **10**, 341, (1991)
64. Markovitsi D., Lecuyer I., *Chem. Soc. Faraday Trans.*, **87**, 1785, (1991)
65. Leisen J., Werth M., Boeffel C., Spiess H.W., *Journal Of Chemical Physics*, **97**, 3749, (1992)
66. Voigt-Martin I.G., Garbella R.W., Schumacher M., *Macromolecules*, **25**, 961, (1992)
67. Ono I., Kondo S., *Bulletin of the Chemical Society of Japan*, **65**, 1057, (1992)
68. Beattie D.B., Hindmarsh P., Goodby J.W., Haslam S., Richardson R.M., *Journal of Materials Chemistry*, **2**, 1261, (1992)
69. Hindmarsh P., Hird M., Styring P., Goodby J.W., *Journal of Materials Chemistry*, **3**, 1117, (1993)
70. Idziak S.H.J., Heiney P.A., Mc Cauley J.P., Carroll P., Smith A.B., *Molecular Crystals and Liquid Crystals Science and Technology Section A*, **237**, 271, (1993)
71. Boden N., Borner R.C., Bushby R.J., Cammidge A.N., Jesudason M.V., *Liquid Crystals*, **15**, 851, (1993)
72. Boden N., Bushby R.J., Clements J., *Journal of Chemical Physics*, **98**, 5920, (1993)
73. Adam D., Closs F., Frey T., Funhoff D., Haarer D., Ringsdorf H., Schumacher P., Siemensmeyer K., *Physical Review Letters*, **70**, 457, (1993)
74. Adam D., Haarer D., Closs F., Frey T., Funhoff D., Siemensmeyer K., Schuhmacher P., Ringsdorf H., *Berichte der Bunsen Gesellschaft fur Physikalische Chemie-An International, Journal Of Physical Chemistry*, **97**, 1366, (1993)
75. Bengs H., Closs F., Frey T., Funhoff D., Ringsdorf H., Siemensmeyer K., *Liquid Crystals*, **15**, 565, (1993)

76. Bengs H., Finkelmann H., Kupfer J., Ringsdorf H., Schuhmacher P., *Makromolekulare Chemie-Rapid Communications*, **14**, 445, (1993)
77. Tsukruk V.V., Reneker D.H., Bengs H., Ringsdorf H., *Langmuir*, **9**, 2141, (1993)
78. Osipov M.A., Hess S., *Molecular Physics*, **78**, 1191, (1993)
79. Phillips T.J., Jones C.J., Mc Donnell D.G., *Liquid Crystals*, **15**, 203, (1993)
80. Kruk G., Kocot A., Wrzalik R., Vij J.K., Karthaus O., Ringsdorf H., *Liquid Crystals*, **14**, 807, (1993)
81. Neff V.D., Gulrich L.W., Brown G.H., *Liquid Crystals*, Gordon and Breach, p 21, (1965)
82. Chandrasekhar S., *Liquid Crystals*, **14**, 3, (1993)
83. Diele S., Liebmann A., Nütz U., Ringsdorf H., Schumacher P., Abstract 14th International Liquid Crystal Conference, Pisa, (1992)
84. Boden N., Bushby R.J., Clements J., *Journal of Materials Science-Materials in Electronics*, **5**, 83, (1994)
85. Boden N., Bushby R.J., Cammidge A.N., *Journal of the Chemical Society-Chemical Communications*, **4**, 465, (1994)
86. Goodby J.W., Hird M., Toyne K.J., Watson T., *Journal of the Chemical Society-Chemical Communications*, **14**, 1701, (1994)
87. Phillips T.J., Jones C.J., *Liquid Crystals*, **16**, 5, 805, (1994)
88. Beattie D.R., Phd Thesis University of Hull, (1994)
89. Voigt-Martin I.G., Garbella R.W., Schumacher M., *Liquid Crystals*, **17**, 775, (1994)
90. Groothues H., Kremer F., Collard D.M., Lillya C.P., *Liquid Crystals*, **18**, 117, (1995)
91. Boden N., Bushby R.J., Cammidge A.N., *Journal of the American Chemical Society*, **117**, 924, (1995)
92. Henderson P., Ringsdorf H., Schuhmacher P., *Liquid Crystals*, **18**, 191, (1995)
93. Plesniviy T., Ringsdorf H., Schuhmacher P., *Liquid Crystals*, **18**, 185, (1995)
94. Phillips T.J., Minter V., *Liquid Crystals*, **20**, 243, (1996)
95. Glüsen B., Heitz W., Kettner A., Wendorff J.H., *Liquid Crystals*, **20**, 627, (1996)

96. Calucci L., Zimmermann H., Wachtel E.J., Poupkoi R., Luz Z., *Liquid Crystals*, **20**, 621, (1997)
97. Sikharulidze D., Chilaya G., Praefcke K., Blunk D., *Liquid Crystals*, **23**, 439 (1997)
98. Wang T., Yan D., Luo J. Zhou E., Karthaus O., Ringsdorf H., *Liquid Crystals*, **23**, 869, (1997)
99. Forget S., Kitzerow H.S., *Liquid Crystals*, **23**, 919, (1997)

References. Chapter 2.

1. Kelker H., *Molecular Crystals and Liquid Crystals*, **21**, 1, (1973)
2. Colling P.J., *Liquid Crystals*, Iop Publishing, Adam Hilger, Ch. 8, 147, (1990)
3. Olympus Manual.
4. Hot stage Linkam Manual.
5. Hot Stage Linkam Controller.
6. VTO 232 Video Text Overlay manual Linkam.
7. Vidi PC Computer Hardware and Software.
8. Beattie D.B., Hindmarsh P., Goodby J.W., Haslam S., Richardson R.M., *Journal of Materials Chemistry*, **2**, 1261, (1992)
9. Beattie D.R., *Phd Thesis University of Hull*, (1994)
10. Hindmarsh P., Hird M., Styring P., Goodby J.W., *Journal of Materials Chemistry*, **3**, 1117, (1993)
11. Goodby J.W., Hird M., Toyne K.J., Watson T., *Journal of the Chemical Society-Chemical Communications*, **14**, 1701, (1994)
12. Destrade C., Tinh N.H., Gasparoux H., *Molecular Crystals and Liquid Crystals*, **71**, 111, (1981)
13. Janning J.L., *Appl. Phys. Lett.*, **21**, 173, (1972)
14. Belarbi Z., *J. Phys. Chem.*, **94**, 7334, (1990)
15. Bengs H., Closs F., Frey T., Funhoff D., Ringsdorf H., Siemensmeyer K., *Liquid Crystals*, **15**, 565, (1993)

16. Vauchier C., Zann A., Le Barny P., Dubois J.C., Billard J., *Molecular Crystals and Liquid Crystals*, **66**, 103, (1981)
17. Raghunathan V.A., Madhusudana N.V., Chandrasekhar S., *Molecular Crystals and Liquid Crystals*, **148**, 77, (1987)
18. Warmerdam T.W., Frenkel D., Zijlstra R.J.J., *Liquid Crystals*, **3**, 369, (1988)
19. Warmerdam T.W., Frenkel D., Zijlstra R.J.J., *Liquid Crystals*, **3**, 1105, (1988)
20. Phillips T.J., Jones C.J., Mc Donnell D.G., *Liquid Crystals*, **15**, 203, (1993)
21. Beattie D.B., Hindmarsh P., Goodby J.W., Haslam S., Richardson R.M., *Journal of Materials Chemistry*, **2**, 1261, (1992)

References. Chapter 3.

1. Bragg L., *The Development of X-ray Analysis*, G. Bell and Sons Ltd.s, Ch. 1 (1975)
2. Ewald P.P., *Fifty Years of X-ray Diffraction*, NVA Oosthoek's Uitgeversmaatschappij Utrecht, Ch. 1 (1962)
3. Lipson H.S., *Crystals and X-rays*, Wykeham publications, Ch. 2 (1970)
4. Roberts I.F., *Crystals and Their Structure*, Methuen Educational, Ch. 1 (1974)
5. Milburn G.H.W., *X-ray Crystallography*, Butterworths, Ch. 1 (1973)
6. Philips X-ray Manual

References. Chapter 4.

1. Kemp W., *Organic Spectroscopy*, Mac Millan, Ch. 1-2, (1987).
2. *Galaxy FT-IR spectrometer User's manual*, Mattson Instruments, Ch. 2, (1992).
3. Griffiths P.R., *Fourier Transform Infra red spectrometry*, John Wiley and Sons Ltd., Ch. 1-3, (1986).
4. Colthup N.B., *Introduction to Infra-red and Raman Spectroscopy*, Academic Press N.Y., p111-112, (1975).

5. Chamberlain J., *The Principles of Interferometric Spectroscopy*, John Wiley and Sons Ltd., Ch. 1 + Ch. 4, (1979).
6. Fellgett P.B., Doctoral Thesis, University of Cambridge, (1951).
7. Cooley J.W., Tukey J.W., *Math. Comput.*, **19**, 297, (1965).
8. Kauppinen J.K., Moffatt D.J., Mantsch H.H., Cameron D.G., *Applied Spectroscopy*, **35**, 3, (1981).
9. Mattson, *FIRST Fourier Software Tools User's Manual - Advanced FIRST Section*, (1990).
10. *IR Heater Spec. Sheet*.
11. Cross A.D., *An introduction to practical IR Spectra.*, Butterworth, Ch. 1-3, (1969)
12. Flett M.St.C., *Characteristic Frequencies of chemical groups in the Infra-red.*, Elsevier Pub., p 30-55, (1963).
13. Barron C., *Reversed Hexagonal Phase Structure in Lithium Phenyl Stearate.*, PhD Thesis, Sheffield City Polytechnic, (1993).
14. Williams, *Spectroscopic Methods in Organic Chemistry*, 5th Edition, **C2**, Mc Graw-Hill International, (1995).
15. Silverstein, *Spectroscopic Identification of Organic Compounds*, 5th Edition, **C3**, John Wiley and Son Inc., (1991).
16. Maroncelli M., Qi S.P., Strauss H.L., Snyder R.G., *J.Am Chem. Soc*, **104**, 6237, (1982).
17. Senak L., Davies M.A., Mendelsohn R., *J. Phys. Chem.*, **95**, 2565, (1991).
18. Flory P.J., *Statistical Mechanics of Chain Molecules*, Hanser - New York, (1988).
19. Kruk G., Kocot A., Wrzalik R., Vij J.K., Karthaus O., Ringsdorf H., *Liquid Crystals*, **14**, 807, (1993)
20. Neff V.D., Gulrich L.W., Brown G.H., *Liquid Crystals*, Gordon and Breach, p 21, (1965)

References. Chapter 5.

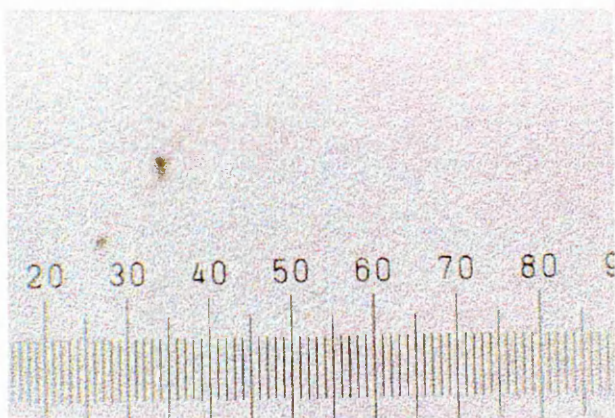
1. Cerius 3.2 Manual, *Molecular Simulations*, Ch. 7, (1993)
2. Mayo S.L., Olafson B.D., Goddard III W.A., *J. Phys. Chem.*, **94**, 8897, (1990)
3. Kao J., Allinger N.L., *J. Am. Chem. Soc.*, **99**, 975, (1977)
4. Liljefors T., Tai J.C., Li S., Allinger N.L., *J. Comp. Chem.*, **8**, 1051, (1987)
5. Sprague J.T., Tai J.C., Yuh Y., Allinger N.L., *J. Comp. Chem.*, **8**, 581, (1987)
6. Wiener S.J., Kollman P.A., Case D.A., Singh U.C., Ghio C., Alagona G., Weiner P., Profeta Jr. S., *J. Amer. Chem. Soc.*, **106**, 765, (1984)
7. Wiener S.J., Kollman P.A., Nguyen D.T., Case D.A., *J. Comp. Chem.*, **7**, 230, (1986)
8. Rappé A.K., Casewit C. J., Colwell K.S., Goddard III W.A., Skiff W.M., *J. Amer. Chem. Soc.*, **114**, 10024, (1992)
9. Cerius 3.2 Manual, *Molecular Simulations*, Ch. 3, (1993)

References. Chapter 6.

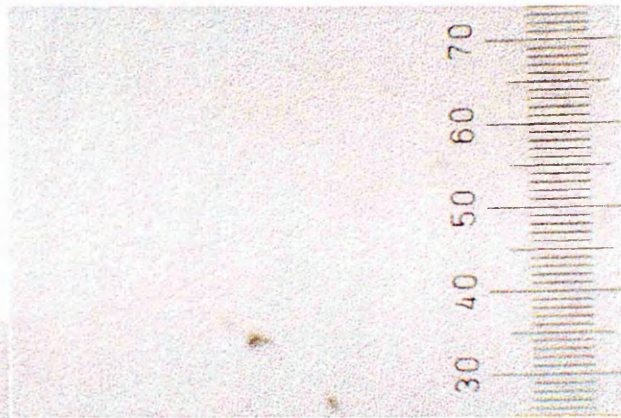
1. Vauchier C., Zann A., Le Barny P., Dubois J.C., Billard J., *Molecular Crystals And Liquid Crystals*, **66**, 103, (1981)
2. Raghunathan V.A., Madhusudana N.V., Chandrasekhar S., Destrade C., *Molecular Crystals And Liquid Crystals*, **148**, 77, (1987)
3. Maroncelli M., Qi S.P., Strauss H.L., Snyder R.G., *J. Am Chem. Soc.*, **104**, 6237, (1982).
4. Senak L., Davies M.A., Mendelsohn R., *J. Phys. Chem.*, **95**, 2565, (1991).
5. Phillips T.J., Minter V., *Liquid Crystals*, **20**, 2, 243, (1996)
6. Calucci L., Zimmermann H., Wachtel E.J., Poupkoi R., Luz Z., *Liquid Crystals*, **20**, 5, 621, (1997)
7. Sikharulidze D., Chilaya G., Praefcke K., Blunk D., *Liquid Crystals*, **23**, 3, 439 (1997)

Optical Microscopy Scale

The optical photographs in Appendix A were taken using a 20 times objective combined with a 10 times eye-piece given a magnification of 200x. The following two images were used as calibration and show the scale for each axis with 100 divisions corresponding to 1 mm. The photographs in Appendix A display an area of 0.75mm x 0.50mm.

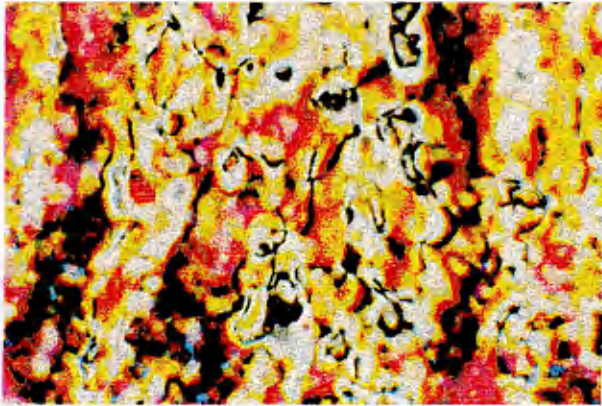


X-axis scale, 100 Divisions = 1mm

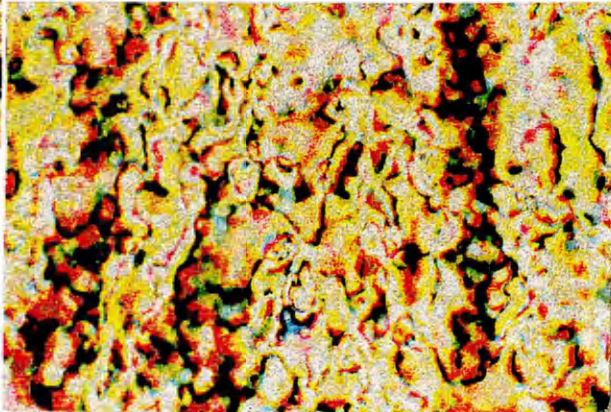


Y-axis scale, 100 Divisions = 1mm

DB26



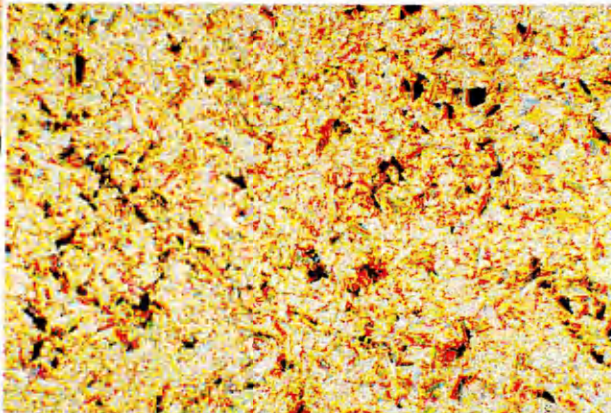
Nematic 235°C



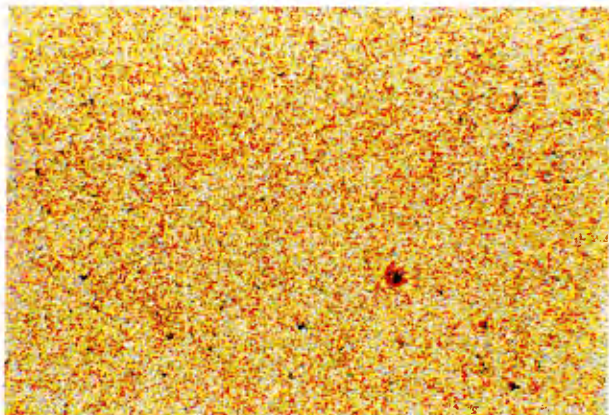
Nematic 187°C



Phase transition. 165.5°C



Crystal 157°C

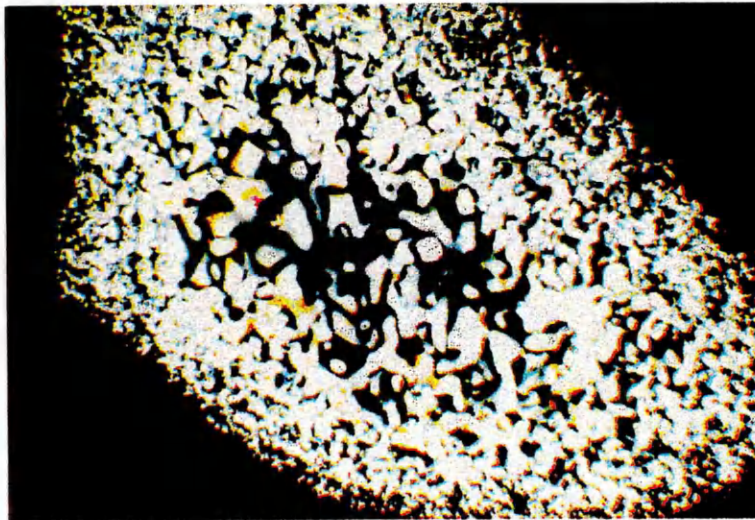


Crystal 70°C

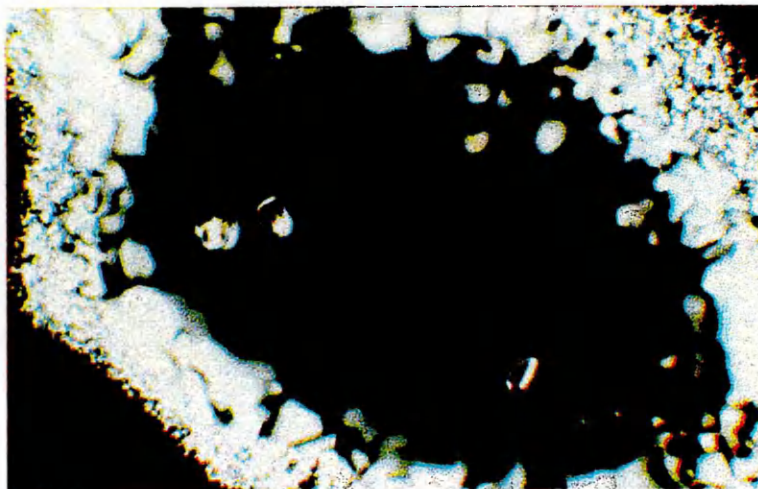
DB118



Nematic 206.6°C

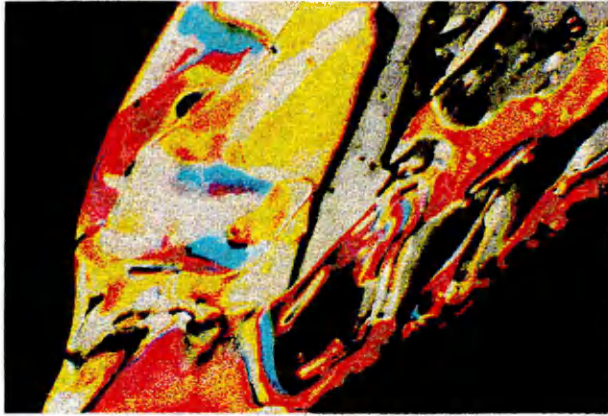


Nematic 206.5°C

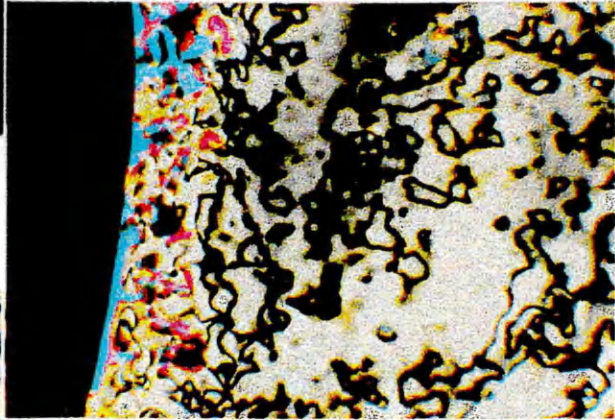


Aligned Nematic 206.3°C

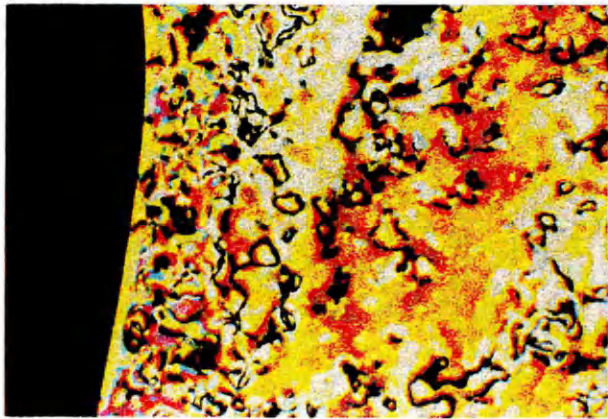
DB125



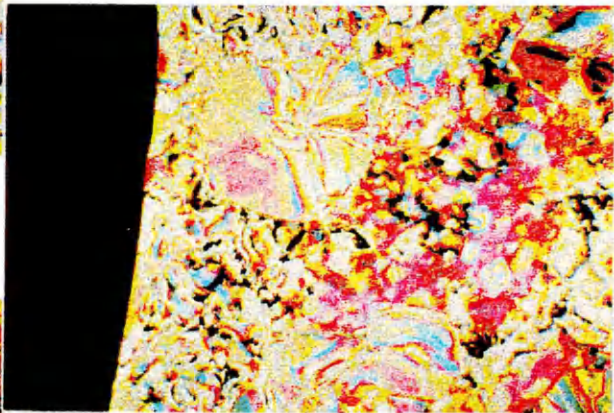
Nematic 200°C on heating



Nematic 188.8°C



Nematic 150°C

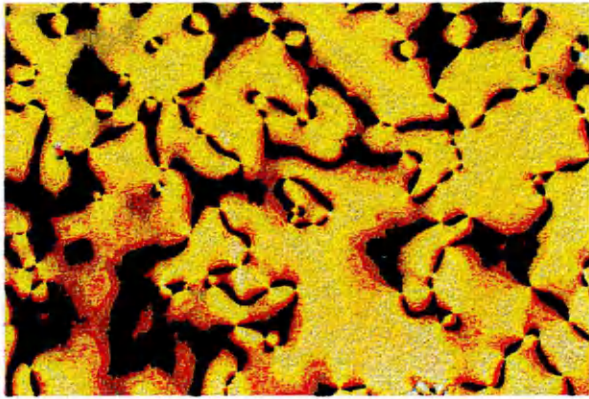


Phase transition. 105°C

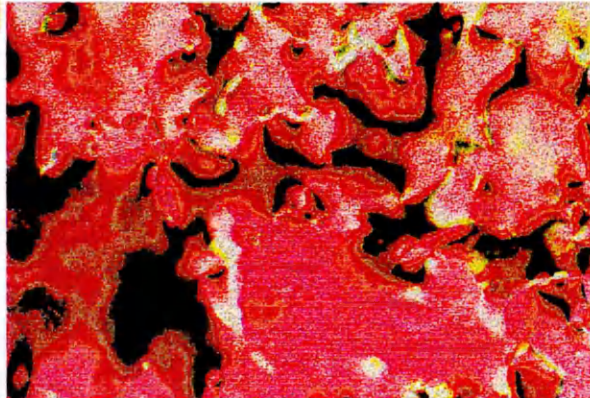


Crystal 90°C

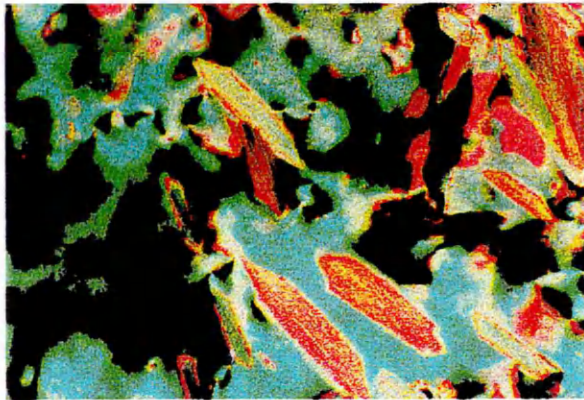
PH64



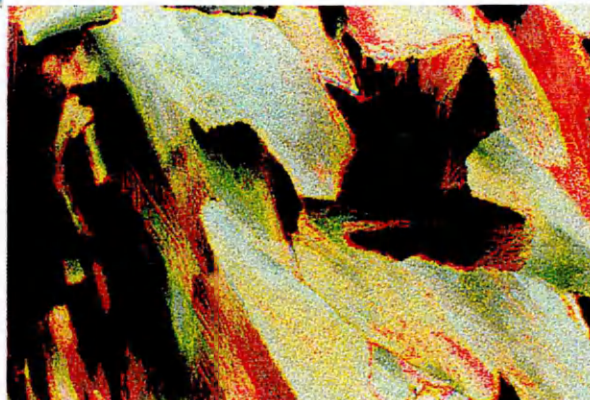
Nematic 214°C



Nematic 210°C

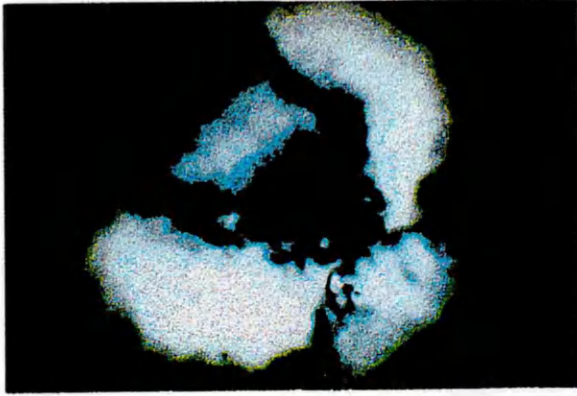


Phase transition. 194.2°C

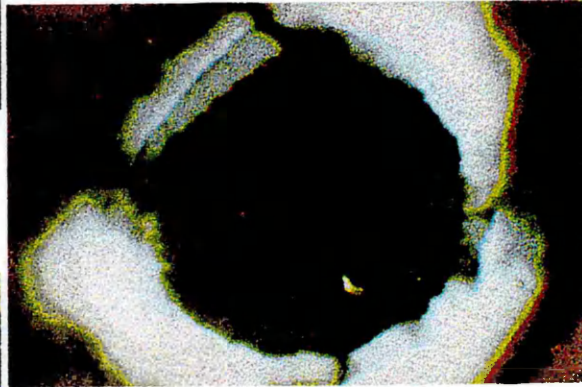


Crystal 185°C

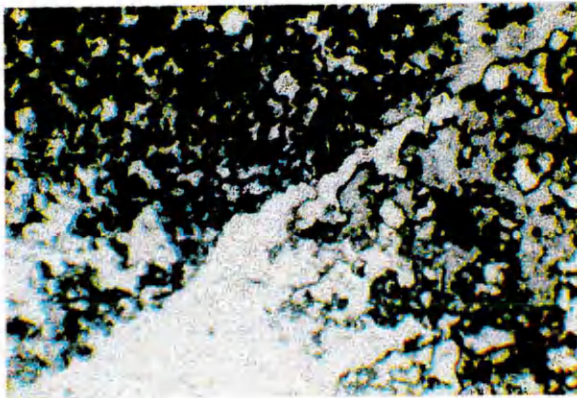
PH76



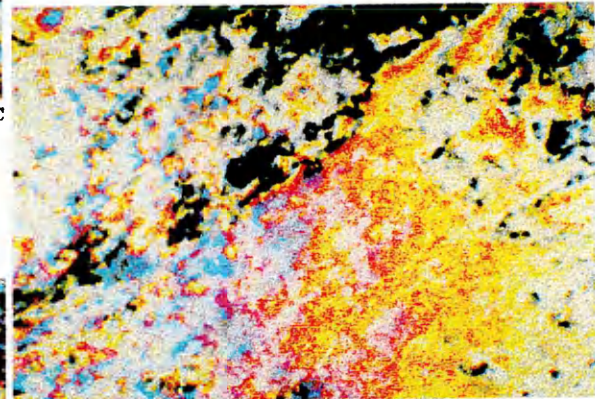
Nematic 172.7°C



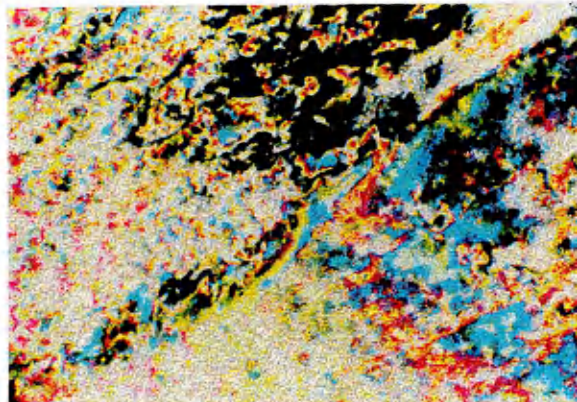
Aligned Nematic 172.6°C



Nematic 155°C



Crystal 122°C

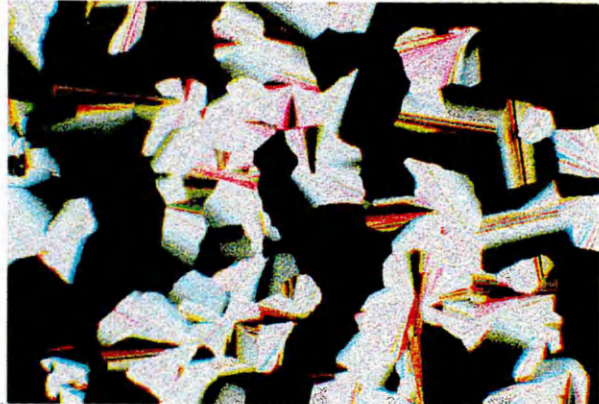


Crystal 48°C

TW75



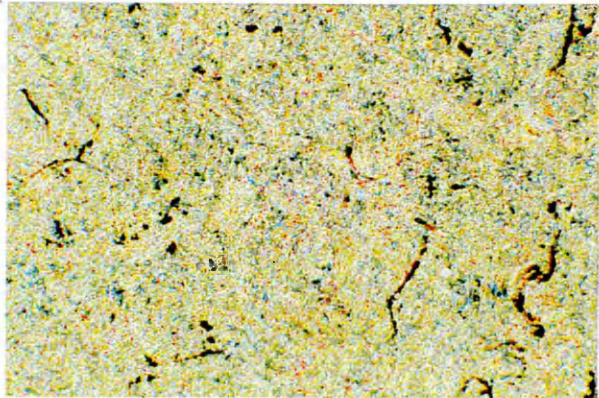
Nematic 83.6°C



Nematic 57.0°C



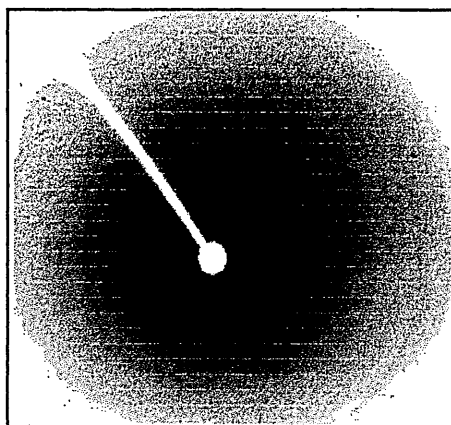
Phase transition. 28.0°C



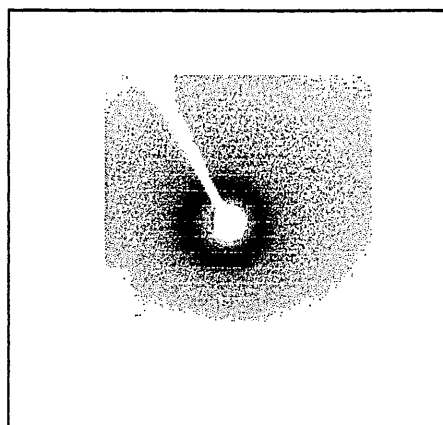
Crystal 28.0°C

Appendix B

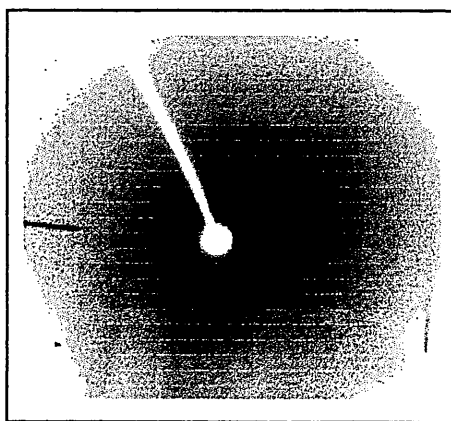
X-ray Diffraction Photographs.



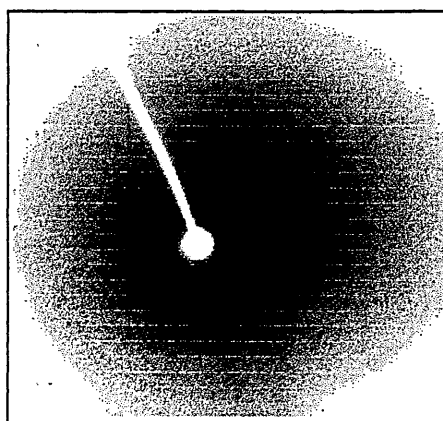
PH76 25°C
Crystal



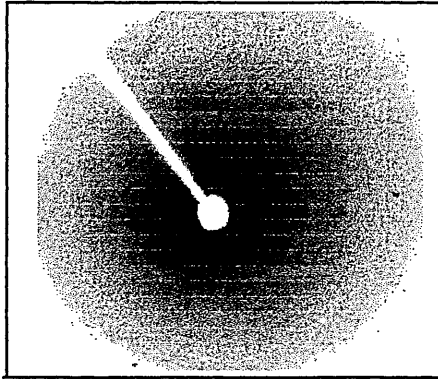
PH76 166.5°C
Nematic



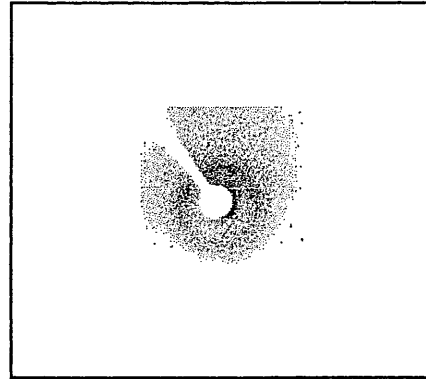
PH 64 Nematic
0.5 Tesla magnetic field.
177.4°C



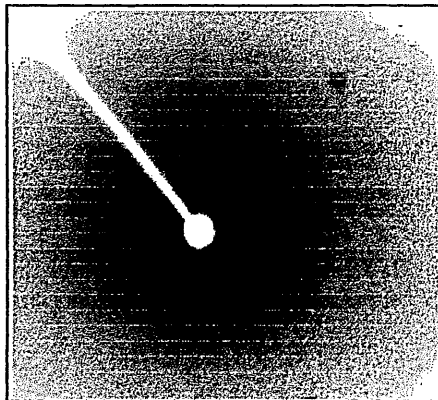
PH74 Nematic
0.5 Tesla magnetic field.
176.9°C



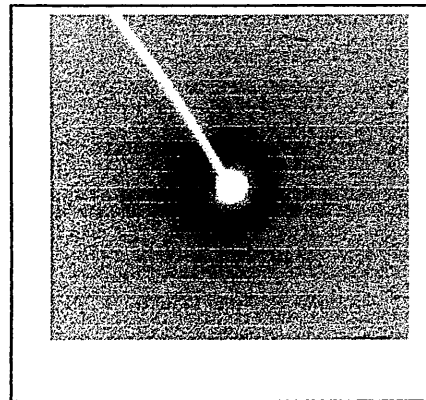
**PH64 Crystal
25°C**



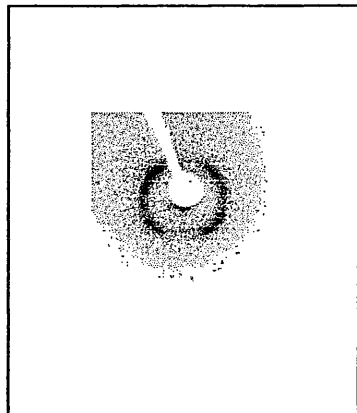
**PH64 Nematic
210.5 - 213.1°C**



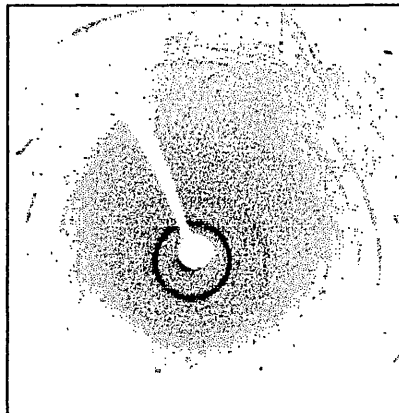
**PH74 Crystal
25°C**



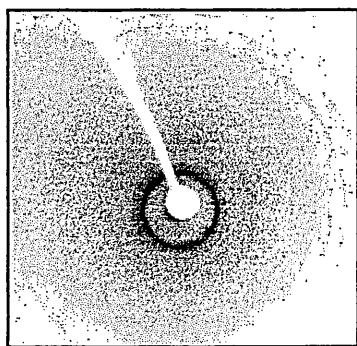
**PH74 Nematic
212.8 - 212.7°C**



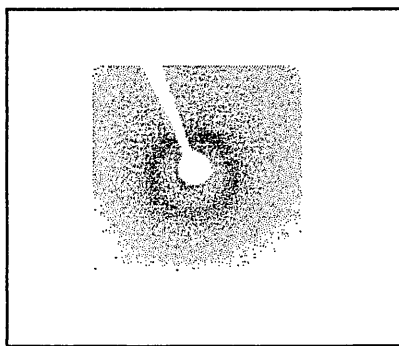
DB118 Crystal
No previous heating.
Room temperature.



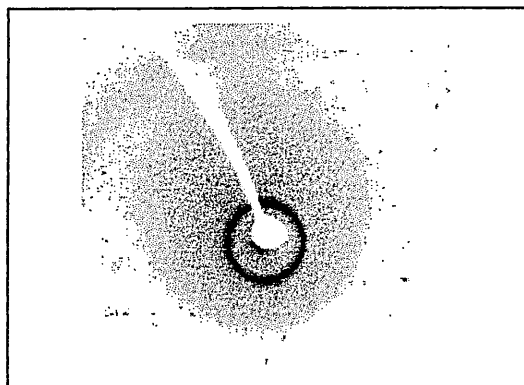
DB118 Crystal
After heating to isotropic.
Room temperature.



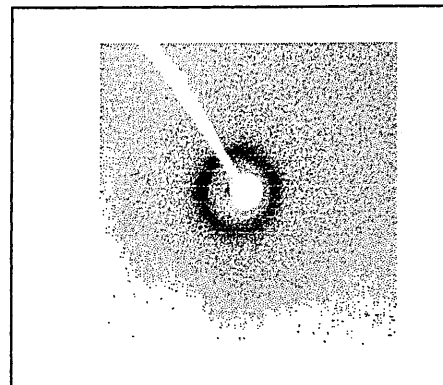
DB118 Crystal
84.3°C



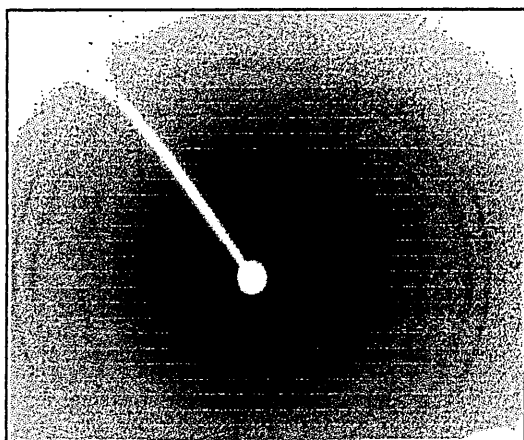
DB118 Nematic
169°C



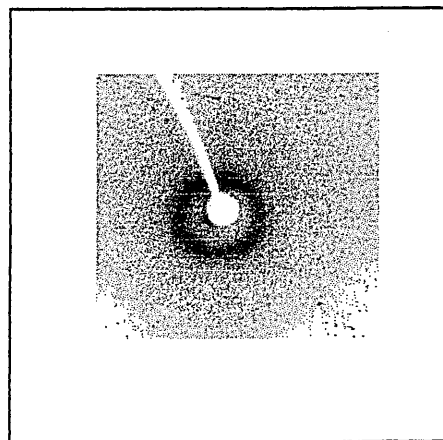
DB26 Crystal
Room temperature.



DB26 Nematic
209.8 - 211.5°C



DB125 Crystal
Room temperature.



DB125 Nematic
171.2°C